อนุพันธ์โลหะ-ซาเลนสำหรับรีดักชันเชิงไฟฟ้าของคาร์บอนไดออกไซด์

นางสาวกันทิมา จิตจักร

วิทยานิพนธ์นี้เป็นส่วนหนึ่งของการศึกษาตามหลักสูตรปริญญาวิทยาศาสตรดุษฎีบัณฑิต
สาขาวิชาปิโตรเคมี
คณะวิทยาศาสตร์ จุฬาลงกรณ์มหาวิทยาลัย
ปีการศึกษา 2560

METAL-SALEN DERIVATIVES FOR ELECTRO-REDUCTION OF CARBON DIOXIDE

Miss Kantima Chitchak

A Dissertation Submitted in Partial Fulfillment of the Requirements
for the Degree of Doctor of Philosophy Program in Petrochemistry
Faculty of Science
Chulalongkorn University
Academic Year 2017

Thesis Title	METAL-SALEN DERIVATIVES FOR ELECTRO-REDUCTION OF CARBON DIOXIDE
By	Miss Kantima Chitchak
Field of Study	Petrochemistry
Thesis Advisor	Parichatr Vanalabhpatana, Ph.D.

Accepted by the Faculty of Science, Chulalongkorn University in Partial Fulfillment of the Requirements for the Doctoral Degree

.....Dean of the Faculty of Science

(Associate Professor Polkit Sangvanich, Ph.D.)

THESIS COMMITTEE

.....Chairman

(Assistant Professor Warinthorn Chavasiri, Ph.D.)

.....Thesis Advisor

(Parichatr Vanalabhpatana, Ph.D.)

.....Examiner

(Assistant Professor Varawut Tangpasuthadol, Ph.D.)

.....Examiner

(Associate Professor Patchanita Thamyongkit, Dr.rer.nat.)

.....External Examiner

(Assistant Professor Nantanit Wanichacheva, Ph.D.)

กันทิมา จิตจักร : อนุพันธ์โลหะ-ซาเลนสำหรับรีดักชันเชิงไฟฟ้าของคาร์บอนไดออกไซด์ (METAL-SALEN DERIVATIVES FOR ELECTRO-REDUCTION OF CARBON DIOXIDE) อ.ที่ปรึกษาวิทยานิพนธ์หลัก: อ. ดร.ปาริฉัตร วนลาภพัฒนา, 98 หน้า.

คอปเปอร์(II) ซาเลน ลิแกนด์ฐานซาโลเฟน และสารประกอบเชิงซ้อนคอปเปอร์ของลิแกนด์ฐานซาโลเฟนถูกเตรียมและใช้สำหรับการเร่งปฏิกิริยารีดักชันของคาร์บอนไดออกไซด์ ศึกษาอิเล็กโทรไลซิสแบบควบคุมศักย์ไฟฟ้าของตัวเร่งปฏิกิริยาเชิงไฟฟ้าคอปเปอร์(II) ซาเลนกับคาร์บอนไดออกไซด์ในสารละลายที่ไม่ใช่น้ำเป็นตัวทำละลายเพื่อให้ได้ภาวะการอิเล็กโทรไลซิสที่เหมาะสม ได้แก่ ศักย์ไฟฟ้าที่ให้ และปริมาณของตัวให้โปรตอน ด้วยศักย์ไฟฟ้าที่ให้ –2.10 โวลต์ ได้คาร์บอนมอนอกไซด์ (3.50-16.30%) เป็นผลิตภัณฑ์ที่ได้ในวัฏภาคแก๊สเท่านั้น พบมีเทนเพิ่มเติมเมื่อมีการเติมตัวให้โปรตอน และมีปริมาณร้อยละสูงสุด (0.39 ± 0.00%) จากอิเล็กโทรไลซิสด้วยตัวให้โปรตอน 25.00 มิลลิโมลาร์ และคอปเปอร์(II) ซาเลน 2.00 มิลลิโมลาร์ ยิ่งไปกว่านั้นประสบความสำเร็จในการสังเคราะห์ พิสูจน์เอกลักษณ์และนำซาโลเฟนและอนุพันธ์ รวมทั้งสารประกอบเชิงซ้อนคอปเปอร์มาประยุกต์ใช้เป็นตัวเร่งปฏิกิริยาทางไฟฟ้าเอกพันธ์สำหรับรีดักชันเชิงไฟฟ้าของคาร์บอนไดออกไซด์ ลิแกนด์และสารประกอบเชิงซ้อนฐานซาโลเฟนแสดงถึงความเป็นไปได้ในการเร่งปฏิกิริยารีดักชันเชิงไฟฟ้าของคาร์บอนไดออกไซด์ ในหมู่สารประกอบฐานซาโลเฟน คอปเปอร์(II) โบรโม-ซาโลเฟนแสดงประสิทธิภาพการเป็นตัวเร่งปฏิกิริยาที่ดีที่สุดโดยการเพิ่มขึ้นของกระแสสูงที่สุด (360%) ในการทดลองไซคลิกโวลแทมเมทรี คล้ายกับอิเล็กโทรไลซิสของคอปเปอร์(II) ซาเลน–คาร์บอนไดออกไซด์ อิเล็กโทรไลซิสของคาร์บอนไดออกไซด์ด้วยคอปเปอร์(I) ซาโลเฟนที่เกิดโดยวิธีทางไฟฟ้าและอนุพันธ์ให้คาร์บอนมอนอกไซด์เป็นผลิตภัณฑ์แก๊ส (5.90-8.87%) ในขณะที่มีเทนถูกพบเพิ่ม (0.57 ± 0.00%) เมื่อเติมตัวให้โปรตอน

สาขาวิชา ปิโตรเคมี ลายมือชื่อนิสิต .....

ปีการศึกษา 2560 ลายมือชื่อ อ.ที่ปรึกษาหลัก .....

5472909123 : MAJOR PETROCHEMISTRY
KEYWORDS: ELECTROCATALYST / CARBON DIOXIDE REDUCTION / SALEN / SALOPHEN / COPPER COMPLEX

KANTIMA CHITCHAK: METAL-SALEN DERIVATIVES FOR ELECTRO-REDUCTION OF CARBON DIOXIDE. ADVISOR: PARICHATR VANALABHPATANA, Ph.D., 98 pp.

Copper(II) salen, salophen-based ligands, and their corresponding copper complexes were prepared and utilized for the electrocatalytic reduction of carbon dioxide. Controlled-potential electrolysis of copper(II) salen electrocatalyst with carbon dioxide in non-aqueous solution was investigated to obtain the optimized electrolysis condition including the applied potential and proton donor quantity. With the applied potential of –2.10 V, carbon monoxide (3.50-16.30%) was obtained as the only product in gas phase. Methane was additionally found with the addition of proton donor and its maximum percentage (0.39 ± 0.00%) were obtained from the electrolysis with 25.00 mM proton donor and 2.00 mM copper(II) salen. Moreover, salophen and its derivatives as well as corresponding copper complexes were successfully synthesized, characterized, and applied as homogeneous electrocatalysts for the electro-reduction of carbon dioxide. Salophen-based ligands and complexes presented possibilities in electrochemically catalyzing the carbon dioxide reduction. Among all salophen-based compounds, copper(II) bromo-salophen showed the best electrocatalytic efficiency with the highest current enhancement (360%) in cyclic voltammetric experiment. Similar to the copper(II) salen–carbon dioxide electrolysis, the electrolysis of carbon dioxide by electrogenerated copper(I) salophen and its derivatives gave carbon monoxide as gaseous product (5.90-8.87%), whereas methane was additionally found (0.57 ± 0.00%) when a proton donor was added.

Field of Study: Petrochemistry Student's Signature .....

Academic Year: 2017 Advisor's Signature .....

ACKNOWLEDGEMENTS

Firstly, I would like to express my gratitude to my advisor, Dr. Parichatr Vanalabhpatana, for continuously providing important guidance and unwavering encouragement throughout my six years of graduate study at Chulalongkorn University.

I also would like to thank my thesis examination committee members, Assistant Professor Dr. Warinthorn Chavasiri, Assistant Professor Dr. Varawut Tangpasuthadol, Associate Professor Dr. Patchanita Thamyongkit, and Assistant Professor Dr. Nantanit Wanichacheva, who give helpful comments and advice in this thesis.

I am grateful to the financial supports from Electrochemistry and Optical Spectroscopy Research Unit (EOSRU) and Cooperation of Proactive Research on Molecular Sensory Science and Optoelectronic Devices Project, Rachadapisek Sompote Fund.

Finally, I am affectionatly thankful to my Chitchak family and my friends for their unlimited support, belief, and encouragement throughout my education.

CONTENTS

Page

Page

Page

Page

Page

LIST OF TABLES

LIST OF FIGURES

LIST OF SCHEMES

LIST OF ABBREVIATIONS

s	Second
V	Volt
ν	Scan rate
g	Gram
μA	Microampere
N_2	Nitrogen
Ar	Argon
CO_2	Carbon dioxide
CO	Carbon monoxide
CH_4	Methane
°C	Degree celsius
Ag/AgCl	Silver/silver chloride
Ag/Ag^+	Silver/silver ion
SCE	Saturated calomel electrode
RVC	Reticulated vitreous carbon

ACN	Acetonitrile
DMF	Dimethylformamide
DMSO	Dimethyl sulfoxide
PC	Propylene carbonate
HFIP	1,1,1,3,3,3-Hexafluoro-2-propanol
$TMABF_4$	Tetramethylammonium tetraflouroborate
$TBABF_4$	Tetrabutylammonium tetraflouroborate
TBAP	Tetrabutylammonium perchlorate
TEHFP	Tetraethylhexaflourophosphate
M	Molar
mM	Millimolar
mL	Milliliter
min	Minute
ppm	Part per million
vs.	Versus

obsd.	Observed
calcd.	Calculated
E_p	Peak potential
E_{pa}	Anodic peak potential
E_{pc}	Cathodic peak potential
i_{pa}	Anodic peak current
i_{pc}	Cathodic peak current
$E_{1/2}$	Half wave potential
E^0	Formal potential
m/z	Mass-to-charge ratio
λ_{abs}	Absorption wavelength
FE	Faradaic efficiency
TON	Turnover number
Q	Charge

CHAPTER I
INTRODUCTION

1.1. Introduction

Increasing concerns about the rising level of atmospheric carbon dioxide (CO_2), the major cause of global warming, and an energy crisis have prompted the development of new technologies for decreasing carbon dioxide. The problem of atmospheric carbon dioxide concentrations can be alleviated by various technologies such as biological [1-3], geochemical [4-6], and chemical methods [7-9]. Although many technologies and processes seem to be perfect solutions of reducing carbon dioxide, their high budgets and complicated procedures are main obstacles. Electrocatalytic reduction of carbon dioxide has tendencies to be attractive avenue for converting carbon dioxide into high value-added chemicals and energy-rich molecules [10] since it can provide a sustainable low temperature redox cycle for energy storages and conversions [11]. Electro-reduction of carbon dioxide can proceed through two-, four-, six-, and eight-electron reduction pathways in gaseous, aqueous, and non-aqueous phases at both low and high temperatures. The major reduction products are carbon monoxide (CO), formic acid (HCOOH) or formate ion ($HCOO^-$) in basic solution, oxalic acid ($H_2C_2O_4$) or oxalate ion ($C_2O_4^{2-}$) in basic solution, formaldehyde (CH_2O), methanol (CH_3OH), methane (CH_4), ethylene (CH_2CH_2), and ethanol (CH_3CH_2OH) [12]. Nevertheless, the electrochemical reduction of carbon dioxide at bare electrodes requires efficient electrocatalysts to overcome overpotential problems. A wide variety of metallic transition metal complexes have been utilized as catalysts for carbon dioxide electro-reduction. Metal electrodes [13-16] and complexes with pyridine [17-19], phosphorus [20-22], and macrocyclic ligands [23-25] generally exhibit good catalytic activity, selectivity, and stability [26]. Previous work in our laboratory studied electrocatalytic reduction of carbon dioxide by macrocyclic and Schiff base catalysts, *i.e.*, phatalocyanine and salen complexes, and found that copper(II) salen acts as an effective electrocatalyst towards this reaction [27]. Therefore, this research investigates thoroughly the carbon dioxide reduction

using copper(II) salen electrocatalyst by means of controlled-potential electrolysis to obtain the optimized electrolysis conditions and gain insight into the electrocatalytic properties of this complex. Furthermore, salen derivatives such as salophen and its corresponding metal complexes were synthesized and explored as electrocatalysts for carbon dioxide reduction. In addition, the effects of the substituents on salophen ligand were investigated.

1.2. Literature Review

Electro-reduction of carbon dioxide is energetically attractive process that converts carbon dioxide to high value-added chemicals (C–C coupled products) and energy-rich molecules (*e.g.*, carbon monoxide, methane, methanol, and formic acid) [10] under low pressure and temperature. For instance, carbon dioxide reduction in non-aqueous solution at an inert electrode produces a mixture of carbon monoxide and oxalate ion. The electrolysis catalyzed by radical anions of aromatic esters and nitriles suggested the mechanism of carbon dioxide reduction as shown in equations 1.1-1.8 [28].

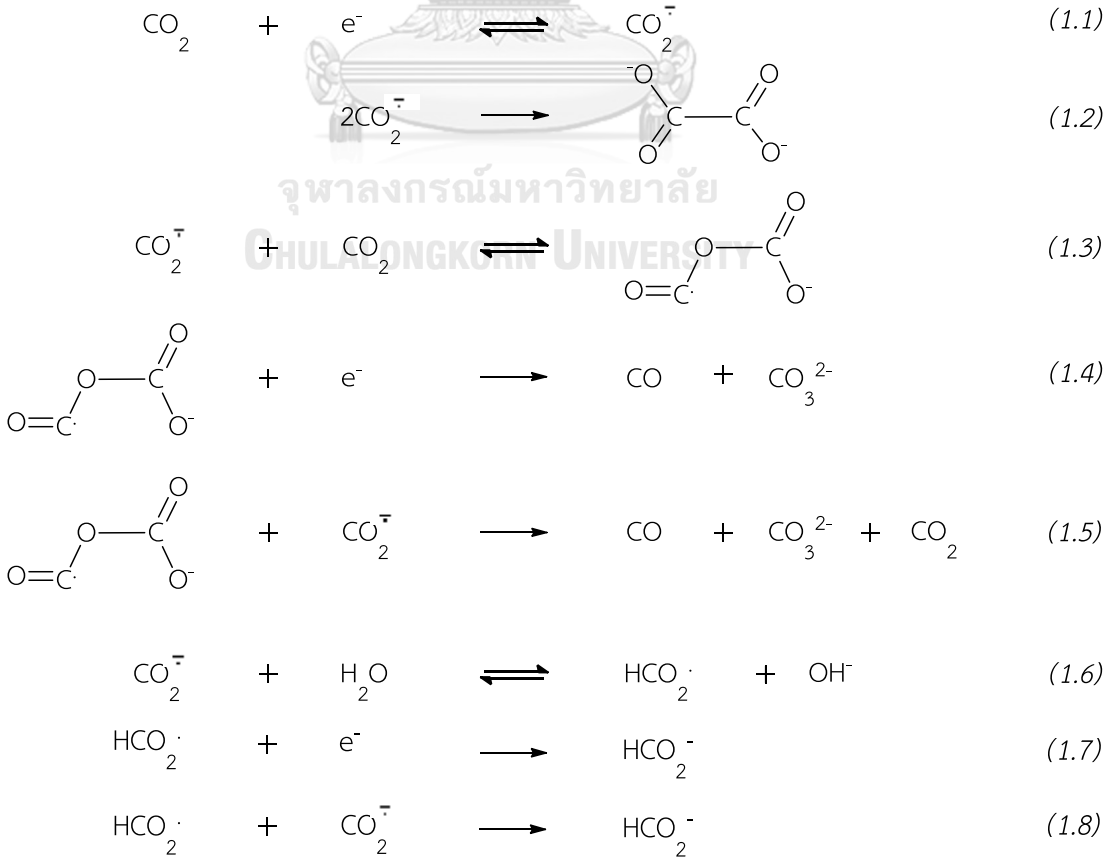

(1.1)

(1.2)

(1.3)

(1.4)

(1.5)

(1.6)

(1.7)

(1.8)

To improve electrochemical kinetics and product distribution of carbon dioxide reduction, high efficiency electrocatalysts are required. A large number of transition metal (*e.g.*, iron, cobalt, nickel, copper, zinc, ruthenium, and silver) complexes have been applied as catalysts for carbon dioxide reduction because of selectivity and tunable activity [29]. Among them, Schiff base complexes such as metal salens appear to be high potential electrocatalysts for carbon dioxide reduction due to their electrically conductive conjugated bonds, easy preparation, and affordable prices. For example, Peiris and co-workers [30] studied the electrocatalytic reduction of carbon dioxide by *N*,*N*′-bis(salicylidene)-ethylenediaminonickel(II) or nickel(II) salen. Cyclic voltammetric experiments were carried out in dimethylformamide (DMF) solution containing tetraethylhexaflouro-phosphate (TEHFP) electrolyte at a glassy carbon electrode. The results revealed that nickel(II) salen-nikel(I) salen reduction peak takes place at –1.80 V and electrogenerated Ni(I) salen is capable of catalyzing carbon dioxide reduction. The electrolysis provided clues for the formation of oxalate ion via carbon dioxide reduction.

In 2002, Zolezzi *et al*. [31] investigated the electrochemical reduction of copper(II) with salen ligands synthesized from ethylenediamine, (*R*,*R*)-, and (*S*,*S*)-1,2-diphenylethylenediamine, with 5-methoxy, 5-bromo, and 5-nitrosalicylaldehyde in dimethyl sulfoxide (DMSO) solution by means of cyclic voltammetry. The resulting voltammograms consist of single quasi-reversible one-electron peaks attributable to copper(II) salen/copper(I) salen redox couple. Trends of the cathodic peak potentials show good correlation with the electronic effect of the ligand substituents.

In 2013, Ourari *et al*. [32] reported the synthesis, characterization, and electrode modification of novel copper(II)-Schiff base complex (Cu(II) complex with salen derivative containing pyrrole ring). Electrochemical experiments were recorded by a glassy carbon electrode in acetonitrile (ACN) solution containing tetrabutyl-ammonium perchlorate (TBAP). The copper(II)-Schiff base complex acted as an effective electrocatalyst with high catalytic activity for carbon dioxide reduction, giving carbon monoxide and formic acid as electrolysis products.

In 2015, Khoshro *et al*. [33] observed the electrochemical behaviors of two copper(II)-Schiff base complexes: *N*,*N*′-bis(2-*R*-phenyl-salicylidenaminato)copper(II) (CuL_2–Me for *R* = Me and CuL_2–Cl for *R* = Cl) and *N*,*N*′-bis(salicylaldimine)propylene-diimino-copper(II) (CuL′). These complexes exhibited excellent electrocatalytic behaviors via ligand-based reduction for the reduction of carbon dioxide and promote the electrocatalytic reduction of carbon dioxide better than the free ligands.

There have been several researches using metal-salophen for the carbon dioxide reduction. In 1993, Gennaro *et al*. [34] used cobalt(II) salophen and nickel(II) salophen as catalysts for electrochemical reduction of carbon dioxide by means of cyclic voltammetric experiments and controlled-potential electrolyses. In the case of nickel(II) salophen, no catalysis was observed. The first electron uptake is ligand-based reduction yielding the radical anion [nickel(II) salophen]$^{\bullet-}$ which dimerizes rapidly. On the contrary, the electron transfer of cobalt(II) salophen is metal-centered process giving the [cobalt(I) salophen]$^{-}$ complex which appears to catalyze the carbon dioxide reduction to yield carbon monoxide and carbonate (CO_3^{2-}) ion in ACN containing lithium perchorate ($LiClO_4$).

In 2015, Singh *et al*. [35] synthesized and evaluated 4-nitro-*N*,*N*′-disalicylidine-1,2-phenylenediamine or nitro-salophen and its corresponding Ni(II) and copper(II) complexes as electrocatalysts for carbon dioxide reduction. The complexes were found to be quite efficient for the reduction process and resulted in the production of hydrocarbons (C1 and C2) and carbon monoxide. The total Faradaic efficiency was found to be 74% for nikel(II) complex and 25% for Cu(II) complex at 1.50 V and 1.80 V, respectively. Moreover, the nikel(II) complex showed better efficiency towards carbon monoxide formation as compared to copper complex. The overpotential of metal complexes was reduced significantly ranging from 10% to 25% against their pure metal counterparts.

1.3. Objective and Scopes of the Thesis

The objective of this work is to investigate the electrocatalytic properties of copper(II) salen for carbon dioxide reduction by means of controlled-potential

electrolysis. Various parameters, *e.g.*, proton donor, applied potential, and electrolysis time will be carefully optimized to improve yields of the targeted products of carbon dioxide electro-reduction. Gaseous products of electrocatalytic reduction of carbon dioxide were analyzed by means of gas chromatography. Morphology and structure of the working electrodes after the electrolysis were studied. Furthermore, salophen ligands and their metal complexes will be synthesized and studied their electrocatalytic activity for carbon dioxide reduction. Nuclear magnetic resonance (NMR) spectroscopy, mass spectrometry, and ultraviolet–visible (UV–vis) spectroscopy were used to characterize and investigate the complexes properties. In addition, metal salophen complexes were investigated for the electrocatalytic reduction of carbon dioxide in comparison with copper(II) salen electrocatalyst.

CHAPTER II

THEORY

2.1. Methods of Carbon Dioxide Removal

The emission of greenhouse gases such as carbon dioxide is the main cause of global warming. Many carbon dioxide-removal techniques have been proposed including biological, geochemical, and chemical technologies. One of these methods is carbon dioxide separation and capture. Figure 2.1 summarizes various options for post-combustion carbon dioxide capture. Although these techniques are well-developed, but their equipment complexity, energy consumption, and capital costs are high [36].

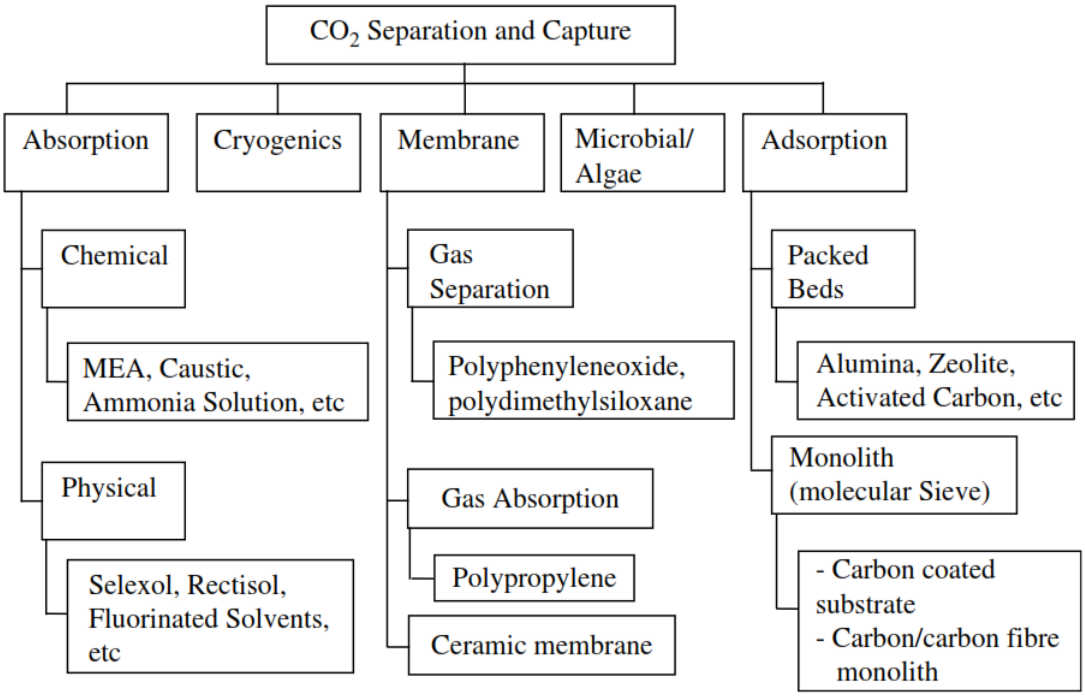

Figure 2.1 Carbon dioxide separation and capture technologies

2.2. Electrochemical Reduction of Carbon Dioxide

Electrochemical techniques have been widely developed to reduce or convert carbon dioxide into more useful products such as carbon monoxide, methane, methanol, and formic acid. Carbon dioxide electro-reduction in non-aqueous solution was suggested the mechanism as shown in Chapter 1 (pp. 2-3). Since electrochemical reduction of carbon dioxide has unfavorable electron transfer kinetics, an effective electrocatalyst is required for electro-reduction of carbon dioxide.

2.3. Electrocatalysis

Electrochemical reaction (reduction or oxidation) can possibly arise at high overpotential due to poor kinetics. This reduction or oxidation needs an electrocatalyst, a catalyst for electrochemical reaction, to improve the reaction rate. Electrocatalysts can be divided into two types which are heterogeneous and homogeneous electrocatalysts [37].

2.3.1. Types of electrocatalysts

2.3.1.1. Heterogeneous electrocatalyst

Heterogeneous electrocatalyst is an electrocatalyst that has different phase from a reactant (substrate). Commonly, it is modified on an electrode surface to help transport electrons between the electrode and substrate. Figure 2.2 exhibits typical example of heterogeneous electrocatalytic system [37]. The electrocatalytic process contains three steps:

(i) A substrate from bulk solution moves to adsorb at the electrode surface ($S_{(bulk)} \longrightarrow S_{(ad)}$).

(ii) Electron exchange occurs between the substrate and the electrode at the immobilized electrocatalyst layer; and

(iii) The product of electron exchange desorbs from the electrode surface and diffuses away into bulk solution ($P_{(ad)} \longrightarrow P_{(bulk)}$).

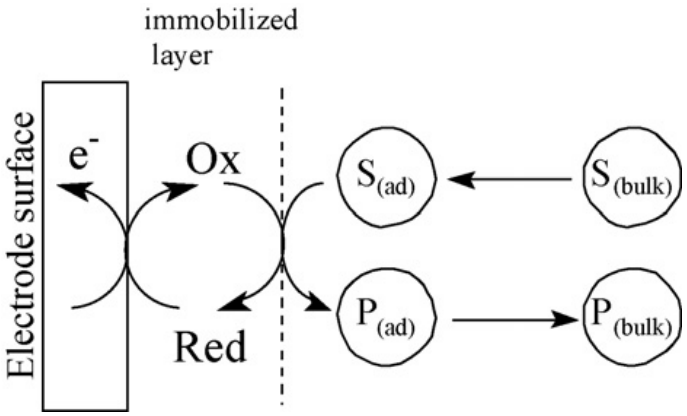

Figure 2.2 Scheme of heterogeneous electrocatalysis

2.3.1.2. Homogeneous electrocatalyst

Homogeneous electrocatalyst is an electrocatalyst that is in the same phase with a reactant (substrate). As shown in Figure 2.3 [37], electron transfer of a substrate cannot occur on the electrode surface directly, but it can take place in the bulk solution via an intermediate or mediator that is in the same phase with the substrate. This mediator can be considered as a homogeneous electrocatalyst.

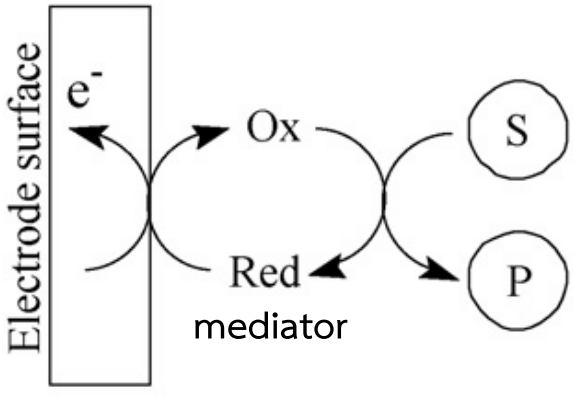

Figure 2.3 Scheme of homogeneous electrocatalysis

2.3.2. Requirements for metal complex electrocatalysts

C. Gosden, *et al*. and J.Y. Becker, *et al*. [38, 39] describe features of a metal complex that can be used as an electrocatalyst.

(i) Metal central atom in the complex gives reversible redox couple peaks for reduction–oxidation process.

(ii) Metal complex electrocatalyst should be either more positively reduced than substrate direct reduction or more negatively oxidized than substrate direct oxidation.

(iii) Regeneration of starting electrocatalyst should be occurred.

(iv) Metal complex should have many turnovers without loss of activity.

2.4. Electrochemical Techniques

2.4.1. Electrochemical system

2.4.1.1. Electrochemical cell

Electrochemical measurement of sample solution is normally performed in a three-electrode cell containing a working electrode, a reference electrode, and an auxiliary electrode (Figure 2.4) [40].

Figure 2.4 An electrochemical cell

2.4.1.1.1. Working electrode

The working electrode is the electrode in an electrochemical system on which the reaction of interest is occurring. Common working electrodes can be made of inert materials such as gold, silver, platinum, glassy carbon as well as mercury drop and film electrodes. The size and shape of the working electrode also varies and depends on the application. The potential of the working electrode is quoted with the reference electrode which provides a stable and reproducible potential.

2.4.1.1.2. Reference electrode

Reference electrode is an electrode which has a stable and well-known electrode potential, and it is used as a point of reference in the electrochemical cell for potential control and measurement. High stability of the reference electrode potential is usually reached by employing a redox system with constant (buffered or saturated) concentration of each participant of the redox reaction. Moreover, the current flow through the reference electrode is kept close to zero (ideally zero) which is achieved by using the auxiliary electrode to close the current circuit in the cell together with a very high input impedance on the electrometer. Silver/silver chloride (Ag/AgCl) reference electrode or saturated calomel electrode (SCE) is commonly used as a reference electrode for the electrochemical measurement in an agueous solution whereas silver/silver ion (Ag/Ag^{+}) reference electrode serves as a reference electrode for the measurement in organic media. For deaeration procedure, gas diffusion tube is used for purging the solution in the electrochemical cell with inert gas (nitrogen or argon) [40].

2.4.1.1.3. Auxiliary electrode

The auxiliary electrode (also known as a counter electrode), is an electrode which is used to complete the current circuit in the electrochemical cell. It is usually made of an inert material and does not interfere with the electrochemical reaction at working electrode. An electrochemically inert material such as a platinum wire or a graphite rod serves as an auxiliary electrode.

2.4.1.2. Solvent and supporting electrolyte

The choice of solvent depends on sample solubility as well as its electrochemical properties including chemical reactivity and electrical conductivity. A solvent should not react with an analyte and other components in a sample. To decrease the solution resistance, eliminate analyte migration, and maintain a constant ionic strength, a supporting electrolyte must be added into a sample solution. Supporting electrolytes can be inorganic salts, organic salts, acids, bases, or buffers. For aqueous system, potassium nitrate, sodium hydroxide, and hydrochloric acid are common examples of supporting electrolytes. In case of non-aqueous system, organic salts whose structures are substituted by alkyl groups to improve solubility in an organic solvent such as tetrabuthylammonium tetrafluoroborate ($TBABF_4$) and tetramethylammonium perchlorate (TMAP) are commonly used as supporting electrolytes. The concentration range of supporting electrolyte is generally 0.10-1.0 M.

2.4.2. Cyclic voltammetry

2.4.2.1. General theory

Cyclic voltammetry [41] is one of the most widely used electrochemical techniques since it provides not only qualitative information, but also quantitative information of electrochemical reactions. Cyclic voltammetry consists of the linearity of scanning potential with a triangular wave form (as shown in Figure 2.5), sweeping over the potential range in forward and backward directions. The potential range depends on whether reduction or oxidation reaction is interested.

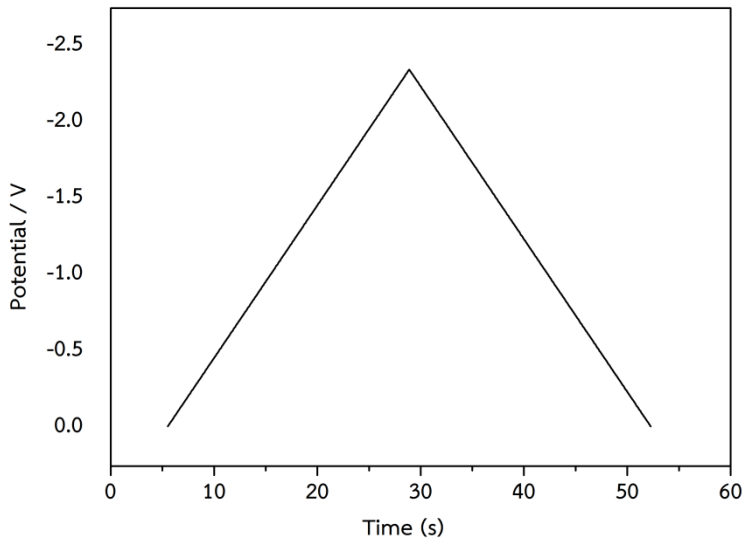

Figure 2.5 Cyclic voltammetric waveform

The obtained current from electrochemical reaction is recorded as a function of the applied potential and a plot between the current and applied potential is called a cyclic voltammogram. The potential is measured between the working electrode and the reference electrode, and the current is measured between the working electrode and the auxiliary electrode. According to Figure 2.6, the obtained data from a cyclic voltammogram are cathodic peak potential (E_{pc}), anodic peak potential (E_{pa}), cathodic peak current (i_{pc}), and anodic peak current (i_{pa}). The cathodic and the anodic peaks can be occurred from the reduction reaction:

$$O + ne^- \rightleftharpoons R$$

where O is the oxidized form and R is the reduced form.

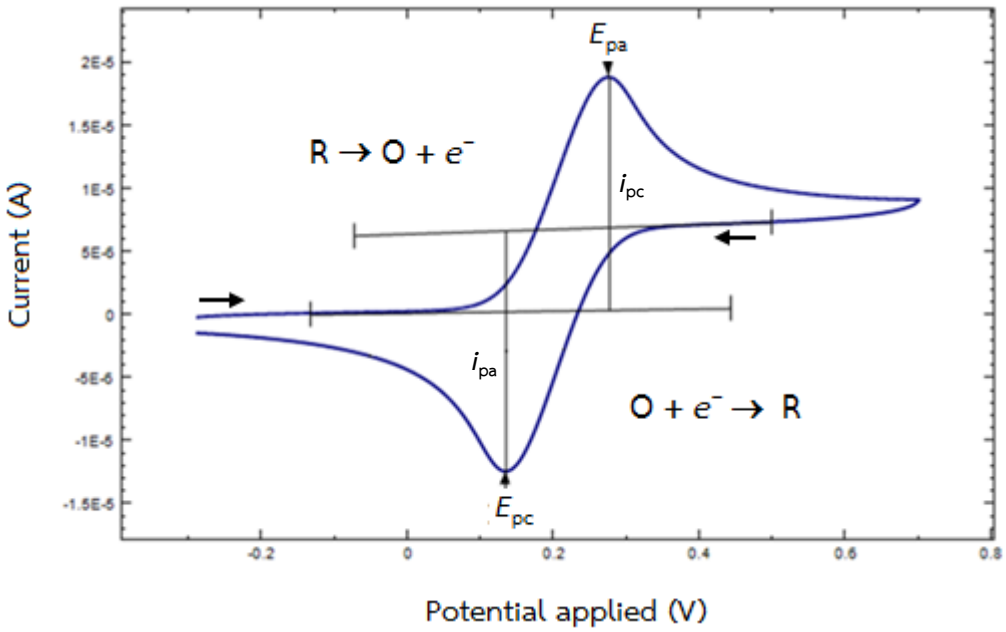

Figure 2.6 A reversible cyclic voltammogram

Cyclic voltammetry can be employed to describe reversibility of any electrochemical reaction.

(i) Reversible system

For a reversible reaction, cathodic and anodic peaks are observed in a cyclic voltammogram and the current ratio between cathodic and anodic peaks is equal to 1. A peak current (i_p) at 25°C is given by Randles–Sevcik equation.

$$i_p = (2.69 \times 10^5)\, n^{3/2} ACD^{1/2} \nu^{1/2} \qquad (2.1)$$

where n is the number of moles of electrons, A is the electrode area (cm^2), C is the concentration ($mol \cdot cm^{-3}$), D is the diffusion coefficient ($cm^2 \cdot s^{-1}$), and ν is the scan rate ($V \cdot s^{-1}$).

The difference of peak potentials (ΔE_p) is related to the number of moles of electron involved in redox reaction. Hence, the possibly involved electrons of redox reaction can be obtained from ΔE_p value of reversible redox couple at 25°C as displayed in equation 2.2.

$$\Delta E_p = E_{pa} - E_{pc} = \frac{0.0592}{n} \text{ V} \qquad (2.2)$$

The half wave potential ($E_{1/2}$) is located at the center between cathodic and anodic peak potential position and is related to the formal potential ($E^{0'}$) as shown in the equation 2.3.

$$E^{0'} \cong E_{1/2} = \frac{E_{pa} + E_{pc}}{2} \qquad (2.3)$$

These equations can be used to determine the number of moles of electrons involved in a redox reaction and other Nernstian behavior. For a reversible system, the peak positions (E_{pc} and E_{pa}) do not change as a function of the scan rate whereas the peak currents are directly proportional to the square root of the scan rate.

(ii) Irreversible system

Due to sluggish electron transfer, a single oxidation or reduction will be observed without reversible peak. The peak position will be altered as a function of scan rate as described in equation 2.4.

$$E_p = E^0 - \frac{RT}{\alpha nF}\left[0.78 - \ln\frac{k^0}{D^{1/2}} + \ln\left(\frac{\alpha nF\nu}{RT}\right)^{1/2}\right] \qquad (2.4)$$

where α is the transfer coefficient and n is the number of electrons involved in the charge-transfer step. Hence, E_p will be obtained at the potential higher than E^0, with the overpotential related to the standard rate constant (k^0) and transfer coefficient. The peak potential and half-peak potential at 25°C will be different from those of reversible system.

The peak current (i_p) is proportional to the bulk concentration and square root of scan rate as the equation 2.5.

$$i_p = \left(2.99\times10^5\right)n(\alpha n)^{1/2}ACD^{1/2}\nu^{1/2} \qquad (2.5)$$

(iii) Quasireversible system

Quasireversible systems have current that is controlled by charge transfer and mass transfer, and exhibit larger separation of peak potentials in comparison with reversible systems.

2.4.3. Controlled-potential electrolysis

Controlled-potential electrolysis employs a large ratio of the electrode area to a volume of solution, and applies a constant potential to allow the reduction or oxidation of all electroactive species. The measured signal corresponds to the current and time as shown in Figure 2.7 [41].

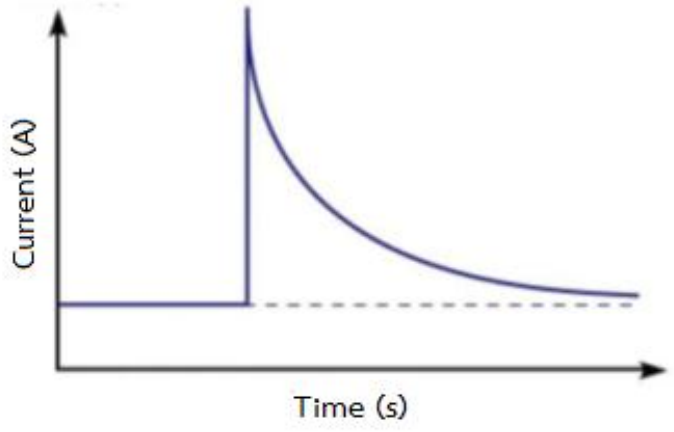

Figure 2.7 Current-time response for controlled-potential electrolysis

Controlled-potential electrolysis uses large surface area working electrode, reference electrode, and auxiliary electrode. An analyte is converted to a new reduced form or oxidized form. When the analyte in the solution is consumed, the current decreases. Product distribution of the electrolysis can be investigated by chromatographic methods. Platinum gauze and reticulated vitreous carbon (RVC) electrodes (Figure 2.8) are normally performed as working electrodes.

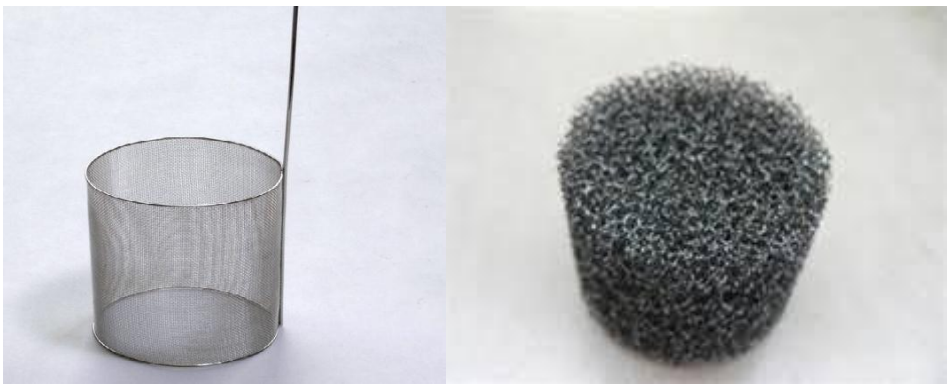

Figure 2.8 Platinum gauze electrode (left) and reticulated vitreous carbon electrode (right) for controlled-potential electrolysis

2.5. Gas Chromatography

Gas chromatography [42] is a commonly used analytical technique in many research and industrial laboratories for quality control as well as identification and quantitation of compounds in mixtures. Samples can be investigated depending on their thermal stability and volatility. A mobile phase and a stationary phase are required for this technique. Mobile phase (or carrier gas) is an inert gas such as helium, argon, or nitrogen whereas the stationary phase is a column which is a pack of solid support as a stationary phase or coated with liquid stationary phase of high boiling polymer. The separation of analyte compounds depends on the different of interaction between the compound and the stationary phase. If the compound has strong interaction with the stationary phase, it will take longer time to migrate through the column giving longer retention time.

The factors of component separation are vapor pressure, polarity of components *versus* the polarity of stationary phase on column, column temperature, carrier gas flow rate, column length, and the amount of material injected.

There are many kinds of gas chromatoghrapic detectors. For instance, flame ionization detector (FID) is a detector which is very sensitive towards organic molecules, but insensitive for a few small molecules, *i.e.*, nitrogen, nitrogen oxides, carbon monoxide, and carbon dioxide. Thermal conductivity detector (TCD) is a

commonly suited for preparative application since it does not destroy sample. The detection signal is based on comparison of two gas streams which are carrier gas and the one containing the compound and carrier gas.

2.6. Characterization Techniques

2.6.1. Nuclear magnetic resonance (NMR) spectroscopy

Nuclear magnetic resonance (NMR) spectroscopy [43] is a powerful relatively non-selective analytical tool which ascertains molecular structure including relative configuration, relative and absolute concentrations, and even intermolecular interactions. The NMR phenomenon is based on the fact that nuclei of atoms have magnetic properties that can be utilized to yield chemical information. Quantum mechanically subatomic particles (protons, neutrons, and electrons) have spin. In some atoms (*e.g.* ^{12}C, ^{16}O, and ^{32}S), these spins are paired and cancel each other out so that the nucleus of the atom has no overall spin. However, in many atoms (^{1}H, ^{13}C, ^{31}P, ^{15}N, and ^{19}F), the nucleus does possess an overall spin. To determine the spin of a given nucleus, one can use the following rules. If the number of neutrons and the number of protons are both even, the nucleus has no spin. If the number of neutrons plus the number of protons is odd, then the nucleus has a half-integer spin (*i.e.*, 1/2, 3/2, and 5/2). If the number of neutrons and the number of protons are both odd, then the nucleus has an integer spin (*i.e.*, 1, 2, and 3). Energy levels for a nucleus with spin quantum number of 1/2 are shown in Figure 2.9.

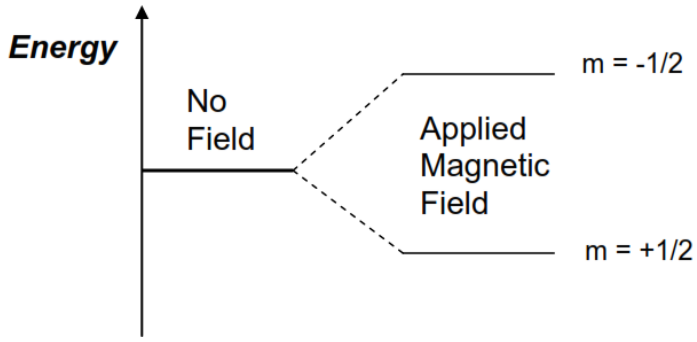

Figure 2.9 Energy levels for a nucleus with spin quantum number of 1/2

2.6.2. Matrix-assisted laser desorption/ionization time-of-flight (MALDI-TOF) mass spectrometry

Matrix-assisted laser desorption/ionization time-of-flight (MALDI-TOF) mass spectrometry [44] has been a popular and useful method to analyze macromolecules. Its general principle involves a rapid photo volatilized sample which is fixed in a UV-absorbed matrix. Matrix will absorb energy from laser source and transfer to molecule of sample to obtain molecular ion. There are many chemical and physical pathways including gas phase photoionization, ion molecule reactions, disproportionation, excited state proton transfer, energy pooling, thermal ionization, and desorption of preformed ions. The molecular ions are induced to a time-of-flight mass spectrometer for analyzing.

2.6.3. Ultraviolet–visible (UV–vis) spectroscopy

In this spectroscopic technique, ultraviolet and visible lights [45] interact with a compound promoting its electron to move from the ground state to the excited state. The ultraviolet region is 190-380 nm whereas the visible region is in the range of 380-750 nm. The outer electron of the molecule is excited from the highest occupied molecular orbital (HOMO) to the lowest unoccupied molecular orbital (LUMO) when the molecule absorbs energy from a light source. The absorbance is directly proportional to the path length (*b)* and the concentration (*c)* of the absorbing species following Beer's Law (equation 2.6).

$$A = \varepsilon bc \qquad (2.6)$$

where ε is a constant of proportionality which is called the absorbtivity.

Different molecules can absorb different wavelengths of radiation source. A number of absorption bands related to structural groups within the molecule will be presented as an absorption spectrum.

2.6.4. X-ray diffraction (XRD) technique

X-ray diffraction (XRD) technique [46] is an efficient technique used for identification and characterization of unknown crystalline materials. When an X-ray beam hits an atom of a solid sample, the electrons around the atom start to oscillate with the same frequency as the incoming X-ray beam. Diffraction beam then occurs when a X-ray beam encounters the sample. It is described as the apparent bending of waves around small samples and the spreading out of waves past small openings. In almost all directions, destructive interference will occur because the combining waves are out of phase and there is no resultant energy leaving the solid sample. However, the atoms in a crystal are arranged in a regular pattern generating constructive interference in a few directions. The combining waves will be in phase causing well defined X-ray beams. Therefore, a diffracted beam may be described as a beam composed of a large number of scattered rays mutually reinforcing one another.

2.6.5. Scanning electron microscopy-energy dispersive X-ray (SEM-EDX) spectroscopy

Scanning electron microscope (SEM) [47] is a type of electron microscope that creates various images by focusing the high energy beam of electrons onto the surface of a sample, and detecting signal from the interaction of the incident electrons with the sample's surface. Three types of signals gathered from a scanning electron microscope are secondary electrons, characteristic X-rays, and back-scattered electrons. In scanning electron microscope, these signals come not only from the primary beam impinging on the sample, but also from other interactions within the sample near its surface. Scanning electron microscope is capable of producing high resolution image of the sample surface in its primary mode, secondary electron imaging. Due to manner in which the images are created, scanning electron microscopic images have great depth of field, yielding a three-dimensional appearance used for understanding the surface structure of a sample. Great depth of field and wide range of magnifications are the most familiar imaging mode for specimens in scanning electron microscopy. Characteristic X-rays are

emitted when the primary beam causes the ejection of inner shell electrons from the sample and they are used to tell the elemental composition of the sample. Emitted from the sample, the back-scattered electrons may be either separately used to form an image or applied in conjunction with the characteristic X-rays as clues to the elemental composition of the sample.

Energy dispersive X-ray spectroscopy [48], also known as EDX, EDS or XEDS, is an analytical technique used for elemental analysis or chemical characterization of a specimen. Being a type of spectroscopy that relies on sample investigation through interaction between electromagnetic radiation and matter, energy dispersive X-ray spectroscopy analyzes the X-ray emitted from the matter in the particular fashion. Its characterization capabilities are large due to the fundamental principle that each element of the periodic table has unique atomic structure, giving distinguishable characteristic X-ray. To stimulate the emission of characteristic X-ray, either the high energy beam of charged particles or the beam of X-ray is focused into a sample. The incident beam may excite an electron in an inner shell of atom within the sample, prompting its ejection that results in the formation of an electron hole within the atom's electronic structure. An electron from an outer, higher energy shell then fills the hole, causing the release of X-ray energy which corresponds to the energy difference between the higher energy shell and the lower energy shell. The released X-ray is then detected and analyzed by energy dispersive spectrometer and can be used as the characteristics of the atomic structure of each element.

CHAPTER III

EXPERIMENTAL

3.1. Chemicals

As summarized in Table 3.1, each of the following chemicals was purchased and used as received.

Table 3.1 List of chemicals

Chemicals	Supplier company (Country)
N,*N*'-bis(salicylidene)ethylenediamine (salen ligand), 98%	Sigma-Aldrich (Germany)
o-Phenylenediamine, 98%	Sigma-Aldrich (Germany)
4-Methyl-*o*-phenylenediamine, ≥98%	Sigma-Aldrich (Germany)
4-Bromo-*o*-phenylenediamine, 97%	Sigma-Aldrich (Germany)
Salicylaldehyde, 98%	Sigma-Aldrich (Germany)
Copper(II) acetate (Cu(II) acetate) monohydrate, 98%	Sigma-Aldrich (Germany)
1,1,1,3,3,3-Hexafluoro-2-propanol (HFIP), 99%	Sigma-Aldrich (Germany)
Tetramethylammonium tetrafluoroborate ($TMABF_4$)	Tokyo Chemical Industry (Japan)
Tetrabuthylammonium tetrafluoroborate ($TBABF_4$)	Tokyo Chemical Industry (Japan)
Acetonitrile (ACN)	RCI Labscan (Thailand)
Dimethylformamide (DMF)	RCI Labscan (Thailand)
Ultra-high purity (UHP) argon, 99.999%	Thai-Japan gas (Thailand)
Ultra-high purity (UHP) nitrogen, 99.999%	Thai-Japan gas (Thailand)
Ultra-high purity (UHP) carbon dioxide, 99.998%	Labgaz (Thailand)

Chemicals	Supplier company (Country)
0.3 μM Alumina micropolish	Alpha (USA)
1.0 μM Alumina micropolish	Alpha (USA)

3.2. Instruments and Apparatus

Instruments and apparatus for electrochemical experiments and other techniques are shown in Table 3.2.

Table 3.2 Instruments and apparatus for electromical experiments

Instruments and Apparatus	Company (Country)
Potentiostat/galvanostat	
– PGSTAT101	Metrohm Autolab B.V. (The Netherlands)
– PARC2273	Princeton Applied Research (USA)
Working electrode	
– Glassy carbon electrode	BAS (USA)
– Reticulated vitreous carbon (RVC)	Energy Research and Generation (USA)
Reference electrode	
– Silver/silver ion (Ag/Ag^+) electrode	BAS (Japan)
Auxiliary electrode	
– Laboratory-made platinum wire	
– Graphite rod	

Instruments and Apparatus	Company (Country)
Other electrochemical apparatus – Glass cell – Laboratory-made glass bridge	
Magnetic stirrer	Metrohm (The Netherlands)
Nuclear magnetic resonance (NMR) spectrometer	Bruker (USA)
Matrix-assisted laser desorption/ionization time-of-flight (MALDI-TOF) mass spectrometer	Bruker (USA)
Ultraviolet–visible (UV–vis) spectrophotometer, HP-8453	Agilent (USA)
X-ray diffractometer (XRD)	Rigaku (USA)
Scanning electron microscope with energy dispersive X-ray (SEM-EDX) spectrometer	JEOL (USA)
Gas chromatograph, 7890A – HP-PLOT molesieve column – HP-FFAP column	Agilent (USA)

3.3. Synthesis and Characterization

3.3.1 Salen-based complex

3.3.1.1 Copper(II) salen

Copper(II) salen was prepared following the procedure in our pervious work (Scheme 3.1) [27]. *N*,*N*′-bis(salicylidene)ethylenediamine (1.002 g, 3.734 mmol) and copper(II) acetate monohydrate (0.758 g, 3.80 mmol) were mixed in ethanol. After leaving at room temperature for 1 h, the green precipitate was obtained. Yield: (93%). MALDI-TOF-MS m/z obsd 329.369 [M^+] (Figure A-1), calcd 329.035 [M=$C_{16}H_{14}CuN_2O_2$]; UV–vis (λ_{abs}, nm) 373 [27]. Results of the characterization

are consistent with previous work in our laboratory [27] and described in the literature [49].

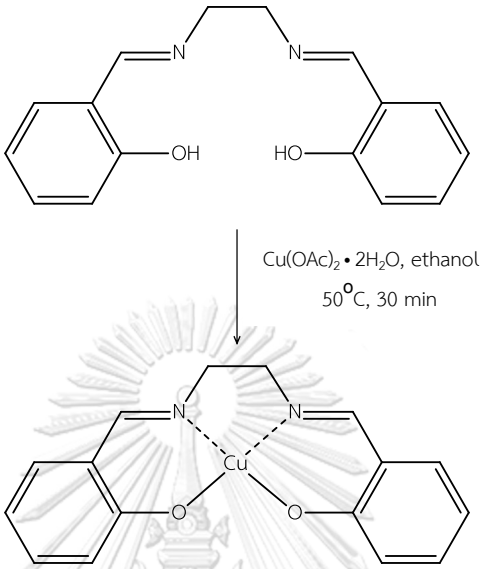

Scheme 3.1 Synthesis of copper(II) salen

3.3.2. Salophen-based complexes

3.3.2.1. Salophen ligand

Adapted from a published procedure [50], salophen was synthesized by mixing 2:1 mol of salicylaldehyde (0.611 g, 5 mmol) and *o*-phenylenediamine (0.270 g, 2.5 mmol) in ethanol solution. After refluxing (40°C) the mixture for 10 h, an orange precipitate was filtered, washed thoroughly with cold methanol, and finally air dried. Yield: (93%). ^{1}H-NMR ($CDCl_3$, δ) 13.00 (2H), 8.60 (2H), 6.70–7.60 (12H) (Figure B-1).; MALDI-TOF-MS m/z obsd 316.443 [M^+], calcd 316.353 [M=$C_{20}H_{16}N_2O_2$]; UV–vis (λ_{abs}, nm) 282, 335. Scheme 3.2 shows the synthesis procedure.

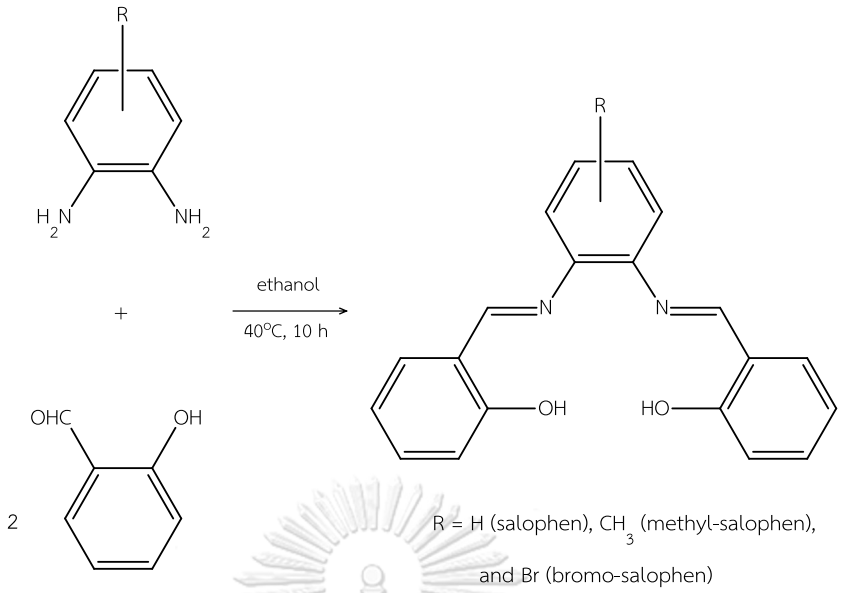

Scheme 3.2 Synthesis of salophen ligand

Salophen derivatives were prepared by a similar method [51]. 4-Methyl-*o*-phenylenediamine (0.305 g, 2.5 mmol) and 4-bromo-*o*-phenylenediamine (0.468 g, 2.5 mmol) were employed instead of *o*-phenylenediamine for the preparation of 4-methyl-*N*,*N*'-disalicylidene-1,2-phenylenediamine (methyl-salophen) and 4-bromo-*N*,*N*'-disalicylidene-1,2-phenylenediamine (bromo-salophen), respectively.

Methyl-salophen: yield (70%); ^{1}H-NMR ($CDCl_3$, δ) 13.20 (2H), 8.80 (2H), 6.80–7.60 (11H), 2.40 (3H) (Figure B-2).; MALDI-TOF-MS m/z obsd 330.497 [M^+], calcd 330.380 [$M=C_{21}H_{18}N_2O_2$]; UV–vis (λ_{abs}, nm) 282, 336.

Bromo-salophen: yield (90%); ^{1}H-NMR ($CDCl_3$, δ) 12.85 (1H), 12.74 (1H), 8.61 (2H), 6.92–7.46 (11H) (Figure B-3).; MALDI-TOF-MS m/z obsd 396.722 [M^+], calcd 395.249 [$M=C_{20}H_{16}N_2O_2$]; UV–vis (λ_{abs}, nm) 274, 337.

3.3.2.2. Copper(II) salophen

Copper(II) salophen and derivatives were prepared using the same procedure as copper(II) salen synthesis (Section 3.3.1.1), but required longer reflux time and using different ligands as shown in Scheme 3.3 [51]. The brownish green precipitates were obtained after refluxing the mixtures for 10 h.

Copper(II) salophen: yield (75%); MALDI-TOF-MS m/z obsd 377.748 [M^+], calcd 377.883 [M=$C_{20}H_{14}CuN_2O_2$]; UV–vis (λ_{abs}, nm) 307, sh 341.

Copper(II) methyl-salophen: yield (57%); MALDI-TOF-MS m/z obsd 391.722 [M^+], calcd 391.910 [M=$C_{21}H_{16}CuN_2O_2$]; UV–vis (λ_{abs}, nm) 308, sh 347.

Copper(II) bromo-salophen: yield (65%); MALDI-TOF-MS m/z obsd 458.010 [M^+], calcd 456.779 [M=$C_{21}H_{16}CuN_2O_2$]; UV–vis (λ_{abs}, nm) 309, 427.

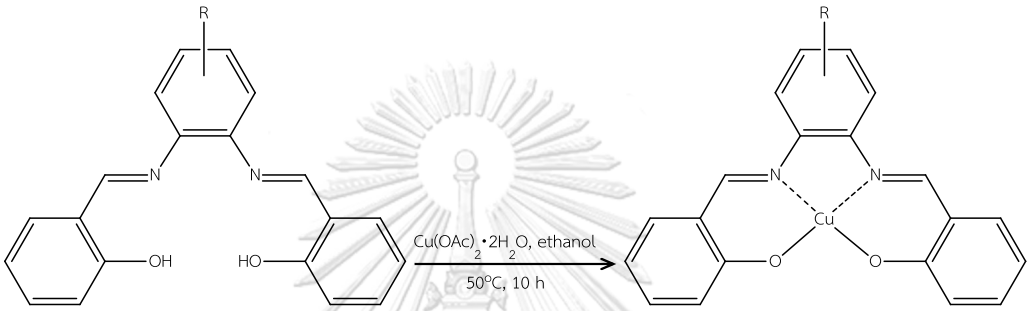

Scheme 3.3 Synthesis of copper(II) salophen and derivatives

3.3.3. Characterization

3.3.3.1. Nuclear magnetic resonance (NMR) spectroscopy

The NMR spectra of salophen-based ligands were recorded in deuterated chloroform ($CDCl_3$) with the frequency of 400 Hz.

3.3.3.2. Ultraviolet–visible (UV–vis) spectroscopy

Each ligand or complex was dissolved in DMF and recorded its UV–vis spectra in the wavelength range of 200–800 nm.

3.3.3.3. Matrix-assisted laser desorption/ionization time-of-flight (MALDI-TOF) mass spectrometry

Small amount of a mixture of ligand or metal complex with dithranol was dissolved in methanol and pasted on MALDI-TOF sample cell. The obtained molecular ion peak [M^+] was compared with the calculated value.

3.4. Electrochemical Procedures

3.4.1. Preparation of electrolyte solution

3.4.1.1. Tetramethylammonium tetrafluoroborate ($TMABF_4$) solution (0.050 M)

$TMABF_4$ (0.8025 g) was dissolved in acetonitrile (100 mL) to obtain a 0.050 M $TMABF_4$ electrolyte solution. This solution was used in the preparation of silver/silver ion (Ag/Ag^+) reference electrode. Before use, $TMABF_4$ was purified by recrystallization from water–methanol and then water. After that, it was filtered, dried, and stored overnight in an oven at 80°C [52].

3.4.1.2. Tetrabutylammonium tetrafluoroborate ($TBABF_4$) solution (0.10 M)

$TBABF_4$ was used as a supporting electrolyte for metal salen-based electrocatalytic systems. $TBABF_4$ was stored at 80°C in an oven before use. $TBABF_4$ (3.2870 g) was dissolved in DMF (100 mL) to gain a 0.10 M electrolyte solution.

3.4.2. Preparation of ligand and metal complex solutions

Calculated amount of the ligand or metal complex was dissolved in freshly prepared electrolyte solution to obtain 2.0 mM of ligand or metal complex solution.

3.4.3. Cyclic voltammetry

Electrocatalytic studies were acquired by means of cyclic voltammetry using a potentiostat/galvanostat. An electrochemical cell containing three-electrode configuration was used throughout this work.

3.4.3.1. Working electrode

A glassy carbon electrode was employed as a working electrode. It was polished with 1.0 and 0.3 μM alumina slurries, washed by Milli-Q water, and dried in air prior to use each time.

3.4.3.2. Reference electrode

Silver/silver ion (Ag/Ag^{+}) in acetonitrile solution containing a 0.05 M $TMABF_4$ was quoted as a reference electrode. This electrode has a potential of 0.298 V *vs*. saturated calomel electrode (SCE) [52].

3.4.3.3. Auxiliary electrode

A laboratory-made platinum wire was employed as an auxiliary electrode to complete the electrochemical circuit.

3.4.3.4. Cyclic voltammetric procedures

Cyclic voltammetric measurements were recorded with a freshly polished glassy carbon electrode at the scan rate of 100 $mV \cdot s^{-1}$. The studied solution was purged and saturated with inert gas (argon or nitrogen) or carbon dioxide before its cyclic voltammograms were recorded. Precentage of cathodic current enhancement of each electrocatalyst was calculated and compared according to equation 3.1.

$$\text{Cathodic current increase (\%)} = \frac{i_{pc} \text{ in carbon dioxide}}{i_{pc} \text{ in argon}} \times 100 \qquad (3.1)$$

where i_{pc} is cathodic peak current.

3.4.4. Controlled-potential electrolysis

Controlled-potential electrolysis experiment was carried out in one-compartment cell with a reticulated vitreous carbon [52] as a working electrode, a graphite rod as an auxiliary electrode, and Ag/Ag^{+} as a reference electrode. Controlled-potential electrolysis was performed under stirring condition for the electro-reduction of 2.0 mM copper(II) salen in DMF containing 0.1 M $TBABF_4$ under saturated nitrogen and saturated carbon dioxide at the applied potential where the electro-reduction of carbon dioxide can occur. Before carbon dioxide purge, the electrolyzed solution was saturated with nitrogen gas. Product distribution of the electro-reduction of carbon dioxide was probed by means of gas chromatography. HP-PLOT molesieve and HP-FFAP columns were employed for the product investigation of gas phase and liquid phase, respectively.

Percentage of composition of post-electrolysis from gas chromatography was calculated according to equation 3.2.

$$\text{Post-electrolysis composition (\%)} = \frac{\text{mol of the obtained composition}}{\text{mol of } CO_2 \text{ before electrolysis}} \times 100 \qquad (3.2)$$

Mole of gaseous product can be calculated using equation 3.3.

$$PV = nRT \qquad (3.3)$$

where V (volume of gas) was calculated from the calibration curve between peak area and injection volume of the standard gas, R is a gas constant (0.08205 $dm^3 \cdot atm \cdot mol^{-1} \cdot K^{-1}$), T is the temperature of the gas (in K), and P is the pressure of the gas (in atm).

In addition, the Faradaic efficiency (FE) and turnover number (TON) were calculated according to equations 3.4 and 3.5, respectively [53, 54]

$$\text{Faradaic efficiency (\%)} = \frac{\text{charge to form the product}}{\text{total charge passed}} \times 100 \qquad (3.4)$$

$$\text{Turnover number (TON)} = \frac{\text{mol of product}}{\text{mol of catalyst}} \times 100 \qquad (3.5)$$

Furthermore, the morphological and structural information of the copper complex-coated reticulated vitreous carbon disks were studied by X-ray diffraction (XRD) analysis recording on a diffractometer (RIGAKU DMAX 2200, USA) at 40 kV and 100 mA with Cu K**α** radiation (**λ**=1.5406 Å). Scanning electron microscopy-energy dispersive X-ray (SEM-EDX) spectroscopy was utilized to observe the images and elemental composition of the copper salen-coated reticulated vitreous carbon disks. JEOL JSM-5410 instrument operating at an electron-accelerating voltage of 15 keV was employed for this analysis.

CHAPTER IV
RESULTS AND DISCUSSION

4.1. Salen-based Complex

4.1.1. Synthesis and characterization of copper(II) salen

Copper(II) salen were obtained in 93% by a reaction between *N*,*N*′-bis(salicylidene)ethylenediamine (salen) and copper(II) acetate monohydrate. This complex was characterized by means of UV–vis spectroscopy and MALDI-TOF mass spectrometry. The absorption spectrum was found at 373 nm corresponding to $\pi^* \rightarrow$ d transitions. For MALDI-TOF mass spectrometric analysis, the observed molecular ion peak of copper(II) salen are consistent with the calculated ones, indicating that copper(II) salen were successfully synthesized. The aboved-mentioned results are consistent with previous work in our laboratory [27].

4.1.2. Electrocatalytic reduction of carbon dioxide by electrogenerated copper(I) salen

Previously our laboratory had investigated salen-based complexes as electrocatalysts for electro-reduction of carbon dioxide in dimethylformamide (DMF) [27]. It was clear that copper(I) salen has a tendency to be an efficient electrocatalyst. As shown in Figure 4.1, cyclic voltammograms of copper(II) salen in the presence and absence of carbon dioxide confirm that carbon dioxide can be electrocatalytic activated by eletrogenerated copper(I) salen. With carbon dioxide (dashed line), a 100-mV positive shift of cathodic peak potential from –1.62 V to –1.56 V, a disappearance of copper(I)-to-copper(II) salen re-oxidation peak, and the presence of new and extremely large cathodic peak were found. This information had already been described in the previous work.

A among the salen-based complexes, copper(II) salen gave the highest percentage of cathodic current enhancement for the electrocatalytic reduction of

carbon dioxide (Table C-1). Hence, this research chose copper(II) salen for electrocatalysis of carbon dioxide reduction.

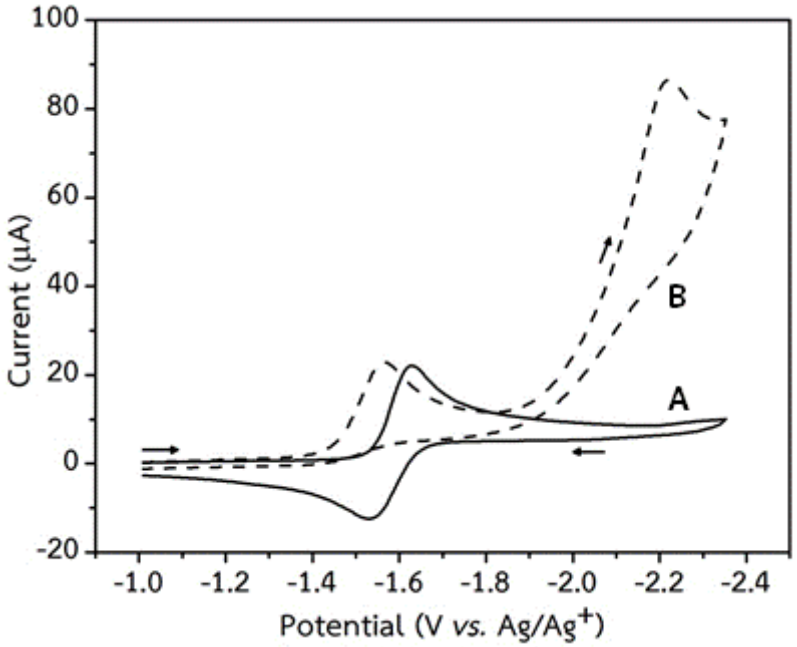

Figure 4.1 Cyclic voltammograms recorded with a glassy carbon electrode at 100 $mV \cdot s^{-1}$ for DMF solution containing 0.10 M $TBABF_4$ in the presence of 2.0 mM copper(II) salen saturated with (A) argon and (B) carbon dioxide

4.1.3. Effect of proton donors on electrocatalytic reduction of carbon dioxide

Due to small pi-conjugated structure of copper(II) salen and insufficiency of protons to catalyze carbon dioxide reduction into valuable products, copper(II) salen can possibly be activated by water and other proton donors. It was found that water can significantly increase the size of the cathodic current for carbon dioxide reduction and can shift the cathodic peak potential towards more positive values. However, cathodic current for carbon dioxide reduction did not increase at high water concentrations (Figure C-1) [27]. Hence, 1.0 M water was added into 2.0 mM copper(II) salen solution when controlled-potential electrolysis of carbon dioxide and copper(II) salen was conducted. Since copper(II) salen were partially transformed by water [55], water was not chosen to improve the electro-catalytic

properties of copper(II) salen for carbon dioxide reduction by means of controlled-potential electrolysis.

In this work, 1,1,1,3,3,3-hexafluoro-2-propanol or hexafluoroiso-propanol (HFIP) was used as a proton donor. HFIP is an acidic alcohol which can be miscible in both water and organic solvent, and commonly used as a proton donor to ascertain the effect of the proton donor in non-aqueous system [56]. The results in previous research [27] revealed that in the presence of HFIP, the cathodic current is higher and peak potential shifts positively (Figure C-2). The increase of the cathodic current with proton donor quantity increase was found. Therefore, the optimization of HFIP quantity and other parameters were accomplished to improve electrocatalytic activity of copper(II) salen for carbon dioxide reduction in bulk electrolysis.

4.1.4. Controlled-potential electrolysis of copper(II) salen in the presence of carbon dioxide

Since copper(II) salen showed the highest cathodic current for electro-reducton of carbon dioxide, bulk electrolysis of carbon dioxide by electrogenerated copper(I) salen was studied using various applied potentials and HFIP quantities. Product distribution for the electrocatalytic reduction of carbon dioxide was investigated by gas chromatographic method. Calibration series of gases by means of gas chromatography are shown in Figure 4.2. High purity carbon dioxide, carbon monoxide, and methane were separately injected into gas chromatograph in nine injection volumes to obtain the calibration plots. The correlation coefficient (r^2) values (0.9950-0.9980) express acceptable linearity of the calibration plot between injection volume and peak area. The calibration curves are further used to calculate percentages of product distribution in gas phase from bulk electrolysis.

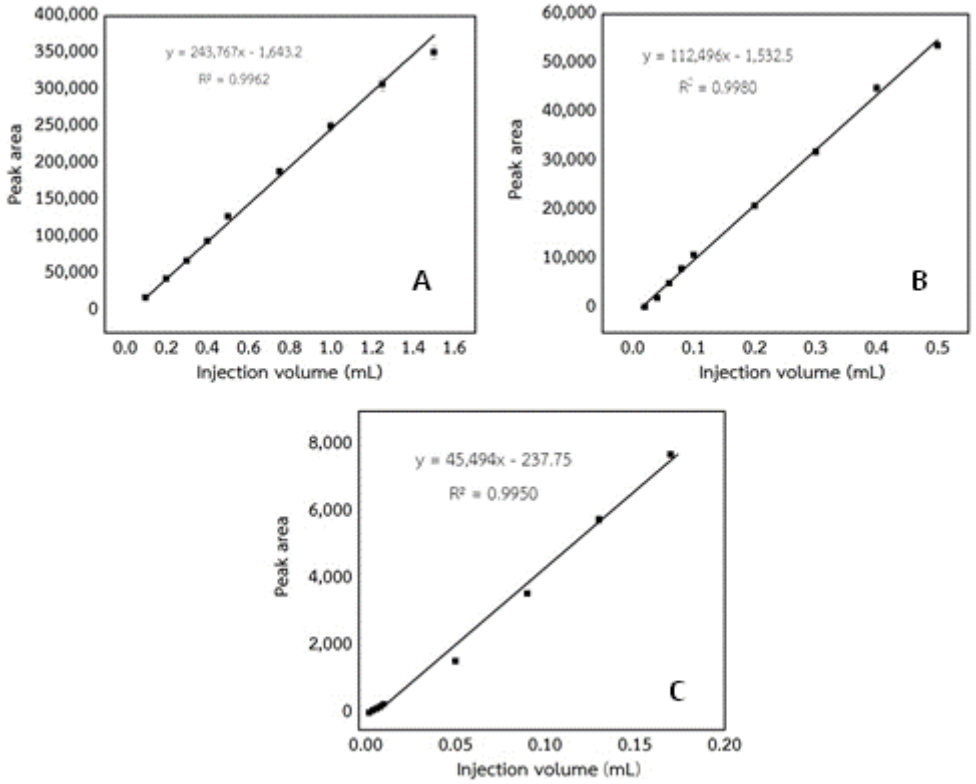

Figure 4.2 Calibration curves of (A) carbon dioxide, (B) carbon monoxide, and (C) methane by means of gas chromatography

Figure 4.3, which are chromatograms of pre- and post-electrolysis of 2.0 mM copper(II) salen in DMF containing 0.10 M $TBABF_4$ and 25.00 mM HFIP with saturated carbon dioxide, reveals the peaks of carbon monoxide and methane as the electrolysis products.

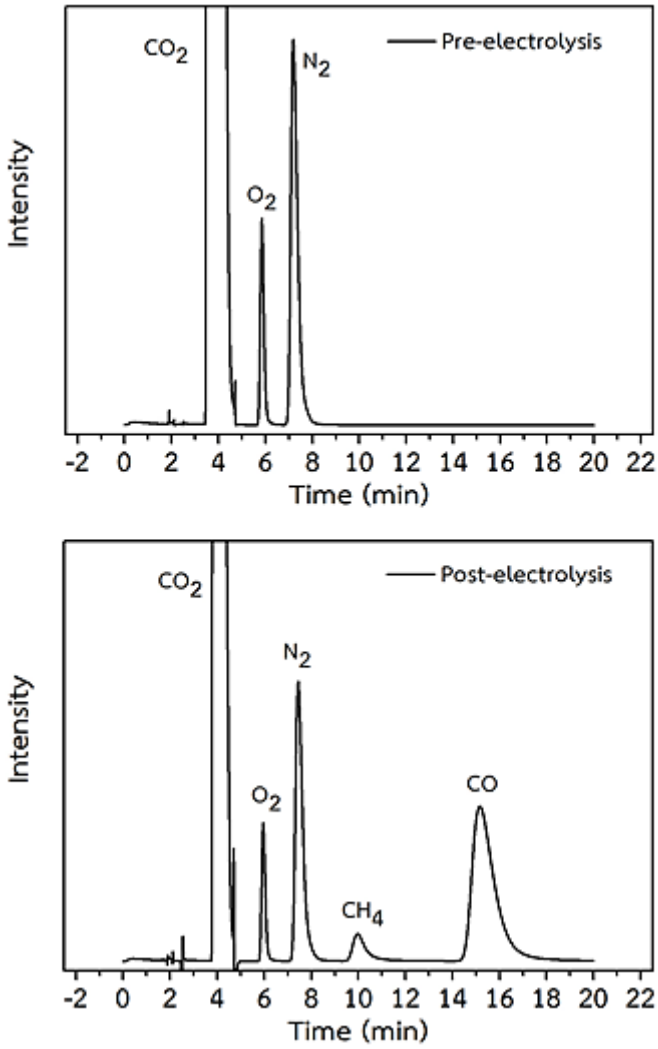

Figure 4.3 Gas chromatograms for headspace samples of pre- and post-electrolysis of 2.0 mM copper(II) salen in DMF/0.10 M $TBABF_4$ with 25.00 mM HFIP under saturated carbon dioxide

4.1.4.1. Opimization of the applied potential

Controlled-potential reduction of carbon dioxide with electrogenerated copper(I) salen, salen legand, and no electrocatalyst was performed in DMF containing 0.10 M $TBABF_4$ at reticulated vitreous carbon (RVC) working electrode at the various applied potentials including –1.60 V corresponding to the half peak potential of copper(II) salen/copper(I) salen redox couple, and –2.00 V and –2.10 V attributing to the onset potential and half peak potential where the

current is half of the cathodic peak current for carbon dioxide reduction, respectively. During the electrolysis, the solution color changed from turquoise of copper(II) salen to brown-greenish of copper(I) salen, and finally to light brown green, revealing the possibility of electrocatalyst modification. Further investigation about this phenomenon will be discussed.

Gas phase of the electrolysis was taken and analyzed by means of gas chromatography. As seen in Table 4.1, only carbon monoxide was observed as a product of the electrocatalytic reduction of carbon dioxide. The highest carbon monoxide amount (3.50 ± 0.04%) was obtained from controlled-potential electrolysis of copper(II) salen at –2.10 V (Example of the electrolysis chronoamperogram is shown in Figure C-3). Small amount of carbon monoxide and no carbon monoxide were obtained from controlled-potential electrolyses with salen ligand and without electrocatalyst, respectively (The chronoamperograms are displayed in Figures C-4 and C-5, respectively). This result indicates that the electrocatalyst choice and the applied potential play key roles in promoting electro-reduction of carbon dioxide. Nevertheless, since methane was found in the presence of HFIP, this research is planned to examine the role of HFIP proton donor and optimize the electrocatalytic system to gain higher percentage yields of products.

Table 4.1 Product distribution for electro-reduction of carbon dioxide in DMF containing 0.10 M $TBABF_4$ with 2.0 mM electrocatalysts

Electrocatalyst	Applied potential (V)	Gaseous composition of post-electrolysis (%)[a]			
		CO_2	CO	CH_4	Total
Copper(II) salen	–1.60	97.12 ± 0.00	1.33 ± 0.00	–	98.45 ± 0.00
Copper(II) salen	–2.00	86.76 ± 0.01	1.36 ± 0.00	–	88.12 ± 0.01
Copper(II) salen	–2.10	81.58 ± 0.04	3.50 ± 0.04	–	85.08 ± 0.02
Salen	–2.10	96.22 ± 0.02	1.22 ± 0.00	–	97.44 ± 0.02
–	–2.10	98.64 ± 0.01	–	–	98.64 ± 0.01

[a] Each entry represents the average of three set of experiments.

%RSD is below 3.00 for each entry.

4.1.4.2. Opimization of proton donor quantity

Figure 4.4 shows the percentages for gaseous composition obtained from electro-reduction of carbon dioxide at the potentials of –2.00 V and –2.10 V using copper(II) salen in the presence of 0-50 mM HFIP. It can be seen that the main gaseous products of carbon dioxide electro-reduction are carbon monoxide and methane. The electrolyses at –2.10 V resulted in larger percentages of products than those of –2.00 V. In the case of the electrolyses at –2.10 V, 25.00 mM HFIP provided highest product yields 16.30 ± 0.00% of carbon monoxide and 0.39 ± 0.00% of methane (Figure 4.4B). In the case of the electrolyses at –2.00 V, highest product yields were also obtained with 25.00 mM HFIP, but at lower percentages (0.18 ± 0.00% of methane and 3.44 ± 0.00% of carbon monoxide (Figure 4.4A). Figures C-6 and C-7 display i-t curves for the electrolyses at –2.00 V and –2.10 V with 25.00 mM HFIP, respectively. Hence, 25.00 mM HFIP is the optimized quantity of HFIP when 2.0 mM copper(II) salen is used to electrochemically reduce carbon dioxide.

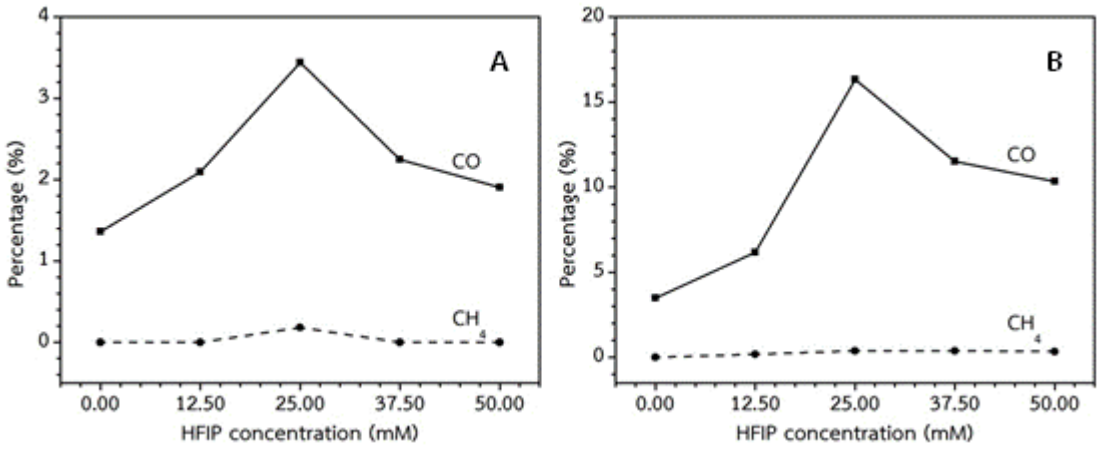

Figure 4.4 Gaseous product distribution obtained from electro-reduction of carbon dioxide using copper(II) salen in the presence of various HFIP concentrations with the applied potentials of (A) –2.00 V and (B) –2.10 V

Using the optimized applied potential and HFIP quantity, the experiments were carried out with the salen ligand and without electrocatalyst for comparison. Table 4.2 shows product distribution for the electrolyses at –2.10 V of

carbon dioxide with copper(II) salen and salen, and without electrocatalyst in the presence of 25.00 mM HFIP. It can be seen that the copper(II) complex gave the highest percentages of products (carbon monoxide and methane) from carbon dioxide electro-reduction, and methane was only found in the presence of copper(II) salen, indicating that copper ion in the salen ligand plays an important role in catalyzing of carbon dioxide electro-reduction.

Table 4.2 Product distribution for electro-reduction at –2.10 V of carbon dioxide in DMF containing 0.10 M $TBABF_4$ with 2.0 mM electrocatalyst and 25.00 mM HFIP

Electrocatalyst	Gaseous composition of post-electrolysis (%)[a]			
	CO_2	CO	CH_4	Total
Copper(II) salen	62.00 ± 0.02	16.30 ± 0.00	0.39 ± 0.00	78.69 ± 0.02
Salen	95.28 ± 0.00	1.21 ± 0.00	–	96.50 ± 0.00
–	97.83 ± 0.01	–	–	97.83 ± 0.01

[a] Each entry represents the average of three set of experiments.
%RSD is below 3.00 for each entry.

4.1.4.3. Faradaic efficiency and turn over number

To determine faradaic efficiency (FE), accumulated charges of the electrolyses for the electro-reduction of carbon dioxide using copper(II) salen at –2.10 V were analyzed. The chronoamperograms used in this calculation are shown in Figures C-3 and C-7. In addition, the turn over numbers (TONs) of the electrolyses were calculated. Table 4.3 shows the faradaic efficiency and turn over number of the carbon dioxide reduction products. In the presence of 25.00 mM HFIP, the faradaic efficiency for carbon monoxide is 16.65 ± 0.86% and that of methane is 1.58 ± 0.06%. However, due to the fact that the total charges of the electrolyses with

Table 4.3 Electrolysis data for the obtained products from electrocatalytic reduction of carbon dioxide at –2.10 V with copper(II) salen in the presence and absence of 25.00 mM HFIP. Each entry represents the average of three set of experiments

Condition	Charge (C)	FE (%)		TON	
		CO	CH_4	CO	CH_4
with HFIP	233.88 ± 2.00	16.65 ± 0.86	1.58 ± 0.06	5.04 ± 0.22	0.12 ± 0.00
without HFIP	43.19 ± 1.04	21.37 ± 4.71	–	1.19 ± 0.25	–

HFIP are higher that those with no HFIP, the obtained faradaic efficiency for carbon monoxide is less than that in the absence of HFIP. For turn over numbers for the electrolysis products, it was found that the turn over number for carbon monoxide from the electrolysis with HFIP is about 5 which it is five times higher than that of electrolysis without HFIP, whereas the turn over number for methane from the electrolysis with HFIP has a value of 0.12 ± 0.00. Table 4.4 compares faradaic efficiency of this work with those of other copper-based electrocatalysts for the electro-reduction of carbon dioxide. It can be seen that this work has gas-phase products similar to other works using copper electrodes in non-aqueous systems [57, 58]. Although the faradaic efficiency of carbon monoxide in this work is lower than that in propylene carbonate (PC) [57], methane was additionally found. These data suggest the capability of copper(II) salen as an electrocatalyst for the electro-reduction of carbon dioxide. Moreover, in comparison with results of aqueous media using different copper-based electrocatalysts [59-62], copper(II) salen in this work gave faradaic efficiency of methane lower than most of the reported copper-based electrocatalysts. Some work [58, 59, 61, 62] also found other products such as formic acid and ethylene. Nevertheless, since this research only detected gas-phase products, the detection of liquid-phase product(s) will be practiced to gain more insightful information about the efficiency of copper(II) salen for carbon dioxide reduction.

Table 4.4 Product comparison with other copper-based electrocatalysts for carbon dioxide electro-reduction

Electrocatalyst	Electrolyte solution	Product(s) (FE%)	Reference
Copper(II) salen	0.10 M $TBABF_4$–DMF and 25.00 mM HFIP	CH_4 (1.58%) and CO (16.65%)	This work
Copper electrode	0.10 M TEAP–PC	CO (70%)	[57]
Copper electrode	0.05 M CH_3COOK–MeOH	CH_4 (8.6%), CO (5.4%), and HCOOH (13.1%)	[58]
Copper electrode	0.10 M $KHCO_3$	CH_4 (18%), C_2H_4 (18%), CO, and HCOOH	[59]
Copper nanoparticles	0.10 M $NaHCO_3$	CH_4	[60]
Copper oxide/copper	0.10 M $KHCO_3$	CH_4 (7%), C_2H_4 (12%), CO, and HCOOH	[61]
Copper phthalocyanine	0.10 M $KHCO_3$	CH_4 (30%), CO, and HCOOH	[62]

4.1.4.4. Investigation of repeatability uses of copper(II) salen electrocatalyst

Since there was some species deposited on RVC disk after the carbon dioxide–copper(II) salen electrolysis, the ability for electrocatalytic reduction of the used RVC disk was investigated by repeatedly employing the used RVC disk for carbon dioxide reduction without the addition of copper(II) salen in the presence and

absence of HFIP as shown in Table 4.5. In total, three electrolyses were conducted using the same RVC disks. In the presence of HFIP, the increase in percentage of methane was found when using RVC disk after the first electrolysis of copper(II) salen in carbon dioxide whereas the carbon monoxide amount decreased, suggesting that the used RVC disk can catalyze the carbon dioxide electro-reduction. After that, the same RVC disk was reused for the third electrolysis and it was found that the percentages of both methane and carbon monoxide decreased. In the absence of HFIP, no methane was found for all three electrolyses.

Table 4.5 Product distributions for the electrocatalytic reduction of carbon dioxide at –2.10 V in DMF containing 0.10 M $TBABF_4$

Electrocatalyst	HFIP (mM)	Gaseous composition of post-electrolysis (%)			
		CO_2	CO	CH_4	Total
Copper(II) salen with new RVC (1st electrolysis)	–	80.48	3.80	–	84.28
Used RVC (2nd electrolysis)	–	74.31	7.96	–	82.26
Used RVC (2nd) (3rd electrolysis)	–	82.97	7.14	–	90.11
Copper(II) salen with new RVC (1st electrolysis)	25.00	62.00 ± 0.02	16.30 ± 0.00	0.39 ± 0.00	78.69 ± 0.02
Used RVC (2nd electrolysis)	25.00	61.02 ± 0.00	7.47 ± 0.01	0.73 ± 0.00	69.22 ± 0.13
Used RVC (2nd) (3rd electrolysis)	25.00	73.44 ± 0.00	5.47± 0.00	0.39 ± 0.00	79.30 ± 0.02

After we found that the species deposited on RVC disks can electrochemically catalyze the electro-reduction of carbon dioxide, the structure and morphology of the deposited species were probed. Figure 4.5 shows XRD patterns of bare RVC disk, and RVC disks after the electrolysis of carbon dioxide with copper(II) salen at –2.10 V in the absence and presence of HFIP proton donor. Two peaks at 2θ values of 21.6 and 43.6 degrees which correspond to the plane (002) and (101) of graphite [63, 64] were found in all RVC disks. The peaks of face centered cubic (FCC) copper at 2θ of 43.64 and 50.80 degrees (corresponding to plane (111) and (200) [65]) appeared for all RVC disks after the electrolysis with copper(II) salen. These results confirmed the deposition of copper on RVC disks via the electrolysis of carbon dioxide with copper(II) salen and suggest that the deposited copper(II) salen for the electro-reduction of carbon dioxide and the deposited copper on RVC disks can also catalyze the carbon dioxide reduction. On the other hand, the formation of copper on the RVC may represent the low stability of copper(II) salen electrocatalyst.

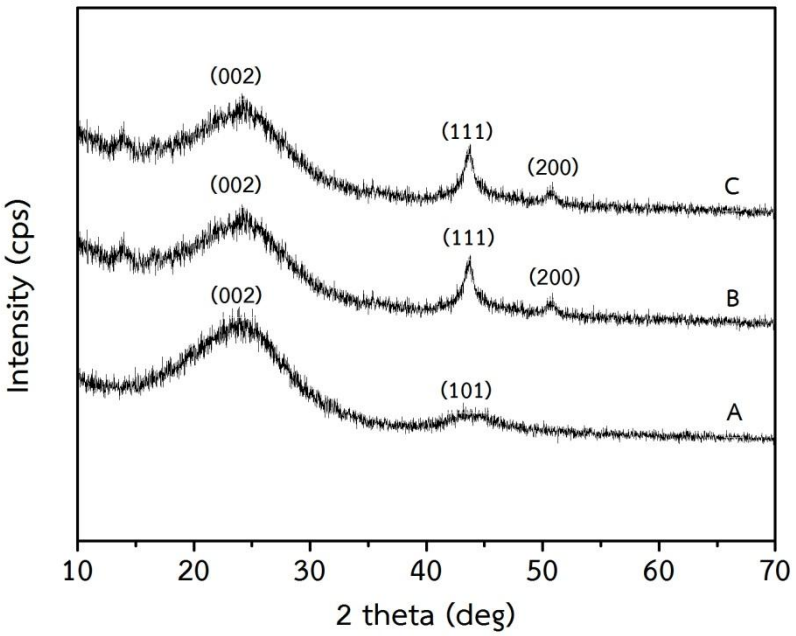

Figure 4.5 XRD patterns of (A) bare reticulated vitreous carbon disk; and reticulated vitreous carbon disks after the electrolysis of carbon dioxide and copper(II) salen at –2.10 V with (B) 0 mM HFIP and (C) 25.00 mM HFIP

Figure 4.6 exhibits scanning electron micrographs of bare RVC disk, and RVC disks after the carbon dioxide electrolysis with copper(II) salen at –2.10 V in the absence and presence of HFIP. In contrast to the smooth and uniform nature of the bare RVC disk material (Figure 4.6A), the RVC disk after the electrolysis in the absence of HFIP proton donor (Figure 4.6B) shows somewhat uniform distribution of copper on the RVC surface. Earlier publications have reported similar observations with copper deposition on bare RVC [66, 67]. As illustrated in Figure 4.7A, scanning electron microscopy-energy dispersive X-ray (SEM-EDX) spectroscopy mapping images support the existence of the copper metal on the RVC disk since carbon, oxygen, and copper are uniformly detected after the elcctrolysis. Figure 4.6C, the SEM image of the RVC disk after the electrolysis with HFIP, reveals that the previously observed structure of the RVC disk after the electrolysis without HFIP (Figure 4.6B) is present, yet the deposited material appears inflated and smoother. SEM-EDX mapping images of this RVC (Figure 4.7B) also indicate the presence of carbon, oxygen, and copper.

To determine the elemental compositions of both copper-coated disks, EDX spectra were obtained (Figure 4.8) and the percentages of all elements are summarized in Table 4.6. For the RVC disks after electrolysis of copper(II) salen in the absence and presence of proton donor, copper was found due to the change of electrogenerated copper(I) salen to copper(0) deposited on RVC surface. The conveniently deformation of copper ions to copper metal presents the stability issue of copper(II) salen, leading to the investigation of copper(II) salen derivatives as electrocatalysts for carbon dioxide electro-reduction. In the case of bare RVC, sulfur was observed in 0.11% and can be considered as a impurity of RVC disk [68].

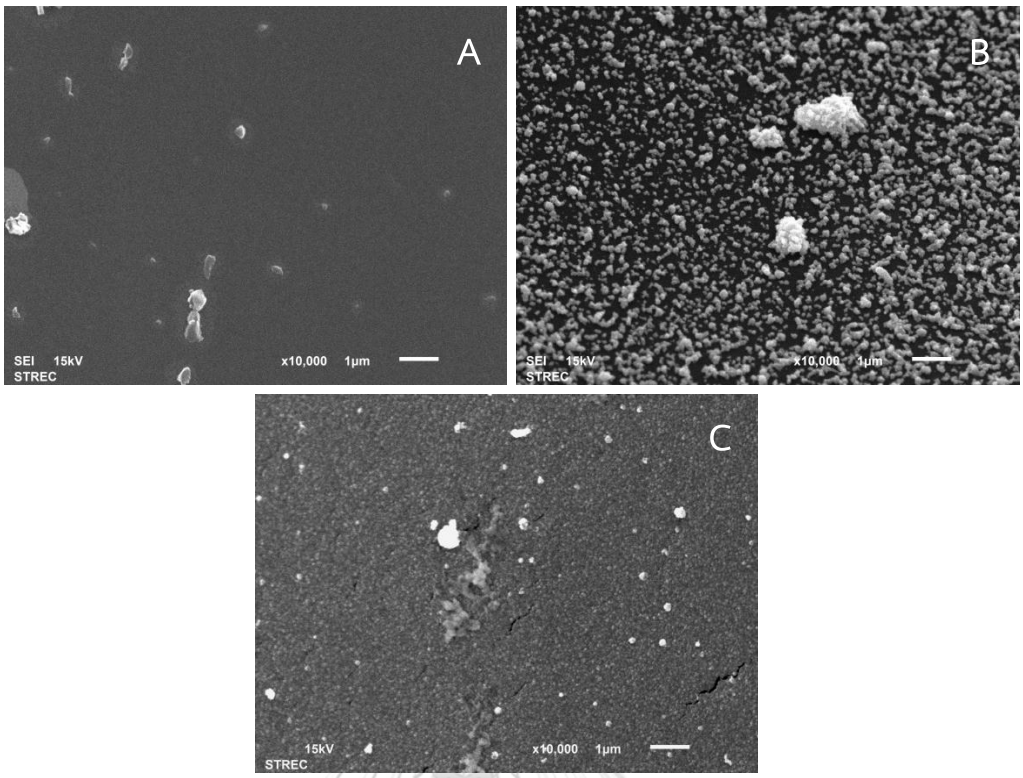

Figure 4.6 Scanning electron micrographs (10,000 X magnification) for (A) bare reticulated vitreous carbon disk; and reticulated vitreous carbon disk after the electrolysis of carbon dioxide and copper(II) salen at –2.10 V with (B) 0 mM HFIP and (C) 25.00 mM HFIP

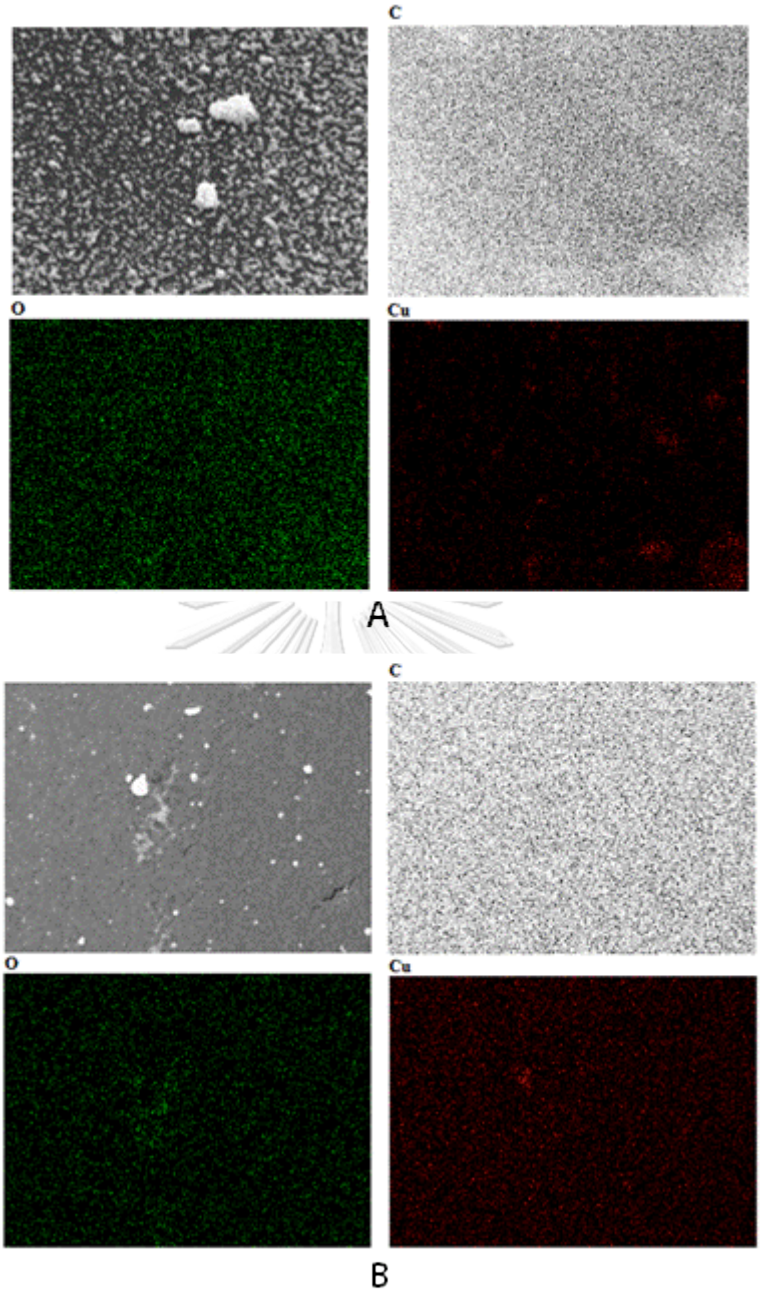

Figure 4.7 SEM-EDX mapping images (10,000 X magnification) for reticulated vitreous carbon disks after the electrolysis of carbon dioxide and copper(II) salen at –2.10 V with (A) 0 mM HFIP and (B) 25.00 mM HFIP

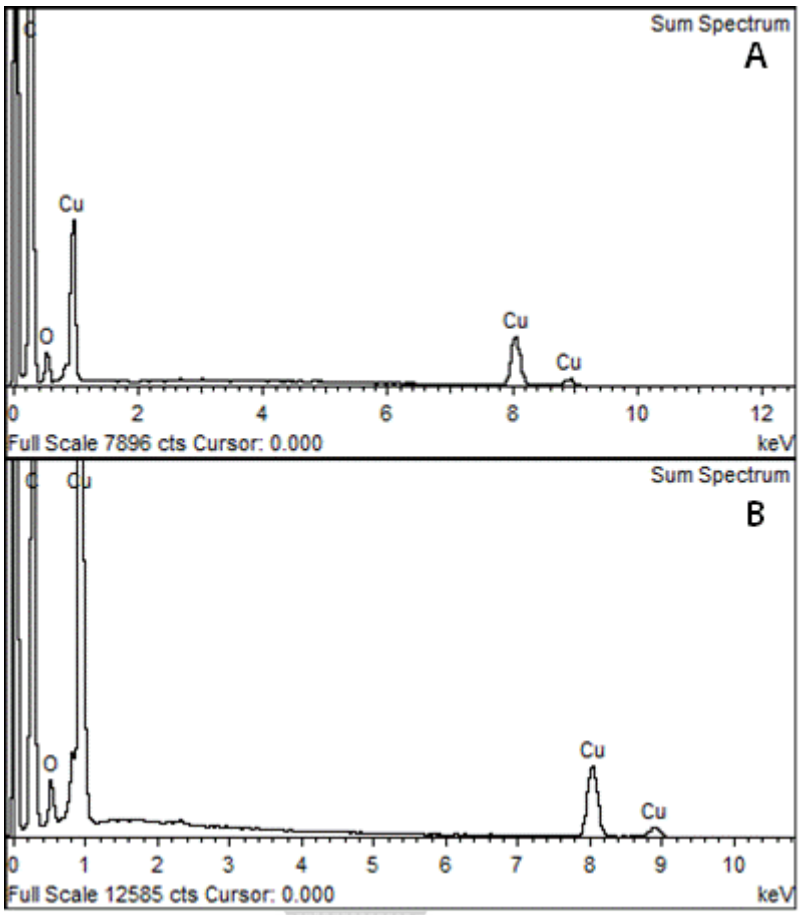

Figure 4.8 EDX spectra of reticulated vitreous carbon disks after the electrolysis of carbon dioxide and copper(II) salen at –2.10 V with (A) 0 mM HFIP and (B) 25.00 mM HFIP

Table 4.6 Elemental composition of bare reticulated vitreous carbon disk and reticulated vitreous carbon disks after the electrolysis of carbon dioxide and copper(II) salen at –2.10 V

Disk	Element (%)				
	C	O	S	Cu	Total
Bare RVC	94.31	5.58	0.11	–	100.00
RVC after the electrolysis with 0 mM HFIP	60.14	6.02	–	33.84	100.00
RVC after the electrolysis with 25.00 mM HFIP	56.52	4.58	–	38.90	100.00

4.2. Salophen-based Complexes

The current ratio of copper(II)/copper(I) salen obtained by cyclic voltammetry is 0.73 which is lower than that of copper(II)/copper(I) salophen (0.97), implying that both oxidation states of copper ion (copper(II) and copper(I)) can be well stabilized by salophen ligand [31]. Therefore, salophen-based complexes have been interested to utilize as electrocatalysts for the carbon dioxide reduction in comparison with copper(II) salen.

4.2.1. Synthesis and characterization of salophen and derivatives

Salophen were obtained in 93% by a reaction between 2:1 mol of salicylaldehyde and *o*-phenylenediamine [51]. Salophen ligand was characterized by means of NMR spectroscopy, UV–vis spectroscopy, and MALDI-TOF mass spectrometry. The wavelengths of maximum absorbances for UV–vis absorption spectrum were found at 282 nm assigning to π–π^* transition involving molecular orbitals located on the phenolic chromophore, and 335 nm corresponding to n–π^* transition involving molecular orbitals of C=N chromophore and benzene ring. These results are consistent with those described in the literature [69]. For MALDI-TOF

mass spectrometric analysis, the observed molecular ion peak of salophen is consistent with the calculated one, demonstrating that salophen ligand was successfully synthesized [51].

Salophen derivatives are 4-methyl-*N*,*N*'-disalicylidene-1,2-phenylene-diamine (methyl-salophen) and 4-bromo-*N*,*N*'-disalicyli-dene-1,2-phenylenediamine (bromo-salophen). They were obtained in 70% [51] and 90%, respectively, by employing 4-methyl-*o*-phenylenediamine and 4-bromo-*o*-phenylenediamine instead of *o*-phenylenediamine in the syntheses. Their NMR spectra were obtained. The UV–vis absorption spectra had absorbance peaks at 282 nm and 336 nm for methyl-salophen as well as 274 nm and 337 nm for bromo-salophen. The π–π^* transition (phenolic chromophore) occurs between 270–320 nm and n–π^* transition involving molecular orbitals of C=N chromophore and benzene ring occurs at 320–350 nm [69]. Their MALDI-TOF mass peaks correspond to the calculated molecules. The above mentioned results are summarized in Table 4.7.

Table 4.7 Characterization data of salophen and derivatives

Ligand	**Absorption[a] maxima (nm)**	**Mass analysis (mass-to-charge ratio, m/z ratio)**	
		MALDI-TOF[b]	**Calculated**
Salophen[c]	282 335	316.443	316.353
Methyl-salophen[c]	282 336	330.497	330.380
Bromo-salophen	274 337	396.722	395.249

[a] Absorption spectra are presented in Figures B-4, B-5, and B-6.

[b] MALDI-TOF mass spectra are shown in Figures A-2, A-3, and A-4.

[c] Data are from reference [51].

4.2.2. Synthesis and characterization of copper(II) salophen and derivatives

Copper (II) salophen, copper (II) methyl-salophen, and copper (II) bromo-salophen were successfully synthesized by metalation of corresponding salophen with copper ion salt as shown in Scheme 3.3. The obtained yields were in a range of 57-75%. The resulting salophen complexes were characterized by means of UV–vis spectroscopy and MALDI-TOF mass spectrometry in comparison with salophen ligand and derivatives (as shown in Table 4.7). In case of copper(II) salophen, the UV–vis absorption spectrum displays an UV band at 200-400 nm with a maximum wavelength of 307 nm and a shoulder peak at 341 nm. The molecular ion peak obtained from MALDI-TOF mass spectrometer was at *m/z* 377.748 which is consistent with the calculated *m/z* value [51]. In case of copper(II) methyl-salophen, its UV–vis absorption peak was found at 308 nm with a shoulder peak at 347 nm. The molecular ion peak appears at *m/z* 391.722, corresponding to the calculated *m/z* value of 391.910 [51]. Copper(II) bromo-salophen showed the UV–vis spectrum with absorption maxima at 309 and 427 nm. The UV–vis absorption spectra of all salophen-based complexes showed intense absorptions in UV-region which are assigned to charge transfer transition from the π orbitals of the donor atoms to the d orbitals of the metal ($\pi \rightarrow$ d) and intraligand n $\rightarrow \pi^*$ transition [69]. The n–π^* transitions of the complexes corresponding to the azomethine group shift to the lower energy. From these results, the nitrogen atom of the imine group appears to be coordinated to the metal ion [70]. The blue shift in the complexes may be due to the donation of a lone pair of electrons by the oxygen of the phenoxy group to the central metal atom [71]. The observed molecular ion peak of this complex (*m/z* 458.010) is in agreement with the calculated values (*m/z* 456.779). The aboved mentioned results are summarized in Table 4.8.

Table 4.8 Characterization data of copper(II) salophen and derivatives

Complex	Absorption[a] wavelength (nm)	Mass analysis (m/z)	
		MALDI-TOF[b]	Calculated
Copper(II) salophen[c]	307	377.748	377.883
	sh 341		
Copper(II) methyl-salophen[c]	308	391.722	391.910
	sh 347		
Copper(II) bromo-salophen	309	458.010	456.779
	427		

[a] Absorption spectra are presented in Figures B-7, B-8, and B-9.

[b] MALDI-TOF mass peaks are shown in Figures A-5, A-6, and A-7.

[c] Data are from reference [51].

sh = shoulder peak.

4.2.3. Electrochemical characterization of salophen ligand and derivatives

All cyclic voltammograms were initially scanned in negative direction in the potential range of –0.50 V to –2.20 V and were obtained with a glassy carbon electrode at a scan rate of 100 $mV \cdot s^{-1}$ in deaerated DMF solution containing 0.10 M $TBABF_4$. As shown in Figure 4.9, there is no peak in this potential range, revealing that DMF–0.10 M $TBABF_4$ solution can be used as an electrolyte solution for this electrochemical studies. One cathodic peak appears at –1.80 to –2.00 V and no anodic peak occurs in the reverse scan, indicating that the reduction process of salophen, methyl-salophen, and bromo-salophen should correspond to irreversible electron transfer. Salophen shows a small shoulder peak at –1.80 V and a cathodic peak at -1.96 V [51]. The shapes of the cathodic waves suggest that they would consist of two overlapped one-electron processes [32]. In case of methyl-salophen, the cathodic peak was observed at –1.94 with a shoulder peak at –2.03 V, whereas bromo-salophen presents an irreversible cathodic peak with the peak potential at –1.84 V [51]. For all studied Schiff bases, the irreversible reduction peak would be

ascribed to an intramolecular reductive coupling of the two imine groups to yield a piperazine [72, 73]. Such a process would involve self-protonation reactions where the phenolic hydroxyl groups act as proton donors. These results are consistent with those described in the literature [31].

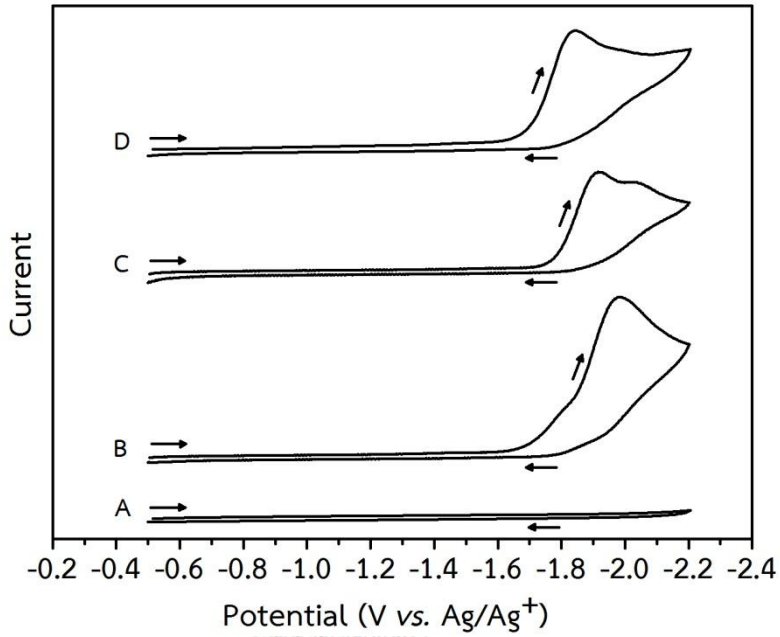

Figure 4.9 Cyclic voltammograms recorded with a glassy carbon electrode at 100 $mV \cdot s^{-1}$ for (A) a DMF solution containing 0.10 M $TBABF_4$; and a DMF solution containing 0.10 M $TBABF_4$ in the presence of (B) 2.00 mM salophen, (C) 2.00 mM methyl-salophen, and (D) 2.00 mM bromo-salophen

Table 4.9 summarizes peak potentials for the reduction of these salophen and derivatives. In each ligand, the cathodic peak potential (E_{pc}) can possibly be affected by the electronic effect of the substituents at aromatic position of diamine [31]. Thus, the cathodic peak potentials become less negative according to the following sequence: $-CH_3 \sim -H > -Br$, possibly due to decrease in electron-donationg qualities of the substituents. Since bromo-salophen contains an electron-withdrawing, –Br group, at the para position of one of the two amine groups, the –Br group reduces the nucleophilic character of the amine moiety. When the reduction of ligand occurs, the cathodic peak potential becomes less negative due to the

effect of –Br group at aromatic ring of diamine [35]. In case of methyl-salophen, $–CH_3$ group acts as the electron-donating group which should shift the reduction potential of salophen ligand to more negative potentials [31]. However, the $–CH_3$ group does not affect the reduction potential of salophen in this work.

Table 4.9 Electrochemical data obtained from cyclic voltammograms of 2.00 mM salophen and derivatives in DMF containing 0.10 M $TBABF_4$

Ligand	Cathodic peak potential, E_{pc} (V)	
	Peak 1	Peak 2
Salophen[a]	–1.80 (sh)	–1.96
Methyl-salophen[a]	–1.94	–2.03
Bromo-salophen	–1.84	–

[a] Data are from reference [51].

sh = shoulder peak.

4.2.4. Electrochemical characterization of copper(II) salophen and derivatives

Figure 4.10 displays cyclic voltammograms obtained with a glassy carbon electrode at a scan rate of 100 $mV \cdot s^{-1}$ for 2.00 mM of salophen complexes with copper ion in DMF solution containing 0.10 M $TBABF_4$ under deaerated condition by nitrogen gas. All cyclic voltammograms were initially scanned in negative direction. Copper(II) salophen (curve B) and copper(II) methyl-salophen (curve C) show similar electrochemical behavior: the reversible one-electron redox couple of copper(II)/copper(I) with cathodic and anodic peak potentials at –1.54 V and –1.45 V for copper(II) salophen and –1.55 V and –1.47 V for copper(II) methyl-salophen, respectively [31], [51]. Curve D, a cyclic voltammogram recorded for the reduction of copper(II) bromo-salophen, shows the reversibility of copperl(II)/copperl(I) redox couple with cathodic and anodic peak potentials at –1.49 V and –1.41 V,

respectively. In addition, the rise of the cathodic wave occurred in the potential range of –2.10 V to –2.20 V.

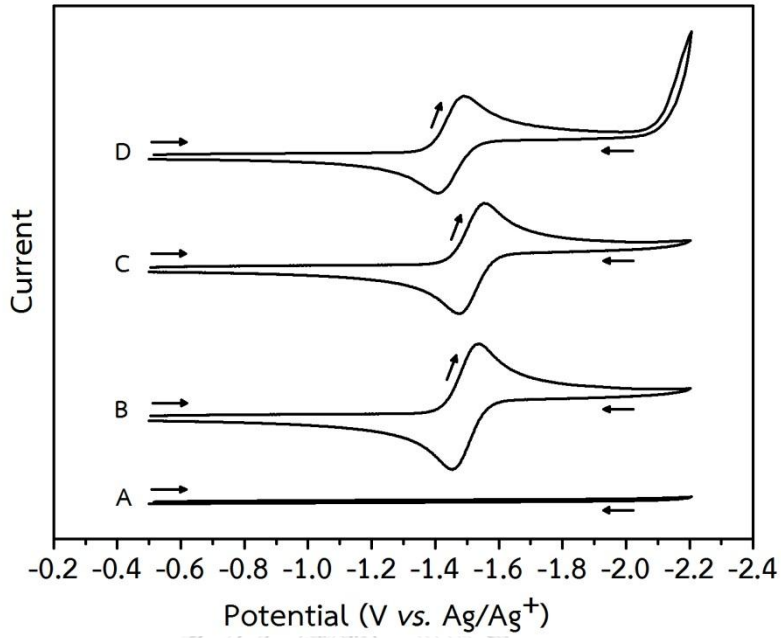

Figure 4.10 Cyclic voltammograms recorded with a glassy carbon electrode at 100 $mV \cdot s^{-1}$ for (A) a DMF solution containing 0.10 M $TBABF_4$; and a DMF solution cantaining 0.10 M $TBABF_4$ in the presence of (B) 2.00 mM copper(II) salophen, (C) 2.00 mM copper(II) methyl-salophen, and (D) 2.00 mM copper(II) bromo-salophen

Theoretically, the difference of two peak potentials: anodic peak potential (E_{pa}) and cathodic peak potential (E_{pc}) or ΔE_p should be 59 mV for a reversible one-electron transfer reaction. As seen in Table 4.10, ΔE_p values of all copper(II) salophen complexes are approximately 80-100 mV in DMF containing 0.10 M $TBABF_4$. Since the obtained ΔE_p of reversible one-electron ferrocene/ferrocenium ion redox couple in DMF–0.10 M $TBABF_4$ solution is 103 mV, it is likely that the copper(II) salophen complexes involve with reversible one-electron reduction. In addition, these cyclic voltammetric results confirm that copper(II) salophen and the derivatives can be successfully synthesized via metallation.

Table 4.10 Electrochemical data obtained from cyclic voltammograms of 2.00 mM copper(II) salophen and derivatives in DMF containing 0.10 M $TBABF_4$

Complex	Potential value (V)			ΔE	ΔE_p (mV)		i_{pa}/i_{pc}
	E_{pc}	E_{pa}	E_{onset}	(mV)	i_{pc}	i_{pa}	
Copper(II) salophen[a]	–1.54	–1.45	–	90	27.90	27.14	0.97
Copper(II) methyl-salophen[a]	–1.55	–1.47	–	80	24.22	23.67	0.98
Copper(II) bromo-salophen	–1.49	–1.41	–2.10	80	22.66	20.53	0.91

E_{pc} = cathodic peak potential; E_{pa} = anodic peak potential;

E_{onset} = onset potential; $\Delta E_p = |E_{pa} - E_{pc}|$.

i_{pc} = cathodic peak current; i_{pa} = anodic peak current.

[a] Data are from reference [51].

4.2.5. Electrocatalytic reduction of carbon dioxide

4.2.5.1. Electrochemical behavior of electrolyte solutions

Cyclic voltammograms of DMF solution containing 0.10 M $TBABF_4$ in the presence and absence of carbon dioxide were recorded with a glassy carbon electrode at a scan rate of 100 $mV \cdot s^{-1}$ in the potential range of –0.50 V to –2.20 V. As seen earlier in Figures 4.9 and 4.10, no significant peak was observed in this potential range so that DMF–0.10 M $TBABF_4$ solution was chosen as supporting electrolyte for this work. In the presence of carbon dioxide, slight enhancement of background current was found, but no cathodic peak for carbon dioxide reduction appeared, indicating that the direct electro-reduction of carbon dioxide did not occur in this potential range.

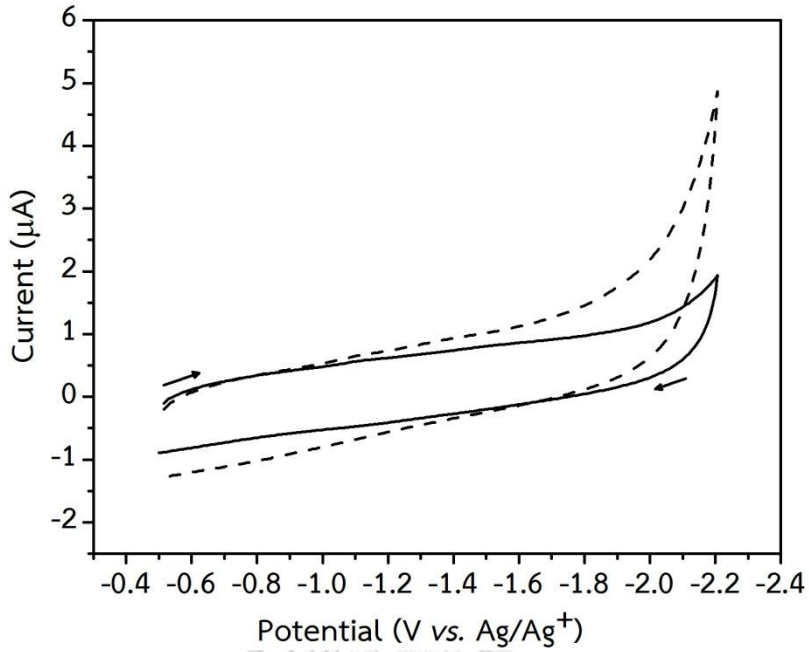

Figure 4.11 Cyclic voltammograms recorded with a glassy carbon electrode at 100 $mV \cdot s^{-1}$ for DMF solution containing 0.10 M $TBABF_4$ in the presence of saturated nitrogen (solid line) and carbon dioxide (dashed line)

4.2.5.2. Electrocatalytic reduction of carbon dioxide by salophen

Electrocatalytic reduction of carbon dioxide by salophen ligand was investigated by means of cyclic voltammetry at the scan rate of 100 $mV \cdot s^{-1}$ in the potential range of –0.50 V to –2.20 V [51]. Dashed line of Figure 4.12 illustrates dramatic increase in the cathodic peak current at the potential around –2.00 V in the presence of carbon dioxide compared with that of nitrogen (solid line). This result indicates that the electrogenerated salophen can possibly interact with carbon dioxide to promote carbon dioxide reduction. Electrochemical behaviors of this salophen including the increase in the peak current for the reduction of the ligand in the presence of carbon dioxide are similar to the salen derivatives in the literature [33].

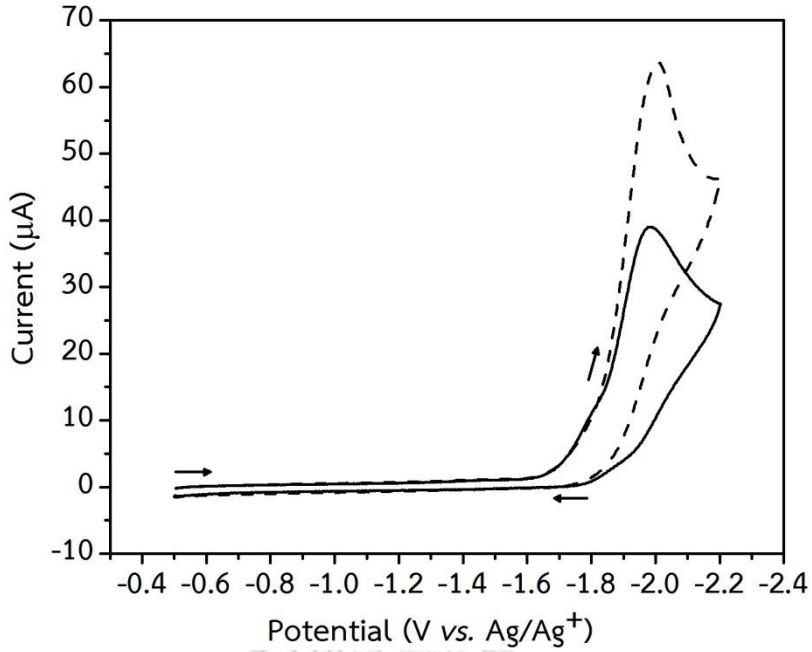

Figure 4.12 Cyclic voltammograms recorded with a glassy carbon electrode at 100 $mV \cdot s^{-1}$ for DMF solution containing 0.10 M $TBABF_4$ in the presence of 2.00 mM salophen saturated with nitrogen (solid line) and carbon dioxide (dashed line)

4.2.5.3. Electrocatalytic reduction of carbon dioxide by metyl-salophen

Electrocatalytic reduction of carbon dioxide by electro-generated methyl-salophen was examined at the scan rate of 100 $mV \cdot s^{-1}$ in the potential range of –0.50 V to –2.20 V [51]. As seen in Figure 4.9, a solid line of Figure 4.13 represents the two-electron reduction of ligand [72, 73] with the peak potentials at –1.94 V and a small wave at –2.03 V. In the presence of carbon dioxide (dashed line), the increase in the cathodic peak current at the potential of –2.00 V was found. This voltammetric result indicates the possibility of electrocatalytic reduction of carbon dioxide via its interaction with electrogenerated methyl-salophen [33].

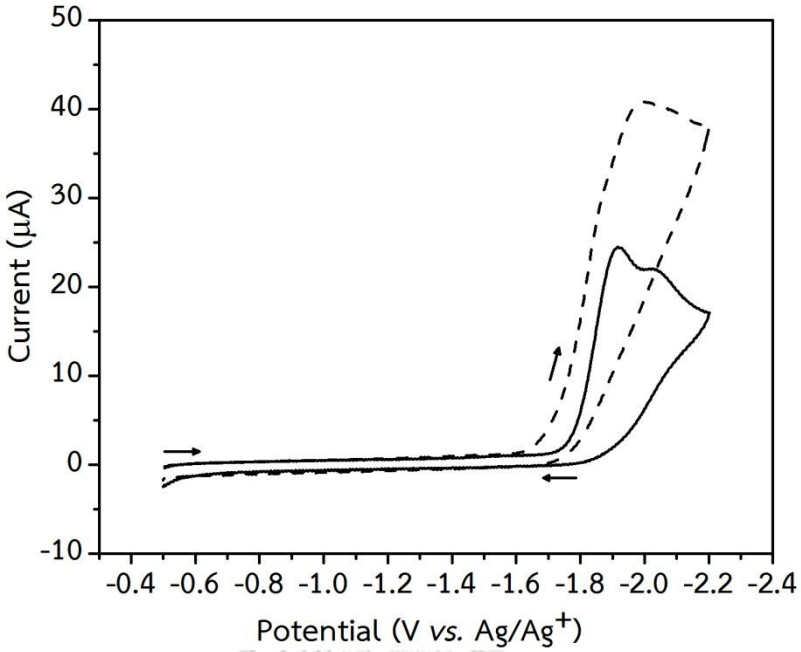

Figure 4.13 Cyclic voltammograms recorded with a glassy carbon electrode at 100 $mV \cdot s^{-1}$ for DMF solution containing 0.10 M $TBABF_4$ in the presence of 2.00 mM methyl-salophen saturated with nitrogen (solid line) and carbon dioxide (dashed line)

4.2.5.4. Electrocatalytic reduction of carbon dioxide by bromo-salophen

Figure 4.14 displays cyclic voltammograms of bromo-salophen in the absence and presence of carbon dioxide recorded at the scan rate of 100 $mV \cdot s^{-1}$ in the potential range of –0.50 V to –2.20 V. Dashed line illustrates the enhancement of the cathodic peak current for bromo-salophen reduction at –1.94 V and the appearance of new shoulder peak at –1.73 V when carbon dioxide was present in bromo-salophen solution. This cyclic voltammetric behavior refects electrocatalytic reduction of carbon dioxide by electrogenerated bromo-salophen [33].

It is clearly that salophen and all derivatives display the increases in cathodic current for the carbon dioxide reduction which are larger than salen (36.87 μA) [27].

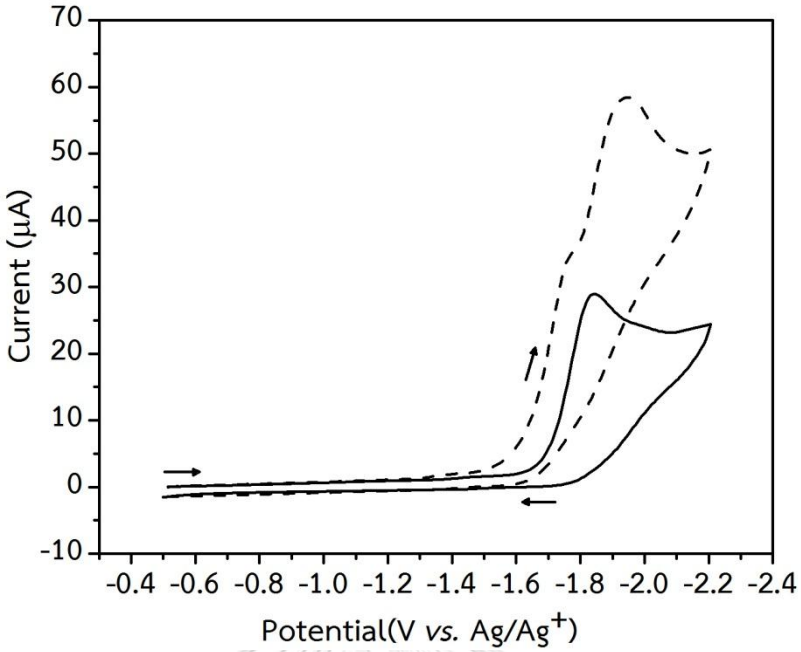

Figure 4.14 Cyclic voltammograms recorded with a glassy carbon electrode at 100 $mV \cdot s^{-1}$ for DMF solution containing 0.10 M $TBABF_4$ in the presence of 2.00 mM bromo-salophen saturated with nitrogen (solid line) and carbon dioxide (dashed line)

4.2.5.5. Electrocatalytic reduction of carbon dioxide by copper(II) salophen

Electrocatalytic reduction of carbon dioxide by electro-generated copper(I) salophen was examined in the potential range of –0.50 V to –2.20 V at 100 $mV \cdot s^{-1}$ [51]. Cyclic voltammetric behavior of the copper(II) salophen solution changed significantly in the presence of carbon dioxide. Without carbon dioxide (solid line), a reversible one-electron copper(II)-to-copper(I) salophen was found at the potential range of –1.40 V and –1.80 V. With carbon dioxide (dashed line), a slight increase in cathodic current and a 20-mV positive shift of cathodic peak potential from –1.54 V to –1.52 V were observed. It was speculated that [copper(I) salophen]$^-$ produced from the reduction potential at –1.52 V would react with the carbon dioxide molecule to form [copper(I) salophen–CO_2]$^-$ [33]. There was also a decrease in size of copper(I)-to-copper(II) salophen re-oxidation peak due to the reaction with carbon dioxide to produce the proposed [copper(I) salophen–CO_2]$^-$.

The appearance of a new cathodic peak at –2.08 V may be attributed to the reduction of the proposed [copper(I) salophen–CO_2]$^-$ causing the reduction of carbon dioxide to carbon dioxide radical anion ($CO_2^{\bullet -}$). Also, carbon dioxide radical anion can behave as a Lewis base and a nucleophile in the synthesis of some organic compounds [33]. According to this result, electrogenerated copper(I) salophen possibly shows the tendency to be an electrocatalyst for electro-reduction of carbon dioxide.

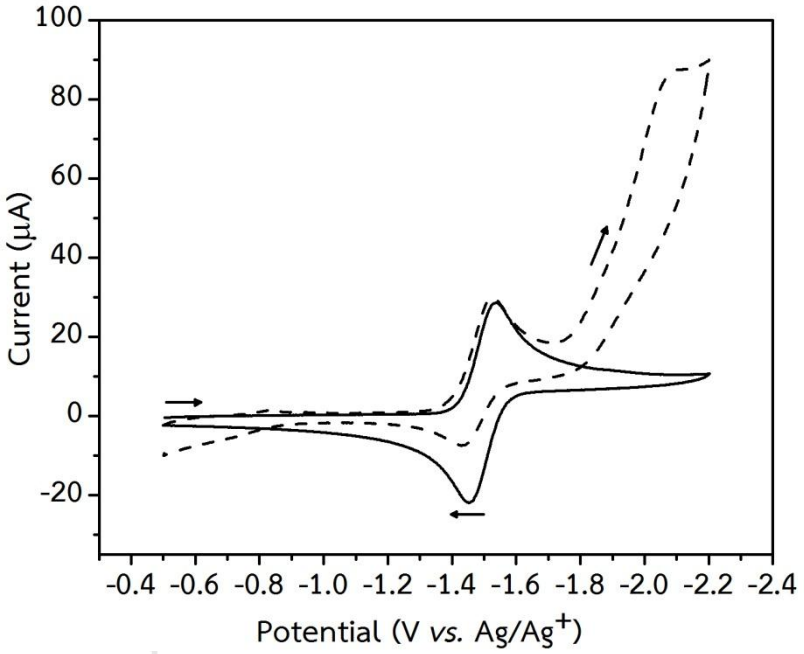

Figure 4.15 Cyclic voltammograms recorded with a glassy carbon electrode at 100 mV·s^{-1} for DMF solution containing 0.10 M $TBABF_4$ in the presence of 2.00 mM copper(II) salophen saturated with nitrogen (solid line) and carbon dioxide (dashed line)

4.2.5.6. Electrocatalytic reduction of carbon dioxide with copper(II) methyl-salophen

Shown in Figure 4.16 are cyclic voltammograms of copper(II) methyl-salophen in DMF solution containing 0.10 M $TBABF_4$ under saturated nitrogen (solid line) and carbon dioxide (dashed line) [51]. In the presence of carbon dioxide (dashed line), a slight increase in cathodic current with no positive shift of cathodic

peak potential (–1.55 V) compared with that of nitrogen atmosphere and the decrease in size of copper(I)-to-copper(II) salophen re-oxidation peak were observed with the presence of new cathodic peak. These results suggest that the electrogenerated copper(I) species from the reduction of copper(II) methyl-salophen might react with carbon dioxide to form new species undergoing further reaction to form carbon dioxide radical anion [33].

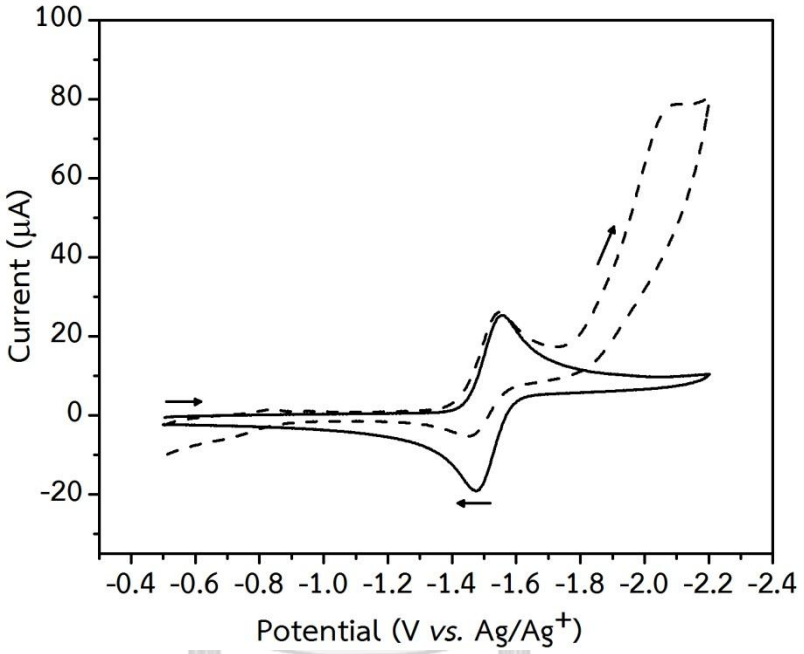

Figure 4.16 Cyclic voltammograms recorded with a glassy carbon electrode at 100 $mV \cdot s^{-1}$ for DMF solution containing 0.10 M $TBABF_4$ in the presence of 2.00 mM copper(II) methyl-salophen saturated with nitrogen (solid line) and carbon dioxide (dashed line)

4.2.5.7. Electrocatalytic reduction of carbon dioxide with copper(II) bromo-salophen

Figure 4.17 depicts cyclic voltammograms of copper(II) bromo-salophen in DMF solution containing 0.10 M $TBABF_4$ in the presence of nitrogen (solid line) and carbon dioxide (dashed line). Higher cathodic peak at –1.47 V with 20-mV positive shift of cathodic peak potential from –1.49 V, a small re-oxidation peak at –1.36 V, and new cathodic peak (–2.05 V) were observed in the presence of carbon

dioxide (dashed line), implying that some interaction between electrogenerated species from copper(II) bromo-salophen reduction and carbon dioxide exists [33].

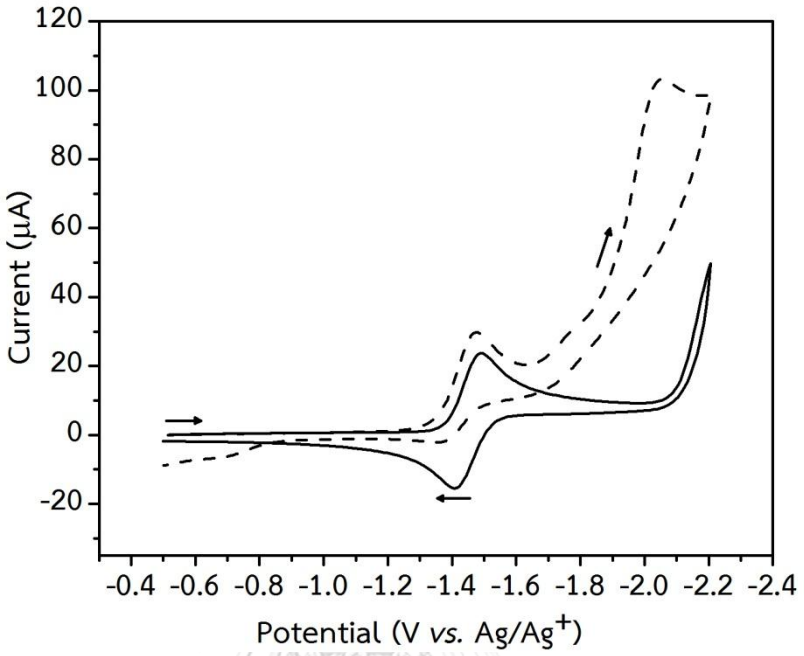

Figure 4.17 Cyclic voltammograms recorded with a glassy carbon electrode at 100 $mV \cdot s^{-1}$ for DMF solution containing 0.10 M $TBABF_4$ in the presence of 2.00 mM copper(II) bromo-salophen saturated with nitrogen (solid line) and carbon dioxide (dashed line).

Table 4.11 summarizes peak potentials, peak currents, and current increase with carbon dioxide for cyclic voltammograms of the salophen-based copper(II) complexes in the presence of carbon dioxide compared with those in the presence of nitrogen. Data indicate that copper(II) bromo-salophen has the highest percentage of cathodic current enhancement (360%) among all salophen-based copper complexes. Therefore, copper(II) bromo-salophen has tendency to be an effective electrocatalyst for carbon dioxide electro-reduction. In the comparison with copper(II) salen [27], copper(II) bromo-salophen exhibited a 20-mV positive shift of cathodic peak potential for a reversible one-electron copper(II)-to-copper(I) salophen which is smaller than that for copper(II)-to-copper(I) salen (100 mV), and although copper(II) bromo-salophen gave cathodic current enhancement (360%) for

carbon dioxide electro-reduction similar to copper(II) salen (358%), the peak corresponding to this reduction occurred much more positively (–2.05 V *vs*. –2.22 V). These results indicate that copper(II) bromo-salophen has tendency to be more efficient electrocatalyst than copper(II) salen. However, to confirm the efficiency of salophen-based complexes, controlled-potential electrolyses of copper(II) salophen, copper(II) methyl-salophen, and copper(II) bromo-salophen in the presence of carbon dioxide were studied.

Table 4.11 Electrochemical data obtained from cyclic voltammograms of 2.0 mM salophen-based ligands and complexes in DMF containing 0.1 M $TBABF_4$ in the presence and absence of carbon dioxide

Compound	Condition	E_{pc1} (V)	E_{pc2} (V)	E_{pa1} (V)	i_{pc1} (μA)	i_{pc2} (μA)	i_{pa} (μA)	Cathodic current increase (%)
salophen	N_2	−1.80	−1.96	ND	ND	37.61	ND	132[c]
	CO_2	−2.00	ND	ND	49.78	ND	ND	
Methyl-salophen	N_2	−1.94	−2.03	ND	23.20	ND	ND	171[b]
	CO_2	−2.00	ND	ND	39.69	ND	ND	
Bromo-salophen	N_2	−1.84	ND	ND	27.38	ND	ND	205[a]
	CO_2	−1.73	−1.94	ND	ND	56.23	ND	
Copper(II) salophen	N_2	−1.54	ND	−1.45	27.90	ND	27.14	241[a]
	CO_2	−1.52	−2.08	−1.44	28.67	67.25	13.32	
Copper(II) methyl-salophen	N_2	−1.55	ND	−1.47	24.22	ND	23.67	252[a]
	CO_2	−1.55	−2.08	−1.45	24.77	60.92	10.11	
Copper(II) bromo-salophen	N_2	−1.49	ND	−1.41	22.66	ND	20.53	360[a]
	CO_2	−1.47	−2.05	−1.36	28.61	81.49	10.09	

[a] Currrent increase = (i_{pc2} (CO_2) / i_{pc1} (N_2)) x 100; [b] Currrent increase = (i_{pc1} (CO_2) / i_{pc1} (N_2)) x 100; and [c] Currrent increase = (i_{pc1} (CO_2) / i_{pc2} (N_2)) x 100. E_{pc} = cathodic peak potential; E_{pa} = anodic peak potential; i_{pc} = cathodic peak current; i_{pa} = anodic peak current; and ND = not available.

4.2.6. Controlled-potential electrolyses of salophen-based complexes in the presence of carbon dioxide

Firstly, bulk electrolyses of salophen-based copper(II) complexes were carried out in DMF solution containing 0.10 M $TBABF_4$ without the addition of HFIP proton donor. The applied potential for the electrolysis was selected at the half-peak potential of the cathodic peak for carbon dioxide reduction in the cyclic voltammogram. Half-peak potential is the potential where the current is half of the cathodic peak current. During the electrolysis, the solution color changed from turquoise of copper(II) salen to brown-greenish of copper(I) salophen, and finally to light brown green, revealing the electrocatalyst modification. Gas chromatography was used to analyze gas-phase composition after the electrolysis. As displayed in Table 4.12, only carbon monoxide was observed as a product in the gas phase of the carbon dioxide electro-reduction with copper(II) salophen derivatives. Their chronoamperograms are shown in Figures C-8, C-9, and C-10. All salophen-based complexes gave similar percentages of carbon monoxide product that are higher than copper(II) salen, implying that three types of copper(II) salophens are more efficient electrocatalysts for carbon monoxide production than copper(II) salen. However, their unreacted percentages of carbon dioxide and total gaseous compositions are higher than that copper(II) salen, implying that copper(II) salen favors the formation of undetected product(s) which might be in the liquid phase. It is also worth to note that the electrolysis parameters for copper(II) salophen reaction have not been optimized yet. The lowest amount of remaining carbon dioxide from copper(II) salophen reaction may reveals that copper(II) salophen can electro-catalytically reduce carbon dioxide better than copper(II) methyl-salophen and copper(II) bromo-salophen. Therefore, copper(II) salophen was firstly chosen as electrocatalyst for the carbon dioxide reduction in the presence of 25.00 mM HFIP.

Table 4.12 Product distribution for electro-reduction of carbon dioxide in DMF containing 0.10 M $TBABF_4$ with copper(II)-based electrocatalysts

Electrocatalyst	E_{app} (V)	Gaseous composition of post-electrolysis (%)			
		CO_2	CO	CH_4	Total
Copper(II) salophen	–2.00[a]	85.66	5.90	–	91.56
Copper(II) methyl-salophen	–2.00[a]	88.99	5.99	–	94.99
Copper(II) bromo-salophen	–1.90[a]	92.92	5.94	–	98.86
Copper(II) salen[b]	–2.10	81.58 ± 0.04	3.50 ± 0.04	–	85.08 ± 0.02

E_{app} = applied potential.

[a] The applied potential was selected at the half-peak potential of the carbon dioxide reduction peak.

[b] Entry represents the average of three set of experiments.

In the presence of HFIP, copper(II) salophen was selected to compare with copper(II) salen for carbon dioxide electro-reduction. Its *i-t* curve is shown in Figure C-11). Table 4.13 shows that the obtained products from the electro-reduction of carbon dioxide in the presence of HFIP were carbon monoxide and methane. Although, copper(II) salophen gave the percentage of carbon monoxide less than copper(II) salen, but the increase in the percentage of methane was found. This result may be refected to the activity and the selectivity of salopen-based electrocatalyst since salophen ligand contains a planar phenylenediamine bridge that can possibly help stabilize the complex square planar structure, which is not the case for salen (ethylenediamine bridge) [74]. In addition, the current ratio (i_{pa}/i_{pc}) of copper(II)/copper(I) salophen is closely related to 1 (Table 4.10) more than that of copper(II)/copper(I) salen [27], indicating good characteristics of metal-centered electrocatalyst. Salophen ligand might provide better interaction of salophen

complex with the electrode material and hence facilitates an electron transfer during the conversion of carbon dioxide to form the products [35]. When the remaining carbon dioxide was considered, it was found that copper(II) salophen gave higher percentage than copper(II) salen, indicating that starting carbon dioxide was less consumed to generate products in gas phase. However, the starting material may react and produce the product(s) in liquid phase as well. Due to the solubility of carbon dioxide in DMF (0.199 ± 0.006 M) [75], the detection of carbon dioxide reduction in both gas and liquid phases is needed. Further experiments including the detection of liquid-phase product(s) and the optimization of the factors affecting the electrocatalytic properties of salophen-based complexes for carbon dioxide electro-reduction should be investigated.

Table 4.13 Product distribution for electro-reduction of carbon dioxide in DMF containing 0.10 M $TBABF_4$ and 25.00 mM HFIP

Electro-catalyst	E_{app} (V)	Gaseous composition of post-electrolysis (%)[a]			
		CO_2	CO	CH_4	Total
Copper(II) salophen	–2.00	71.21 ± 0.02	8.87± 0.00	0.57± 0.00	80.65 ± 0.02
Copper(II) salen	–2.10	62.00 ± 0.02	16.30 ± 0.00	0.39 ± 0.00	78.69 ± 0.02

[a] Each entry represents the average of three set of experiments.
%RSD is below 3.00 for each entry.

CHAPTER V
CONCLUSIONS

Copper(II) salen, salophen-based ligands, and their complexes were successfully synthesized and characterized by mean of NMR spectroscopy, MALDI-TOF mass spectrometry, UV–vis spectroscopy, and cyclic voltammetry. The electrocatalytic activity of copper(II) salen for carbon dioxide reduction was investigated by means of controlled-potential electrolysis. With the applied potential of –2.10 V, carbon monoxide (3.50-16.30%) was obtained as the only product in gas phase. Methane was additionally found with the addition of proton donor and its maximum percentage (0.39 ± 0.00%) were obtained from the electrolysis with 25.00 mM proton donor and 2.0 mM copper(II) salen. In addition, copper coated-reticulated vitreous carbon disks can electrochemically catalyze carbon dioxide reduction. For salophen and derivatives as well as their complexes, the electrocatalytic activity for carbon dioxide reduction was studied by means of cyclic voltammetry. Salophen-based ligands and complexes presented possibility for electrochemically catalyzing carbon dioxide reduction. Among all salophen derivatives and the copper complexes, copper(II) bromo-salophen displayed highest percentage of current enhancement (360%) for carbon dioxide reduction. Controlled-potential electrolyses of carbon dioxide by electrogenerated copper(I) salophen and derivatives were accomplished, giving carbon monoxide as gas-phase main product whereas methane was additionally detected with the addition of HFIP as a proton donor. Due to the good features including the complex stability from salophen structure, more reversibility of copper(II)/copper(I) redox couple, and better electron transfer during carbon dioxide electro-reduction in comparison with copper(II) salen, it is possible that copper(II) salophen has a tendency to be an efficient electrocatalyst.

5.1. Future Aspects

Further studies will focus on the analysis of products in liquid phase of carbon dioxide reduction and the optimization of experimental parameters to improve product yields using salophen-based electrocatalysts.

REFERENCES

[1] Lenton, T.M. The Potential for Land-based Biological CO_2 Removal to Lower Future Atmospheric CO_2 Concentration. Carbon Management 1(1) (2010): 145–160.

[2] Savile, C.K. and Lalonde, J.J. Biotechnology for the Acceleration of Carbon Dioxide Capture and Sequestration. Current Opinion in Biotechnology 22(6) (2011): 818–823.

[3] Acién Fernández, F.G., González-López, C.V., Fernández Sevilla, J.M., and Molina Grima, E. Conversion of CO_2 into Biomass by Microalgae: How Realistic a Contribution May It be to Significant CO_2 Removal? Applied Microbiology and Biotechnology 96(3) (2012): 577–586.

[4] Kawagucci, S., et al. Hydrothermal Fluid Geochemistry at the Iheya North field in the Mid-Okinawa Trough: Implication for Origin of Methane in Subseafloor Fluid Circulation Systems. Geochemical Journal 45(2) (2011): 109–124.

[5] Garcia, B., et al. A Geochemical Approach for Monitoring a CO_2 Pilot Site: Rousse, France. A Major gases, CO_2-carbon Isotopes and Noble Gases Combined Approach. Oil & Gas Science and Technology - Revue d'IFP Energies nouvelles 67(2) (2012): 341–353.

[6] Roberts, J.J., Gilfillan, S.M.V., Stalker, L., and Naylor, M. Geochemical Tracers for Monitoring Offshore CO_2 Stores. International Journal of Greenhouse Gas Control 65(Supplement C) (2017): 218–234.

[7] Abdul Halim, H.N., M. Shariff, A., Tan, L.S., and Bustam, M.A. Mass Transfer Performance of CO_2 Absorption from Natural Gas using Monoethanolamine (MEA) in High Pressure Operations. Industrial & Engineering Chemistry Research 54(5) (2015): 1675–1680.

[8] Binns, M., Oh, S.-Y., Kwak, D.-H., and Kim, J.-K. Analysis of Hybrid Membrane and Chemical Absorption Systems for CO_2 Capture. Korean Journal of Chemical Engineering 32(3) (2015): 383–389.

[9] Moioli, S., Pellegrini, L.A., and Gamba, S. Simulation of CO_2 Capture by MEA Scrubbing with a Rate-Based Model. Procedia Engineering 42(Supplement C) (2012): 1651–1661.

[10] Steinmann, S.N., Michel, C., Schwiedernoch, R., and Sautet, P. Impacts of Electrode Potentials and Solvents on the Electroreduction of CO_2: A Comparison of Theoretical Approaches. Physical Chemistry Chemical Physics 17(21) (2015): 13949–13963.

[11] Kortlever, R., Shen, J., Schouten, K.J.P., Calle-Vallejo, F., and Koper, M.T.M. Catalysts and Reaction Pathways for the Electrochemical Reduction of Carbon Dioxide. The Journal of Physical Chemistry Letters 6(20) (2015): 4073–4082.

[12] Qiao, J., Liu, Y., Hong, F., and Zhang, J. A Review of Catalysts for the Electroreduction of Carbon Dioxide to Produce Low-Carbon Fuels. Chemical Society Reviews 43(2) (2014): 631–675.

[13] Peterson, A.A. and Nørskov, J.K. Activity Descriptors for CO_2 Electroreduction to Methane on Transition-Metal Catalysts. The Journal of Physical Chemistry Letters 3(2) (2012): 251–258.

[14] Nie, X., Luo, W., Janik, M.J., and Asthagiri, A. Reaction Mechanisms of CO_2 Electrochemical Reduction on Cu(111) Determined with Density Functional Theory. Journal of Catalysis 312 (2014): 108–122.

[15] Murugananthan, M., Kumaravel, M., Katsumata, H., Suzuki, T., and Kaneco, S. Electrochemical Reduction of CO_2 using Cu Electrode in Methanol/$LiClO_4$ Electrolyte. International Journal of Hydrogen Energy 40(21) (2015): 6740–6744.

[16] Scialdone, O., Galia, A., Nero, G.L., Proietto, F., Sabatino, S., and Schiavo, B. Electrochemical Reduction of Carbon Dioxide to Formic Acid at a Tin Cathode in Divided and Undivided Cells: Effect of Carbon Dioxide Pressure and Other Operating Parameters. Electrochimica Acta 199 (2016): 332–341.

[17] Elgrishi, N., Chambers, M.B., Artero, V., and Fontecave, M. Terpyridine Complexes of First Row Transition Metals and Electrochemical Reduction of CO_2 to CO. Physical Chemistry Chemical Physics 16(27) (2014): 13635–13644.

[18] Sieh, D., Lacy, D.C., Peters, J.C., and Kubiak, C.P. Reduction of CO_2 by Pyridine Monoimine Molybdenum Carbonyl Complexes: Cooperative Metal–ligand Binding of CO_2. Chemistry – A European Journal 21(23) (2015): 8497–8503.

[19] Nganga, J.K., et al. Electrochemical Reduction of CO_2 Catalyzed by Re(pyridine-oxazoline)$(CO)_3Cl$ Complexes. Inorganic Chemistry 56(6) (2017): 3214–3226.

[20] Dubois, D.L. Development of Transition Metal Phosphine Complexes as Electrocatalysts for CO_2 and CO Reduction. Comments on Inorganic Chemistry 19(5) (1997): 307–325.

[21] Raebiger, J.W., et al. Electrochemical Reduction of CO_2 to CO Catalyzed by a Bimetallic Palladium Complex. Organometallics 25(14) (2006): 3345–3351.

[22] Rao, G.K., Pell, W., Korobkov, I., and Richeson, D. Electrocatalytic Reduction of CO_2 Using Mn Complexes with Unconventional Coordination Environments. Chemical Communications 52(51) (2016): 8010–8013.

[23] Zhang, A., Zhang, W., Lu, J., Wallace, G.G., and Chen, J. Electrocatalytic Reduction of Carbon Dioxide by Cobalt-Phthalocyanine-Incorporated Polypyrrole. Electrochemical and Solid-State Letters 12(8) (2009): E17–E19.

[24] Shen, J., et al. Electrocatalytic Reduction of Carbon Dioxide to Carbon Monoxide and Methane at an Immobilized Cobalt Protoporphyrin. Nature Communications 6 (2015): 8177.

[25] Wu, Y., et al. Electroreduction of CO_2 Catalyzed by a Heterogenized Zn-Porphyrin Complex with a Redox-Innocent Metal Center. ACS Central Science 3(8) (2017): 847–852.

[26] Posada-Perez, S., et al. Highly Active Au/delta-MoC and Cu/delta-MoC Catalysts for the Conversion of CO_2: The Metal/C Ratio as a Key Factor Defining Activity, Selectivity, and Stability. Journal of the American Chemical Society 138(26) (2016): 8269–78.

[27] Jaisabuy, K. Development of Phthalocyanine-based Electrocatalytic Systems for Reduction of Carbon Dioxide. Master, Chemistry Chulalongkorn University, 2014.

[28] Gennaro, A., Isse, A.A., Severin, M.-G., Vianello, E., Bhugun, I., and Saveant, J.-M. Mechanism of the Electrochemical Reduction of Carbon Dioxide at Inert Electrodes in Media of Low Proton Availability. Journal of the Chemical Society, Faraday Transactions 92(20) (1996): 3963–3968.

[29] Manbeck, G.F. and Fujita, E. A Review of Iron and Cobalt Porphyrins, Phthalocyanines and Related Complexes for Electrochemical and Photochemical Reduction of Carbon Dioxide. Journal of Porphyrins and Phthalocyanines 19(01-03) (2015): 45–64.

[30] Peiris, M.C.R. and Udugala-Ganehenege, M.Y. Electrocatalytic Activity of (Bis(salicylaldehyde)ethylenediamino)Ni(II) Complex for CO_2 Reduction. International Journal of Environmental Science and Development 7(2) (2015): 91–94.

[31] Zolezzi, S., Spodine, E., and Decinti, A. Electrochemical Studies of Copper(II) Complexes with Schiff-base Ligands. Polyhedron 21(1) (2002): 55–59.

[32] Ourari, A., Aggoun, D., and Ouahab, L. A Novel Copper(II)-schiff Base Complex Containing Pyrrole Ring: Synthesis, Characterization and its Modified Electrodes Applied in Oxidation of Aliphatic Alcohols. Inorganic Chemistry Communications 33 (2013): 118–124.

[33] Khoshro, H., Zare, H.R., and Vafazadeh, R. New Insight into Electrochemical Behavior of Copper Complexes and their Applications as Bifunctional Electrocatalysts for CO_2 Activation. Journal of CO_2 Utilization 12 (2015): 77–81.

[34] Gennaro, A., Isse, A. A., and Vianello, H. Electrochemical Reduction of CO_2 Catalysed by Transition Metal Complexes. Kluwer Academic, 1993.

[35] Singh, S., Phukan, B., Mukherjee, C., and Verma, A. Salen Ligand Complexes as Electrocatalysts for Direct Electrochemical Reduction of Gaseous Carbon Dioxide to Value Added Products. RSC Advances 5(5) (2015): 3581–3589.

[36] Thiruvenkatachari, R., Su, S., An, H., and Yu, X.X. Post Combustion CO_2 Capture by Carbon Fibre Monolithic Adsorbents. Progress in Energy and Combustion Science 35(5) (2009): 438–455.

[37] Cheung, K., Wong, W., Ma, D., Lai, T., and Wong, K. Transition Metal Complexes as Electrocatalysts—Development and Applications in Electro-oxidation Reactions. Coordination Chemistry Reviews 251(17-20) (2007): 2367–2385.

[38] Gosden, C., Kerr, J.B., Pletcher, D., and Rosas, R. The Electrochemistry of Square Planar Macrocyclic Nickel Complexes and the Reaction of Ni(I) with Alkyl Bromides: Tetradentate Schiff Base Complexes. Journal of Electroanalytical Chemistry and Interfacial Electrochemistry 117(1) (1981): 101–107.

[39] Becker, J.Y., Kerr, J.B., Pletcher, D., and Rosas, R. The Electrochemistry of Square Planar Macrocyclic Nickel Complexes and the Reaction of Ni(I) with Alkyl Bromides: Nickel Tetraamine Complexes. Journal of Electroanalytical Chemistry and Interfacial Electrochemistry 117(1) (1981): 87–99.

[40] Wang, J. Analytical Electrochemistry. John Wiley & Sons, 2006.

[41] Bard, A.J.a.F., L.R. Electrochemical Methods: Fundamentals and Applications. Vol. 2: Wiley New York, 1980.

[42] Blumberg, L.M. Gas Chromatography. in Theory of Gas Chromatography. 2012, Amsterdam: Elsevier. 19–77.

[43] Edwards, J. Principles of NMR. 2009.

[44] Bizzini, A. and Greub, G. Matrix-assisted Laser Desorption Ionization Time-of-Flight Mass Spectrometry, a Revolution in Clinical Microbial Identification. Clinical Microbiology and Infection 16(11) (2010): 1614–1619.

[45] Pavia, D.L., Lampman, G.M., Kriz, G.S., and Vyvyan, J.R. Introduction to Spectroscopy. 2009, Brooks. Cole, Cengage Learning, Nelson Education Ltd Canada.

[46] Whiston, C. X-ray Methods: Analytical Chemistry by Open Learning. Singapore. John Wiley & Sons, Inc., Publication, 1991.

[47] Flegler, S.L., Heckman Jr, J.W., and Klomparens, K.L Scanning and Transmission Electron Microscopy: An Introduction. 1993, Oxford University Press Publication: USA.

[48] Garratt-Reed, A.J.a.B., D.C. Energy Dispersive X-ray Analysis in the Electron Microscope. UK: Taylor & Francis e-Library, Publication, 2005.

[49] Samide, M.J. and Peters, D.G. Electrochemical Reduction of Copper(II) Salen at Carbon Cathodes in Dimethylformamide. Journal of Electroanalytical Chemistry 443(1) (1998): 95–102.

[50] Gholivand, M.B., Ahmadi, F., and Rafiee, E. Solid Phase Extraction and Determination of Ultra Trace Amounts of Copper using Activated Carbon Modified byN,N′-Bis(Salicylidene)-1,2-Phenylenediamine. Separation Science and Technology 42(4) (2007): 897–910.

[51] Tomon, C. Development of Metal-salophen Derivatives as Electrocatalysts for the Reduction of Carbon Dioxide. Bachelor, Chemistry Chulalongkorn University, 2016.

[52] Vanalabhpatana, P., Peters, D.G., and Karty, J.A. Stoichiometric Reduction of Primary Alkyl Monohalides with Electrogenerated Nickel(I) Salen: Formation of Aldehydes. Journal of Electroanalytical Chemistry 580(2) (2005): 300–312.

[53] Cook, T.D., et al. Nickel Complexes of C-Substituted Cyclams and Their Activity for CO_2 and H^+ Reduction. ACS Omega 2(7) (2017): 3966–3976.

[54] Wakerley, D.W. and Reisner, E. Development and Understanding of Cobaloxime Activity through Electrochemical Molecular Catalyst Screening. Physical Chemistry Chemical Physics 16(12) (2014): 5739–46.

[55] Samide, M.J. and Peters, D.G. Electrochemical Reduction of Copper(II) Salen at Carbon Cathodes in Dimethylformamide. Journal of Electroanalytical Chemistry 443(1) (1998): 95–102.

[56] Raess, P.W., et al. Catalytic Reduction of 1-Iodooctane by Nickel(I) Salen Electrogenerated at Carbon Cathodes in Dimethylformamide: Effects of added Proton Donors and a Mechanism Involving both Metal- and Ligand-centered One-electron Reduction of Nickel(II) Salen. Journal of Electroanalytical Chemistry 603(1) (2007): 124–134.

[57] Ikeda, S., Takagi, T., and Ito, K. Selective Formation of Formic Acid, Oxalic Acid, and Carbon Monoxide by Electrochemical Reduction of Carbon Dioxide. Bulletin of the Chemical Society of Japan 60(7) (1987): 2517–2522.

[58] Kaneco, S., Iiba, K., Ohta, K., and Mizuno, T. Electrochemical Reduction of Carbon Dioxide on Copper in Methanol with Various Potassium Supporting

Electrolytes at Low Temperature. Journal of Solid State Electrochemistry 3(7) (1999): 424–428.

[59] Kuhl, K.P., Cave, E.R., Abram, D.N., and Jaramillo, T.F. New Insights into the Electrochemical Reduction of Carbon Dioxide on Metallic Copper Surfaces. Energy & Environmental Science 5(5) (2012): 7050.

[60] Manthiram, K., Beberwyck, B.J., and Alivisatos, A.P. Enhanced Electrochemical Methanation of Carbon Dioxide with a Dispersible Nanoscale Copper Catalyst. Journal of the American Chemical Society 136(38) (2014): 13319–25.

[61] Lee, S., Kim, D., and Lee, J. Electrocatalytic Production of C3-C4 Compounds by Conversion of CO_2 on a Chloride-Induced Bi-Phasic Cu_2O-Cu Catalyst. Angewandte Chemie International Edition in English 54(49) (2015): 14701–5.

[62] Furuya, N. and Matsui, K. Electroreduction of Carbon Dioxide on Gas-diffusion Electrodes Modified by Metal Phthalocyanines. Journal of Electroanalytical Chemistry and Interfacial Electrochemistry 271(1) (1989): 181–191.

[63] Harikrishnan, G., Umasankar Patro, T., and Khakhar, D.V. Reticulated Vitreous Carbon from Polyurethane Foam–Clay Composites. Carbon 45(3) (2007): 531–535.

[64] Rufford, T.E., Zhu, J., and Hulicova-Jurcakova, D. Green Carbon Materials: Advances and Applications. Pan Stanford, 2014.

[65] Theivasanthi, T. and Alagar, M. Nano Sized Copper Particles by Electrolytic Synthesis and Characterizations", Int. Vol. 6, 2011.

[66] Reade, G.W., Bond, P., de Leon, C.P., and Walsh, F.C. The Application of Reticulated Vitreous Carbon Rotating Cylinder Electrodes to the Removal of Cadmium and Copper Ions from Solution. Journal of Chemical Technology & Biotechnology 79(9) (2004): 946–953.

[67] Reade, G.W., Nahle, A.H., Bond, P., Friedrich, J.M., and Walsh, F.C. Removal of Cupric Ions from Acidic Sulfate Solution Using Reticulated Vitreous Carbon Rotating Cylinder Electrodes. Journal of Chemical Technology & Biotechnology 79(9) (2004): 935–945.

[68] Brownson, D.A.C., et al. High Temperature Low Vacuum Synthesis of a Freestanding Three-dimensional Graphene Nano-ribbon Foam Electrode. Journal of Materials Chemistry A 4(7) (2016): 2617–2629.

[69] Kumar, D.N. and Garg, B.S. Synthesis and Spectroscopic Studies of Complexes of Zinc(II) with N_2O_2 Donor Groups. Spectrochim Acta A Mol Biomol Spectrosc 64(1) (2006): 141–147.

[70] Campbell, M.J.M. Transition Metal Complexes of Thiosemicarbazide and Thiosemicarbazones. Coordination Chemistry Reviews 15(2) (1975): 279–319.

[71] Sharma, R.K., Singh, R.V., and Tandon, J.P. Biscyclopentadienyl Titanium(IV) Complexes of Monofunctional Bidentate Ketamines. Journal of Inorganic and Nuclear Chemistry 42(9) (1980): 1382–1384.

[72] Isse, A.A., Gennaro, A., and Vianello, E. Electrochemical Reduction of Schiff Base Ligands H2salen and H2salophen. Electrochimica Acta 42(13) (1997): 2065–2071.

[73] Shono, T., Kise, N., Shirakawa, E., Matsumoto, H., and Okazaki, E. Electroorganic Chemistry. 129. Electroreductive Synthesis of Chiral Piperazines and Enantioselective Addition of Diethylzinc to Aldehydes in the Presence of the Chiral Piperazines. The Journal of Organic Chemistry 56(9) (1991): 3063–3067.

[74] Tzubery, A. and Tshuva, E.Y. Trans Titanium(IV) Complexes of Salen Ligands Exhibit High Antitumor Activity. Inorganic Chemistry 50(17) (2011): 7946–7949.

[75] Jitaru, M. Electrochemical Carbon Dioxide Reduction-Fundamental and Applied Topics. Journal of the University of Chemical Technology and Metallurgy 42 (2007): 333–344.

APPENDIX A

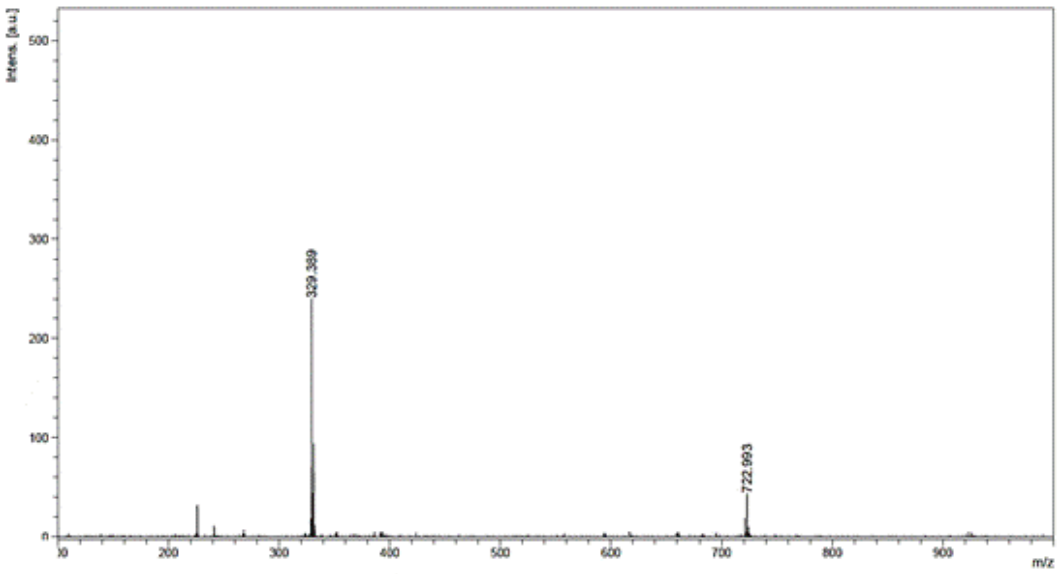

Figure A-1 MALDI-TOF mass spectrum of copper(II) salen [27]

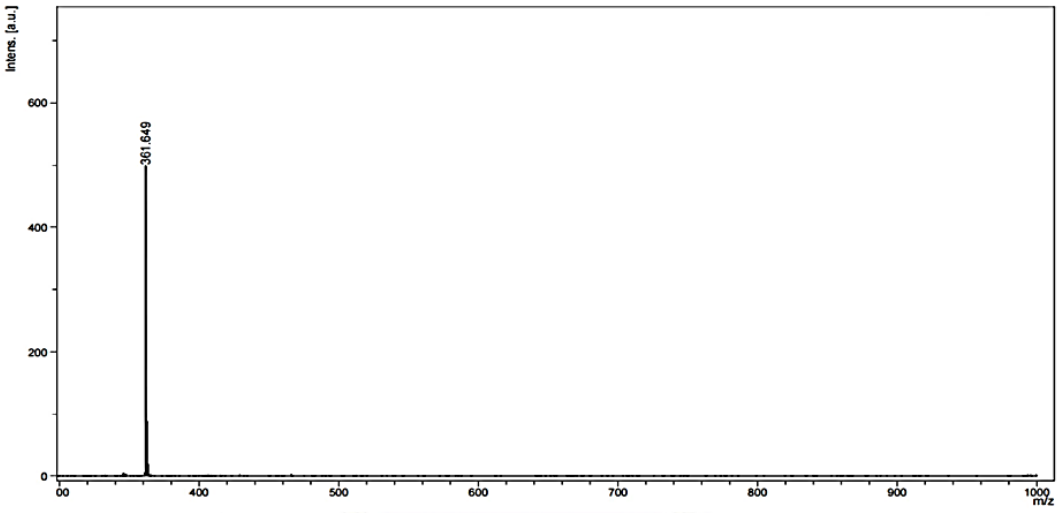

Figure A-2 MALDI-TOF mass spectrum of salophen [51]

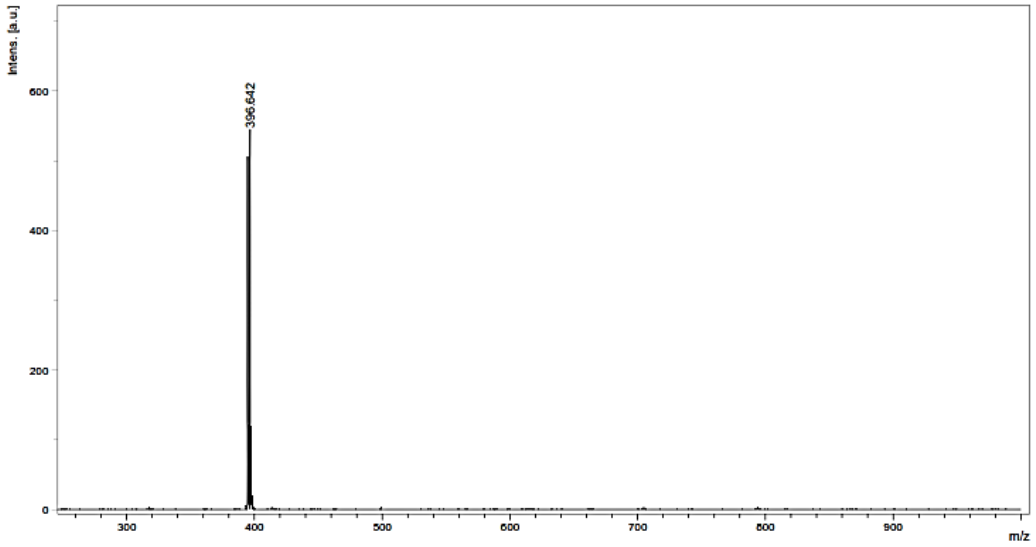

Figure A-3 MALDI-TOF mass spectrum of methyl-salophen [51]

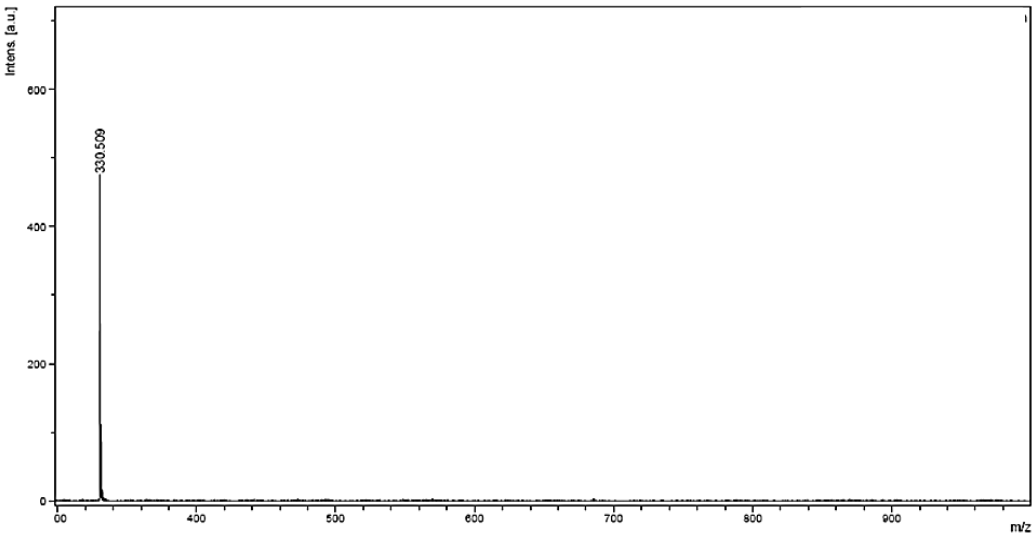

Figure A-4 MALDI-TOF mass spectrum of bromo-salophen

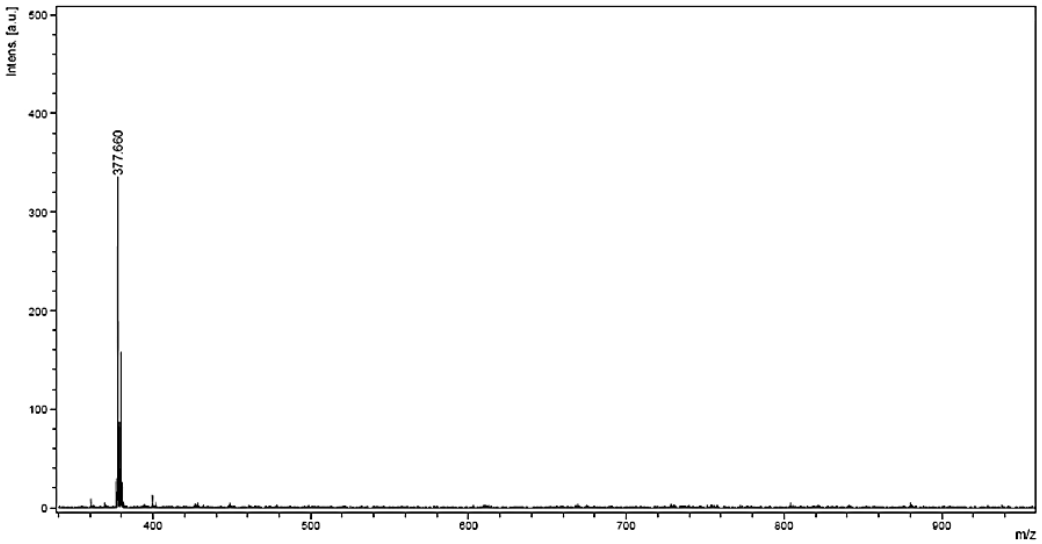

Figure A-5 MALDI-TOF mass spectrum of copper(II) salophen [51]

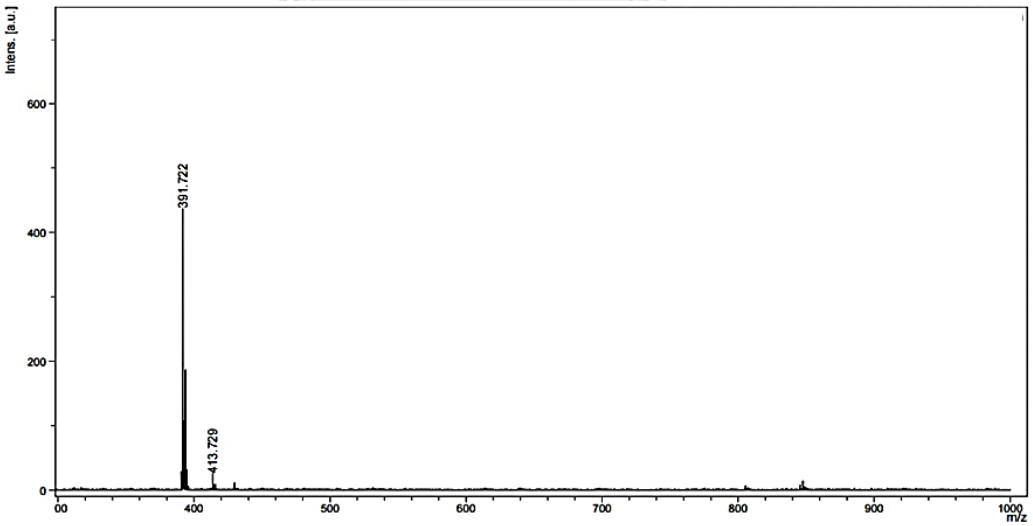

Figure A-6 MALDI-TOF mass spectrum of copper(II) methyl-salophen [51]

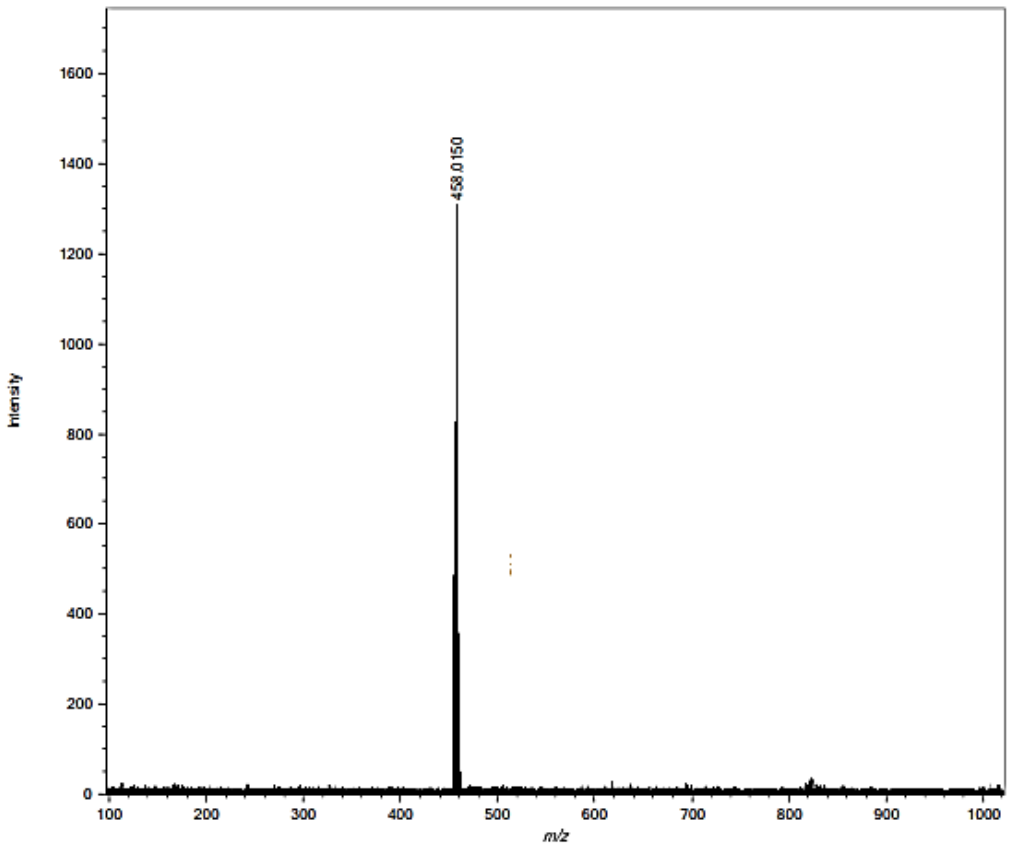

Figure A-7 MALDI-TOF mass spectrum of copper(II) bromo-salophen

APPENDIX B

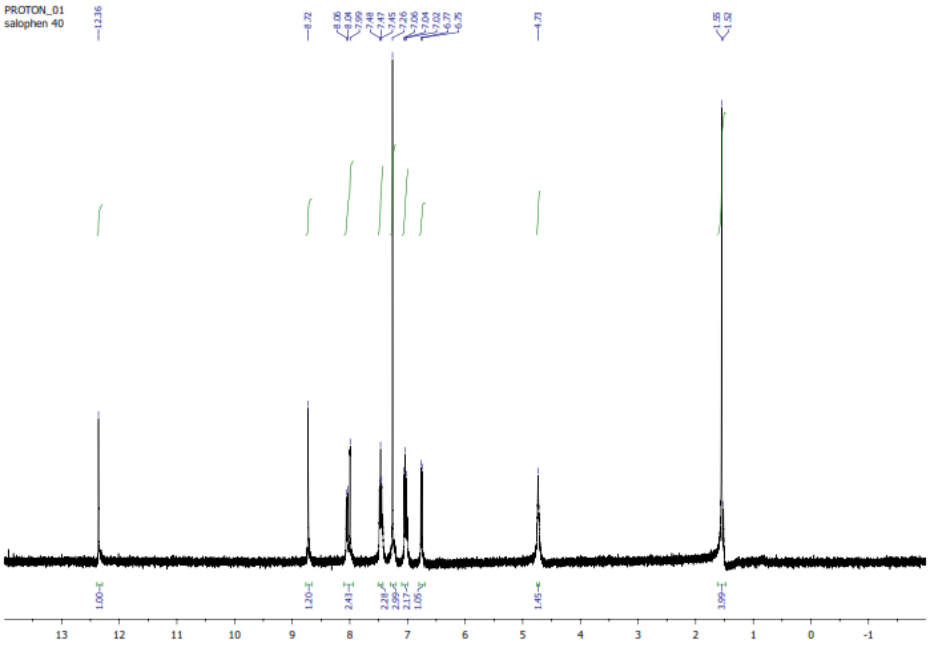

Figure B-1 NMR spectrum of salophen [51]

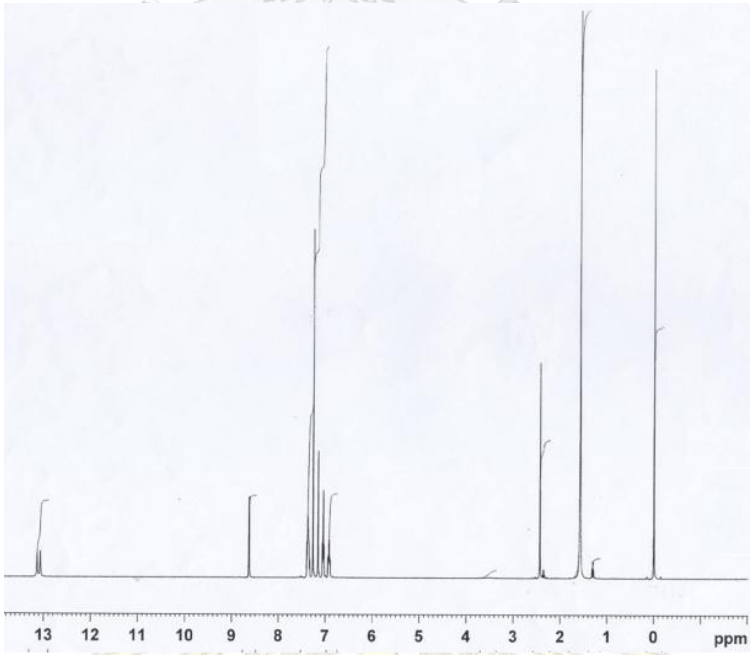

Figure B-2 NMR spectrum of methyl-salophen [51]

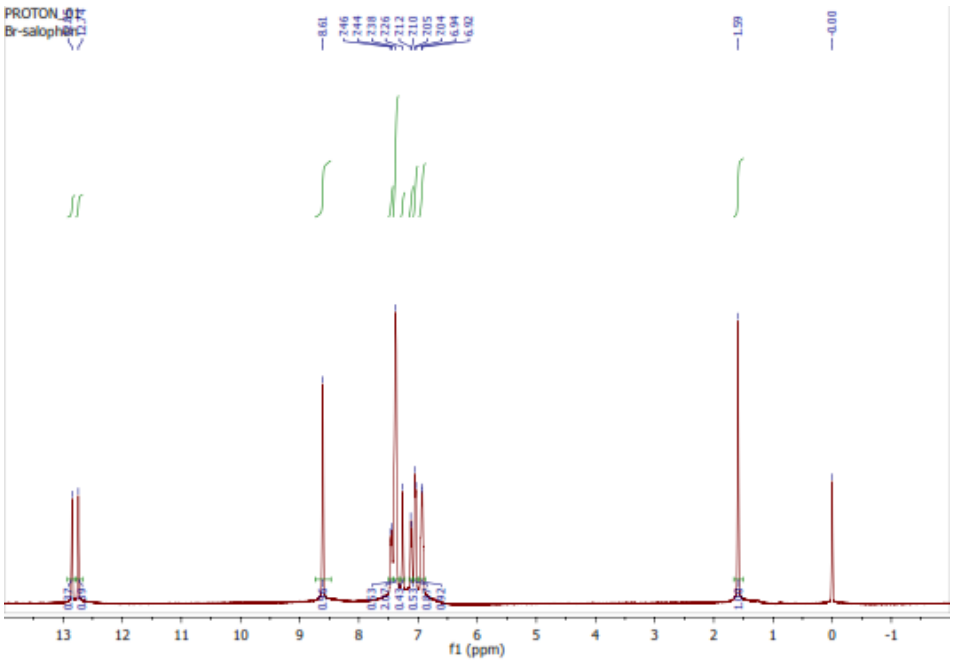

Figure B-3 NMR spectrum of bromo-salophen

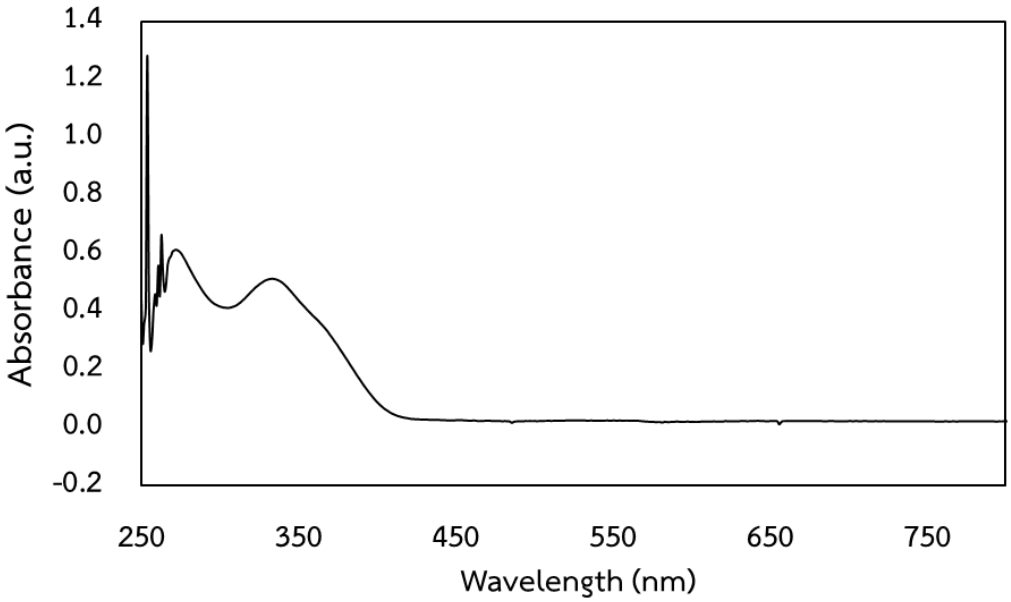

Figure B-4 UV–vis spectrum of salophen [51]

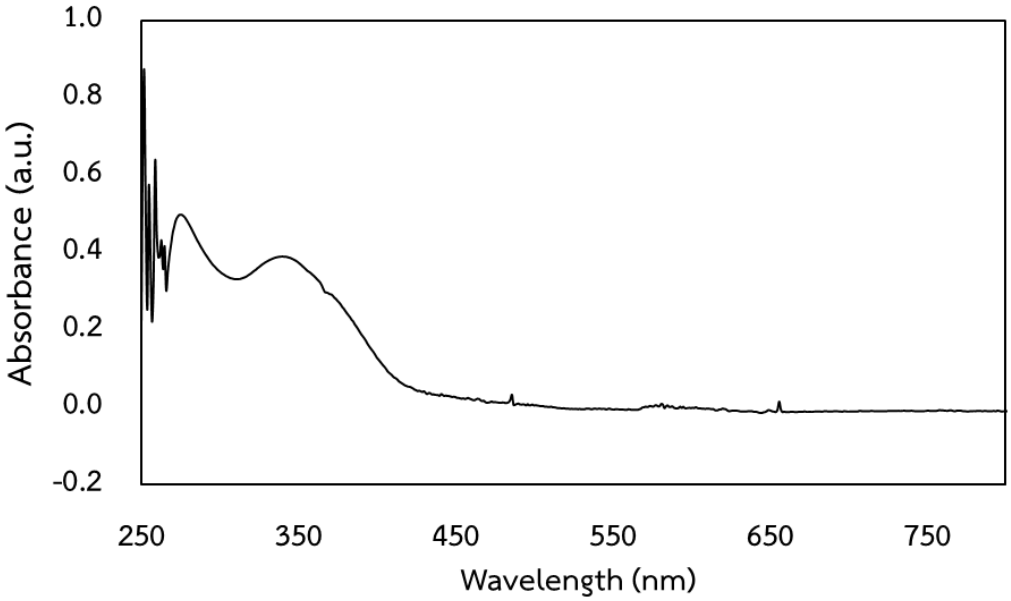

Figure B-5 UV–vis spectrum of methyl-salophen [51]

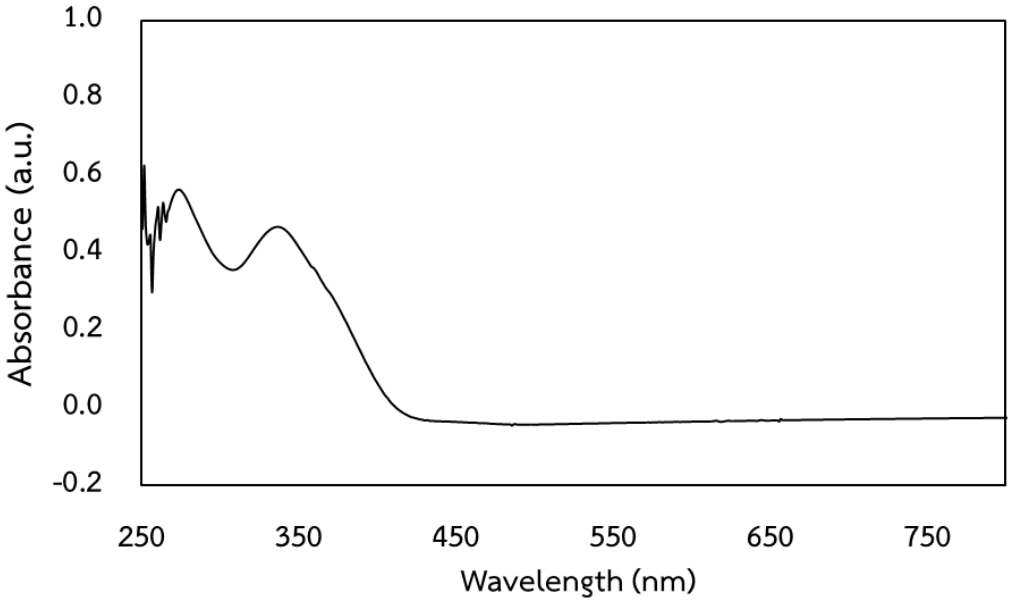

Figure B-6 UV–vis spectrum of bromo-salophen

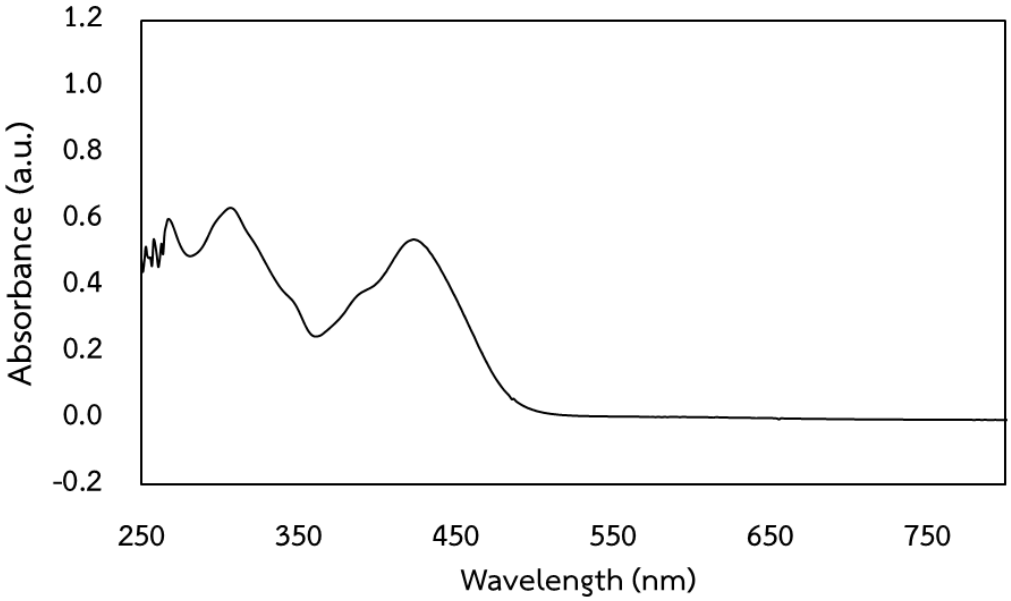

Figure B-7 UV–vis spectrum of copper(II) salophen [51]

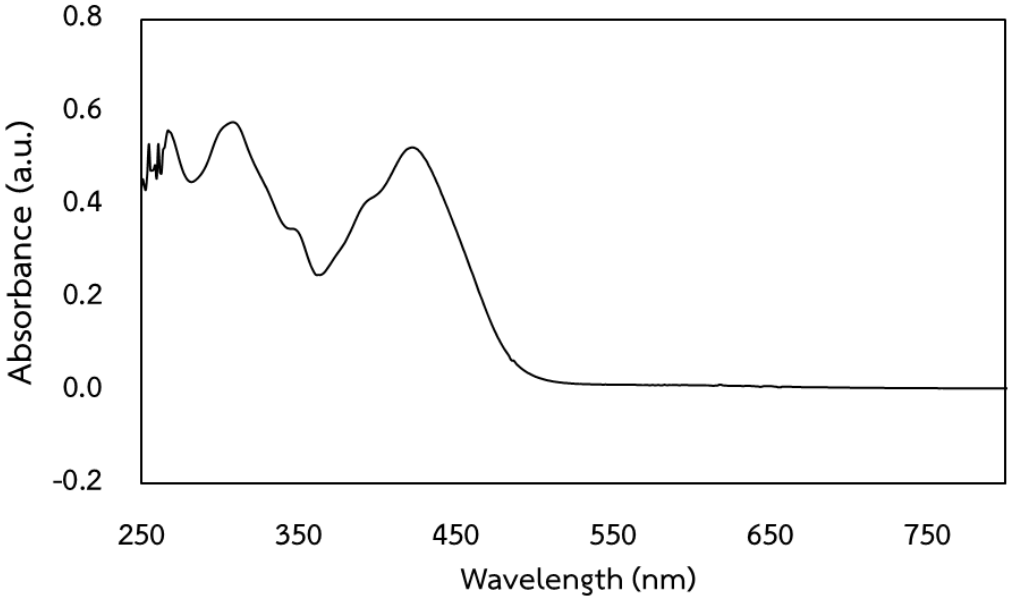

Figure B-8 UV–vis spectrum of copper(II) methyl salophen [51]

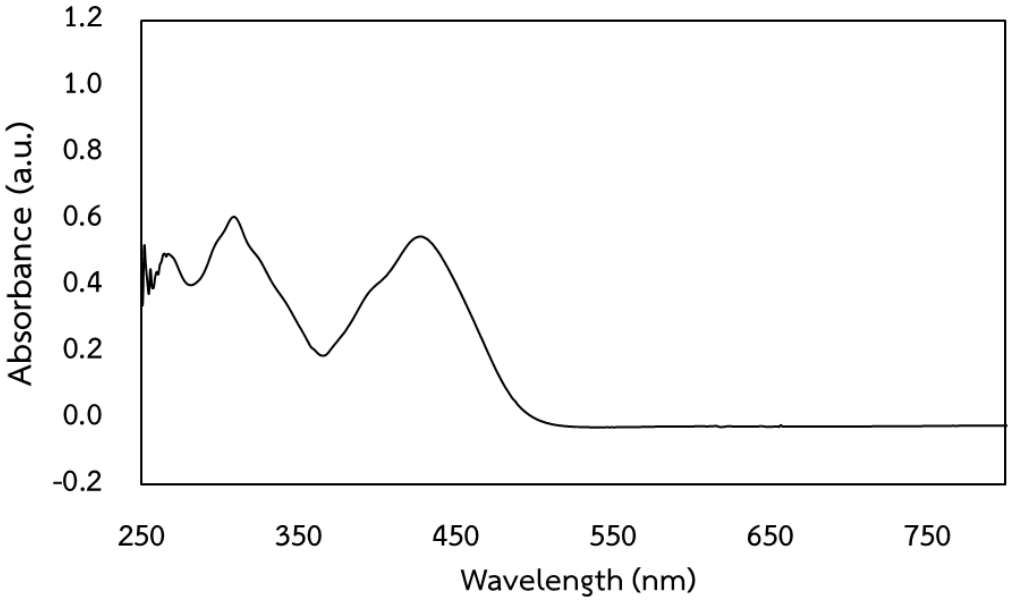

Figure B-9 UV–vis spectrum of copper(II) bromo-salophen

APPENDIX C

Table C-1 Electrochemical data obtained from cyclic voltammograms of 2.0 mM metal salen-based complexes in DMF containing 0.1 M $TBABF_4$ in the presence and absence of carbon dioxide [27]

Complex	Condition	E_{pc} (V)	E_{pa} (V)	i_{pc} (μA)	i_{pa} (μA)	Cathodic current increase (%)
iron(III) salen	Ar	−2.19	−2.10	−24.517	24.698	166.90
	CO_2	−2.19	ND	−65.437	ND	
cobalt(II) salen	Ar	−1.68	−1.60	−24.297	24.594	45.15
	CO_2	−1.68	−1.60	−24.297	20.413	
nickel(II) salen	Ar	−2.05	−1.97	−24.108	24.122	41.39
	CO_2	−2.06	ND	−34.087	ND	
copper(II) salen	Ar	−1.62	−1.52	−20.646	18.047	879.96
	CO_2	−1.56	ND	−20.613	ND	
salen ligand	Ar	−2.20	ND	−24.607	ND	49.86
	CO_2	−2.12	ND	−36.875	ND	

E_{pc} = cathodic peak potential; E_{pa} = anodic peak potential; and i_{pc} = cathodic peak current.

ND = not available.

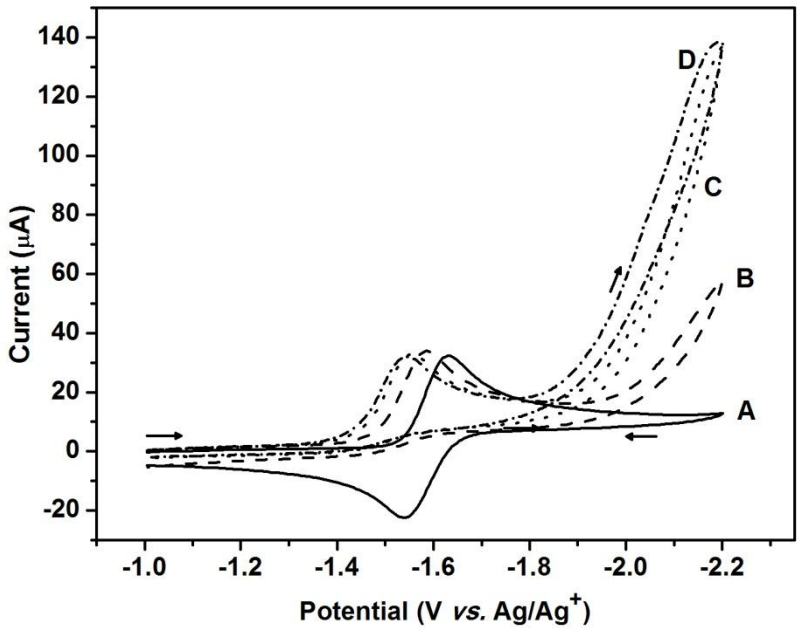

Figure C-1 Cyclic voltammograms recorded with a glassy carbon disk electrode at a scan rate of 100 $mV \cdot s^{-1}$ for DMF solution containing 0.10 M $TMABF_4$ with (A) 2.0 mM copper(II) salen in saturated argon, (B) 2.0 mM copper(II) salen in saturated carbon dioxide, (C) 2.0 mM copper(II) salen and 1.0 M H_2O in saturated carbon dioxide, and (D) 2.0 mM copper(II) salen and 2.0 M H_2O in saturated carbon dioxide [27]

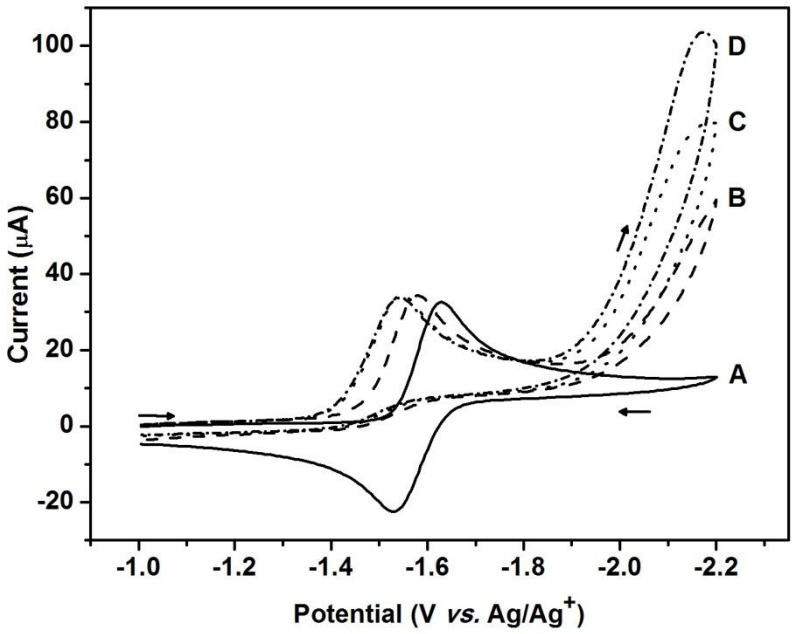

Figure C-2 XRD patterns of (a) reticulated vitreous carbon; and reticulated vitreous carbon after electrolysis of copper(II) salen at –2.10 V (B) without HFIP and (C) with 25.00 mM HFIP [27]

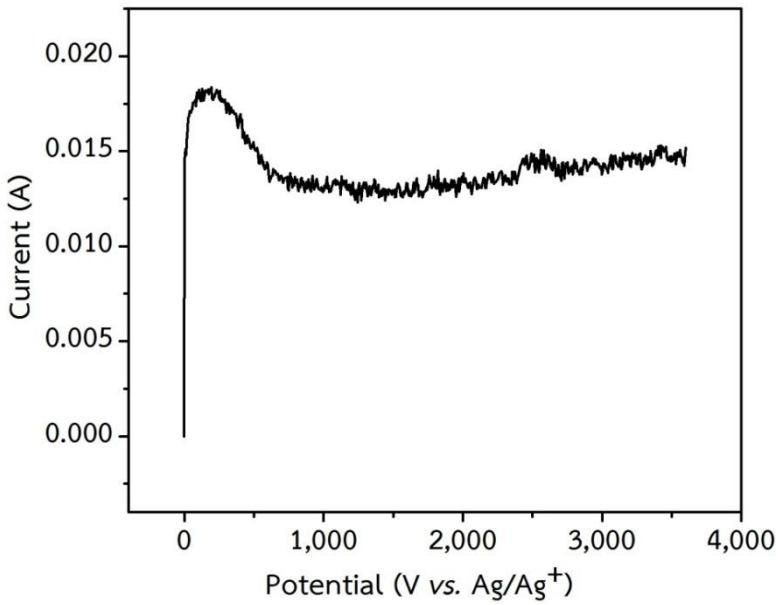

Figure C-3 Chronoamperogram recorded with a reticulated vitreous carbon electrode for 2.0 mM copper(II) salen in DMF solution containing 0.10 M $TBABF_4$ with saturated carbon dioxide at the potential of –2.10 V

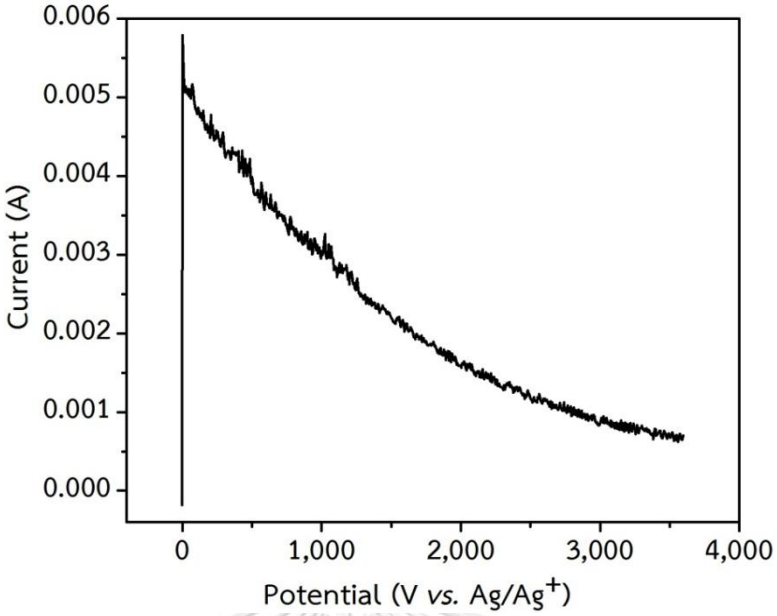

Figure C-4 Chronoamperogram recorded with a reticulated vitreous carbon electrode for 2.0 mM salen ligand in DMF solution containing 0.10 M $TBABF_4$ with saturated carbon dioxide at the potential of –2.10 V

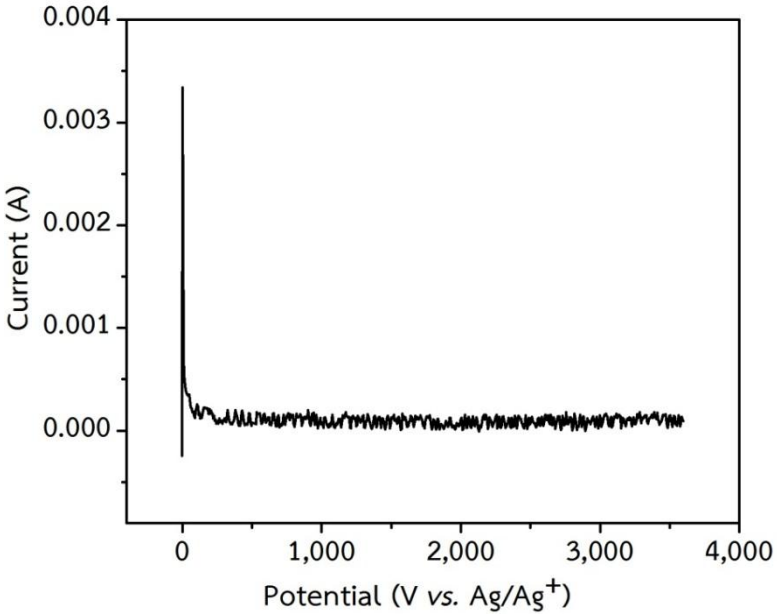

Figure C-5 Chronoamperogram recorded with a reticulated vitreous carbon electrode in DMF solution containing 0.10 M $TBABF_4$ with saturated carbon dioxide at the potential of –2.10 V

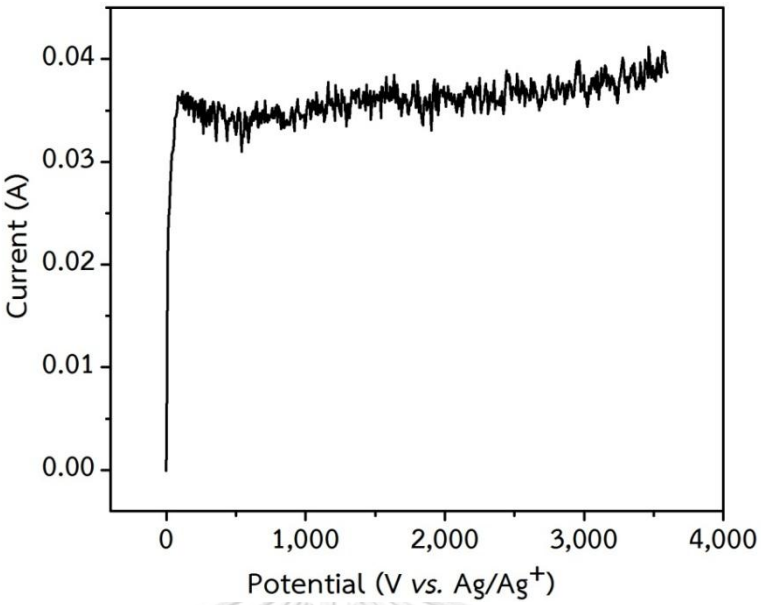

Figure C-6 Chronoamperogram recorded with a reticulated vitreous carbon electrode for 2.0 mM copper(II) salen in DMF solution containing 0.10 M $TBABF_4$ and 25 mM HFIP with saturated carbon dioxide at the potential of –2.00 V

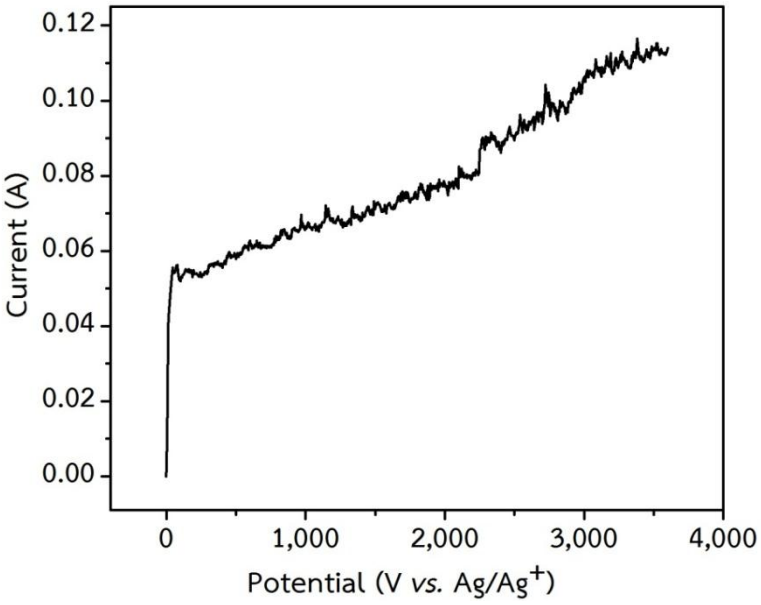

Figure C-7 Chronoamperogram recorded with a reticulated vitreous carbon electrode for 2.0 mM copper(II) salen in DMF solution containing 0.10 M $TBABF_4$ and 25 mM HFIP with saturated carbon dioxide at the potential of –2.10 V

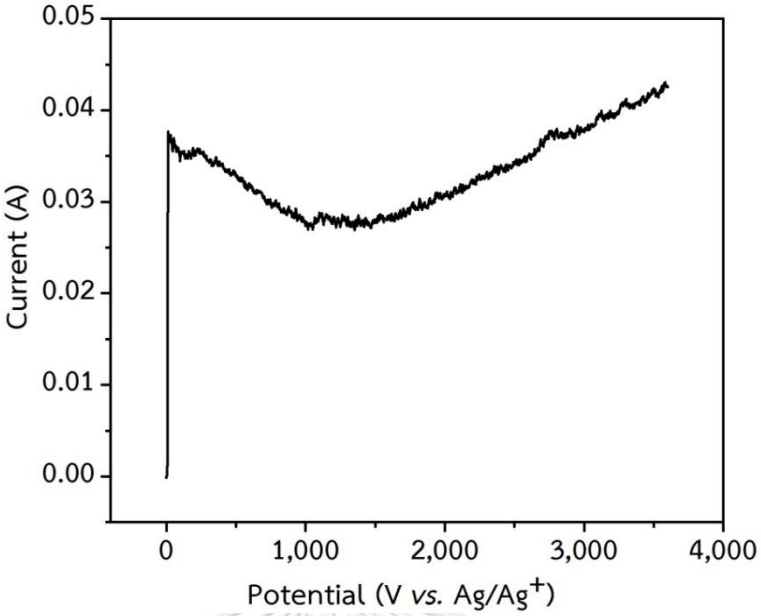

Figure C-8 Chronoamperogram recorded with a reticulated vitreous carbon electrode for 2.0 mM copper(II) salophen in DMF solution containing 0.10 M $TBABF_4$ with saturated carbon dioxide at potential of –2.00 V

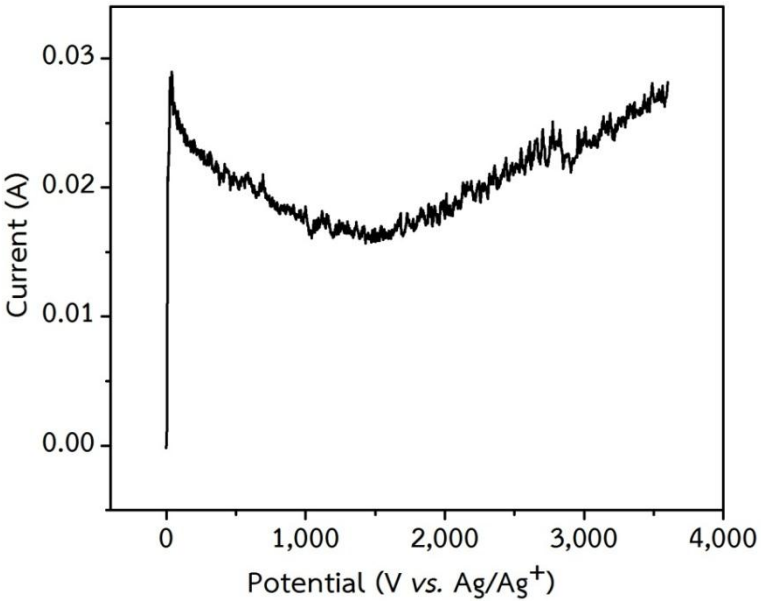

Figure C-9 Chronoamperogram recorded with a reticulated vitreous carbon electrode for 2.0 mM copper(II) methyl-salophen in DMF solution containing 0.10 M $TBABF_4$ with saturated carbon dioxide at the potential of –2.00 V

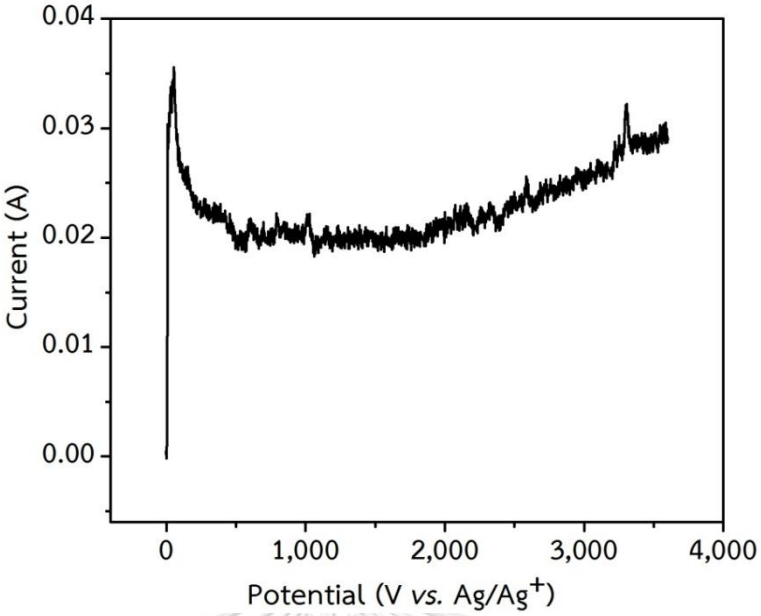

Figure C-10 Chronoamperogram recorded with a reticulated vitreous carbon electrode for 2.0 mM copper(II) bromo-salophen in DMF solution containing 0.10 M $TBABF_4$ with saturated carbon dioxide at the potential of –2.00 V

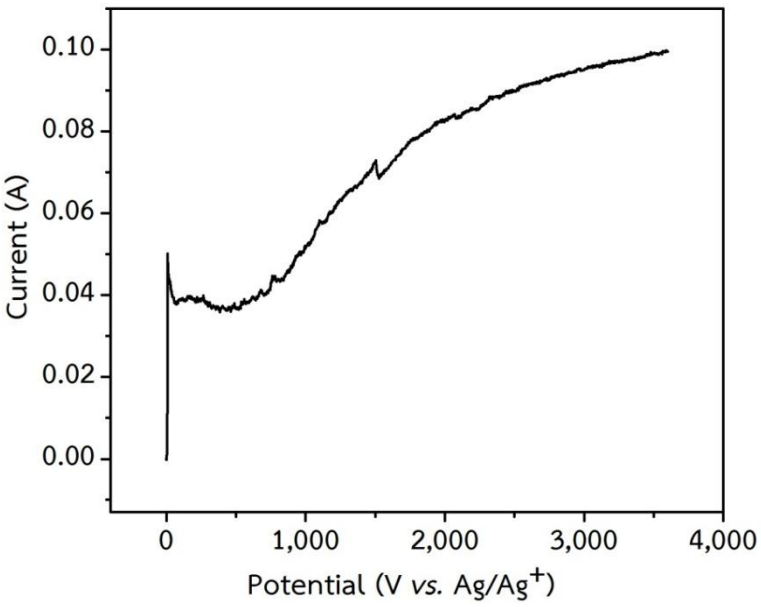

Figure C-11 Chronoamperogram recorded with a reticulated vitreous carbon electrode for 2.0 mM copper(II) salophen in DMF solution containing 0.10 M $TBABF_4$ and 25 mM HFIP with saturated carbon dioxide at the potential of –2.00 V

VITA

Miss Kantima Chitchak was born on October 6, 1985 in Kalasin, Thailand. She graduated with Bachelor's Degree in Petrochemicals and Polymeric materials Engineering, Silpakorn University in 2007. She continued her study in Petrochemical and Polymer Science, Chulalongkorn University and completed with Master's Degree in 2011.

Research experience:

Nov 4-14, 2014: recipient of SAKURA Exchange Program in Science, Nagaoka University of Technology, Nagaoka, Niigata, Japan.